

**MOLECULAR BEAM STUDIES OF
NITRIC OXIDE (NO) REDUCTION
REACTIONS ON Pd(111) SURFACES**

A THESIS SUBMITTED TO THE

**UNIVERSITY OF PUNE
FOR THE DEGREE OF**

**DOCTOR OF PHILOSOPHY
IN**

CHEMISTRY

BY

K. THIRUNAVUKKARASU

**CATALYSIS DIVISION
NATIONAL CHEMICAL LABORATORY**

PUNE 411 008

INDIA

DECEMBER 2006

DECLARATION

I hereby declare that the thesis “**Molecular Beam Studies of Nitric Oxide (NO) Reduction Reactions on Pd(111) Surfaces**” submitted for the degree of Doctor of Philosophy to the University of Pune has not been submitted by me for a degree to any other University.

K. THIRUNAVUKKARASU

CERTIFICATE

This is to certify that the work incorporated in the thesis, “**Molecular Beam Studies of Nitric Oxide (NO) Reduction Reactions on Pd(111) Surfaces**” submitted by **Mr. K. Thirunavukkarasu**, for the Degree of **Doctor of Philosophy**, was carried out by the candidate under my supervision in the Catalysis Division, National Chemical Laboratory, Pune – 411 008, India. Such material as has been obtained from other sources has been duly acknowledged in the thesis.

Dr. C. S. Gopinath

(Research Supervisor)

Acknowledgements

I thank my research supervisor, Dr. C. S. Gopinath for helping me throughout my tenure for his kindness and shaping my dissertation work to a good structure.

I would like to thank the present and past heads of the division, Dr. Rajivkumar and Drs. A. V. Ramaswamy and S. Sivasanker, for providing me all the divisional facilities required for my research work. I would also like to thank all the scientific and non-scientific staffs in the division for their direct and indirect help in various occasions. Many thanks go to the present and past directors, National Chemical Laboratory, for allowing me to carry out the research work in a prestigious and well-equipped laboratory. CSIR, New Delhi is gratefully acknowledged for the research fellowship.

I'm grateful to Professor H-J. Freund and Dr. J. Libuda, Fritz-Haber Institute, Berlin, for their keen interest and collaboration. I thank Mr. S. D. Bakare for making the temperature controller in a timely manner for our work. I admire and thank Dr. S. D. Prasad for in-depth and detailed discussions.

I thank my present and past colleagues, Maitri, Dhanashree, Nagarajan, Vijay, Dr. Thomas, Dr. More, and Moorthy for their support. I thank all of my friends who made my stay here memorable and enjoyable. I've to mention a few among them: Elangovan, Sankar, Dr. Selvakannan, Shankar Raman, Balaji (NMRL), Marivel, Suresh, Sasi Kumar, Victor, Vijay, Muthukumar, Murugan, Moorthy, Marimuthu (C-MET), Khaja, Dr. Senthil, Sathya and his parents from NCL. I would like to thank my important college mates and childhood friends: Praba, Karthik, Babu, Stalin, Dr. Chimbu, Sakthivel(s), Ravi, Kans, Dr. Jeba, Ram, Venketesh, Balu, Desigan and Govind. I specially thank Nitin, for his support as a room-mate.

I would like to thank my e-friends who accepted me as a writer (in Tamil) on this occasion: Iyappan, Ganesh, Mrs. Shylaja, Kanya, KVR.

I thank the great saint, Ramana Maharishi, for guiding me internally throughout my life. I thank my parents and family members for their constant encouragement throughout my Ph D.

K. Thirunavukkarasu

Table of Contents

1.	Introduction	1
1.1.	Heterogeneous Catalysis – Surface Science Approach	1
1.1.1.	Surface Science Approach – Importance of Ultra-High Vacuum	2
1.2.	Various Levels of Study in Catalysis	3
1.3.	Model Studies using Metal Single Crystals	4
1.4.	Pressure and Material Gap Problems	7
1.4.1.	The Material Gap	7
1.4.2.	The Pressure Gap	8
1.5.	Molecular Beam Technique for Kinetic Studies	9
1.5.1.	Advantages of Molecular Beam Studies	10
1.5.2.	Deviations from Conventional Kinetic Theories and Limitations of the Technique	13
1.6.	Present Status of NO Reduction on Pd(111) Surfaces and Scope of the Thesis	14
1.6.1.	The Catalytic Converter	14
1.6.2.	Nitric Oxide (NO) Reduction Reactions on Palladium – Structure of the Thesis	15
2.	Fabrication of Molecular Beam Instrument for Kinetic Studies	17
2.1.	Introduction	17
2.2.	Design Considerations of MBI Chamber	17
2.3.	Design Considerations of the Doser Assembly	20
2.4.	Coverage Calculations - CO Adsorption on Pd(111) Surfaces at 300 K	23
2.5.	Summary	26
3.	NO Adsorption and Decomposition on Pd(111) Surfaces	27
3.1	Introduction	27
3.2.	Experimental	28
3.3.	Results and Discussion	29

Table of Contents

3.3.1.	General Considerations	29
3.3.2.	Temperature-Dependent NO Adsorption and Dissociation on Pd(111)	31
3.3.3.	Surface Oxygen Coverage and Oxygen Diffusion into Subsurface/Bulk	36
3.3.4.	Temperature-Programmed Desorption Studies of NO/Pd(111)	37
3.3.5.	Sticking Coefficient of NO on Pd(111)	39
3.3.6.	Reaction Mechanism	40
3.4.	Summary	42
4.	NO + CO Reaction on Pd(111) Surfaces	43
4.1.	Introduction	43
4.2.	Experimental	44
4.3.	Results	45
4.3.1.	General Aspects on Catalytic Activity Measurements	45
4.3.2.	Transient Kinetics	48
4.3.2.1.	Displacement of CO by NO	48
4.3.2.2.	Restart Experiments	52
4.3.3.	Steady-State Kinetics:	54
4.3.3.1.	Temperature Dependence	54
4.3.3.2.	Composition Dependence	55
4.3.3.3.	Flux Dependence	55
4.3.3.4.	Steady-State Reaction Rates	57
4.3.3.5.	TPD Studies	57
4.4.	Discussion	59
4.4.1.	Reaction Mechanism	59
4.4.2.	Steady-State Kinetics	61
4.4.3.	A Comparison between (NO + CO)/Pd(111) and (NO+ CO)/Rh(111)	64
4.5.	Summary	65
5.	CO + O₂ Reaction on Pd(111) Surfaces	66

Table of Contents

5.1.	Introduction	66
5.2.	Experimental	67
5.3.	Results	68
5.3.1.	Typical Isothermal Kinetic Measurement	68
5.3.2.	Adsorption of Oxygen on Pd(111) surfaces	70
5.3.3.	Transient Kinetics	72
5.3.3.1.	Temperature Dependence	72
5.3.3.2.	Beam Composition Dependence	74
5.3.3.3.	CO+O Coverage Differential ($\Delta\Theta^{\text{TS}}$)	78
5.3.3.4.	CO and O ₂ Initial Sticking Coefficients	81
5.3.3.5.	Any O ₂ poisoning in the CO+O ₂ reaction on Pd(111) Surfaces ?	83
5.3.3.6.	Flux Dependence	84
5.3.4.	Steady State CO+O ₂ /Pd(111) Kinetics	86
5.3.4.1.	Temperature Dependence of Steady State Rate	86
5.3.4.2.	Composition Dependence of CO+O ₂ Reaction on Pd(111) Surfaces at 425 K	86
5.3.4.3.	Steady State Rate of CO ₂ Production on CO+O ₂ /Pd(111)	88
5.3.5.	A Correlation between R _{SS} and Transient Kinetics	89
5.3.6.	Surface Stoichiometry under Steady-State Conditions	90
5.3.7.	Post-reaction TPD	92
5.4.	Discussion	94
5.4.1.	Reaction Mechanism Aspects	94
5.4.2.	Initial Adsorption of CO and O ₂ from CO+O ₂ Beams	96
5.4.3.	Transient Behavior of Surface Coverages	98
5.4.4.	Unusual Transient Kinetics and High Temperature CO-adsorption	99
5.5.	Conclusions	101
6.	NO + CO + O₂ Reaction on Pd(111) Surfaces	102
6.1.	Introduction	102
6.2.	Experimental	103

Table of Contents

6.3.	Results	104
6.3.1.	A Typical Isothermal Kinetic Measurement	104
6.3.2.	Transient Kinetics of NO+CO+O ₂ Reaction on Pd(111)	105
6.3.2.1.	Temperature Dependence	105
6.3.2.2.	Beam Composition Dependence	108
6.3.2.3.	Temporal Evolution of N ₂ and N ₂ O from O ₂ -lean and O ₂ -rich Beams	111
6.3.3.	Steady State Kinetics of NO+CO+O ₂ /Pd(111)	111
6.3.3.1.	The Effect of NO on the Steady State CO ₂ Production for CO+O ₂ Reaction on Pd(111) Surface	115
6.3.4.	Beam Switching Experiments	116
6.4.	Discussion	118
6.4.1.	The Effect of O ₂ on NO Adsorption and Dissociation	119
6.4.2.	The Effect of NO on CO+O ₂ Kinetics	120
6.4.3.	Beam Switching Experiments	120
6.4.4.	Comparison with Previous Reports	121
6.5.	Summary	122
7.	Conclusions and Future Outlook	124
	References	127

Chapter 1

Introduction

“Most finely divided catalysts must have structures of great complexity, and it is probable that the atoms are attached to each other in the form of branching chains so that there are hardly any groups of as little as three or four atoms which are as closely packed as they would be in the crystalline solid. In order to simplify our theoretical consideration of reactions on surfaces, let us confine our attention mainly to reactions on plane surfaces. If the principles in this case are well understood, it should then be possible to extend the theory to the case of porous bodies”.

Langmuir, I. *Trans. Faraday. Soc.* 17, **1922**, 607

Introduction

1.1. Heterogeneous Catalysis – Surface Science Approach

Berzelius introduced the concept of catalysis on 1835. Based on the phase of the reactants and catalysts, catalysis can be divided into homogeneous and heterogeneous. Though, in general, homogeneous catalysts have good catalytic activity and selectivity towards a particular product, the difficulty in the separation of products from reactants and the catalyst makes heterogeneous catalysis more advantageous for the industrial processes. Heterogeneous catalysis occurs at the surfaces/interfaces of the solid catalysts. The gas or liquid phase reactants are brought together on the solid catalyst surface and the chemical transformation of reactants to products occurs. As the surface free energy of solids is always positive [1], the solid surfaces tend to attract foreign species from its immediate atmosphere to keep its surface tension to a low value. In other words, the surface atoms of any solid always want to have the coordination number as the same as that of the bulk atoms; thus they have a thirst to attract foreign molecules from the immediate surroundings.

Depending on the strength of any bond formed between the adsorbed species (adsorbate) and surface atoms (adsorbent/substrate), the adsorption process is classified to physisorption (a weak bond / van der Waals interaction) and chemisorption (a strong bond). Generally, physisorbed species will be desorbed as such by heating the surface; chemisorbed species may be dissociated or get transformed into some other species by thermal energy and lead to the products. At present, nearly 90% of the industrial chemical processes involve catalysis. Particularly heterogeneous catalysis is vital in many industrial processes like steam reforming, catalytic cracking, fine-chemical production, environmental clean-up etc.

The rate equation for a heterogeneously catalyzed reaction, $A + B \xrightarrow{\text{Catalyst}} \text{products}$, may be represented as:

$$\text{Rate} = k[A][B] \quad (1.1)$$

The rate equation gives some information about the mechanism of chemical reactions. However a heterogeneously catalyzed reaction cannot be characterized by macroscopic kinetic parameters alone, as it ignores some important microscopic parameters such as,

elementary steps like adsorption of reactants, surface diffusion (hopping of adsorbates from one site to another), chemical transformation of adsorbed species, and desorption, the identification and characterization of intermediates/products (that comprise the reaction mechanism) and the temporal behavior together with the relevant transport processes which gives the overall rate. [2] The slowest process, with respect to the rate among the elementary reactions, controls the rate of an overall catalytic reaction and determines the macroscopic properties of the reaction, like free energy and enthalpy changes. By observing the dynamic processes that are occurring on the surface during the course of a catalytic chemical reaction through *in-situ* spectroscopic techniques gives most of the fundamental information mentioned above and this approach is known as '*surface science approach*'. General concepts involved in catalysis can be extracted from them and it may be used in the design of the catalyst.

1.1.1. Surface Science Approach – Importance of Ultra-High Vacuum:

Ultra high vacuum (UHV) is required for most surface science experiments for two principal reasons: (i) to enable to prepare atomically clean surfaces, and (ii) such surfaces to be maintained in a contamination-free state for the duration of the experiment and to use the electron/ion/photon-based *in-situ* experimental techniques without undue interference from gas phase scattering. Most spectroscopic techniques are capable of detecting molecules in the gas phase; in these cases it is preferable that the number of species present on the surface substantially exceeds those present in the gas phase immediately above the surface - to achieve a surface/gas phase discrimination of better than 10:1.

In order to begin experiments with a reproducibly clean surface and to ensure that significant contamination by background gases does not occur during an experiment, the background pressure must be kept very low in such a way that the time required for contaminant build-up is substantially greater, i.e. it should be in hours than that required to conduct an experiment. The implication with regard to the required pressure depends upon the nature of the surface, but for the more reactive surfaces this necessitates the use of UHV ($<10^{-9}$ Torr).

1.2. Various Levels of Study in Catalysis

From the above section, it is clear that catalysis is a dynamic phenomenon. The various aspects of the dynamics of the surface reaction may be classified in a hierarchical scheme in terms of a qualitative time and length scales (Fig. 1.1) [2,3].

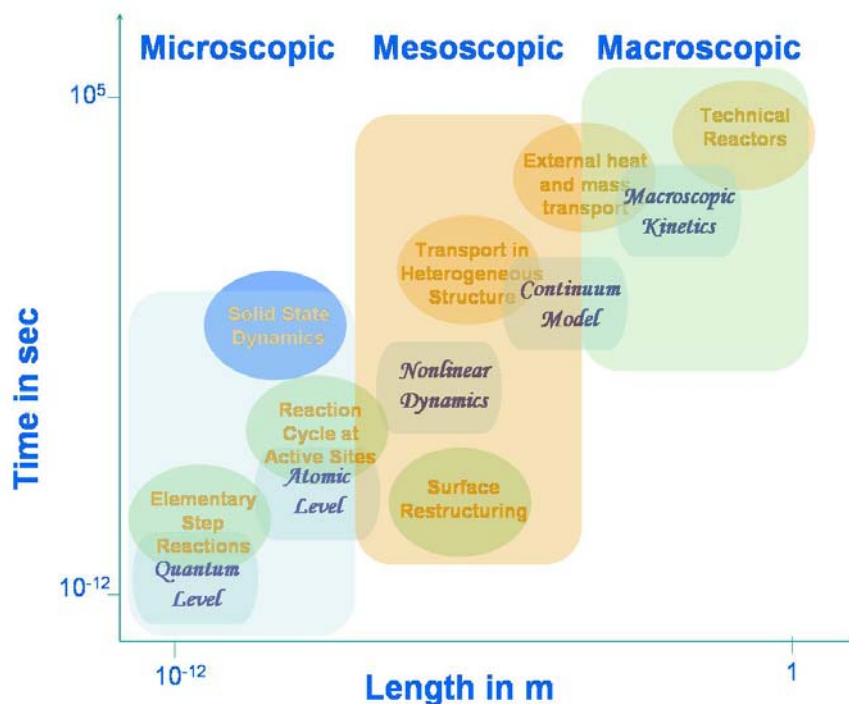


Fig. 1.1 Various aspects of the dynamics of surface reaction (adapted from [2,4]).

Briefly, a macroscopic kinetics is explored by using Eq 1.1 with the macroscopic parameters like temperature, pressure and concentration of the reactants. The efficiency of a catalyst is determined from this *macroscopic kinetics*. Description of the progress of a catalytic reaction is achieved by modeling the macroscopic kinetics. It is measured through connecting the atomic processes with the macroscopic parameters in rate equations in the framework of a suitable *continuum model*. When the *continuum model* fails to provide a good approximation over a range of external parameters, a set of nonlinear differential equations based on the rate laws of individual elemental reactions are derived for the concentrations of the various adsorbed species (coverages) involved. The existence of local variations in surface coverage causes coupling of the reaction with adsorbate diffusion or other transport (e.g., heat transfer) processes. Formulation of rate

equations in a *continuum model* requires detailed knowledge of the surface species involved in the reaction in an atomic scale. Modern surface science techniques provide this information. Processes of energy transfer between the various degrees of freedom on the *quantum level* guide the chemical transformations [2].

Simply, it can be explained as follows [3]: Technological chemical reactors operate in macroscopic dimensions of space and in time scales of years (Fig. 1.1). The transport of mass and energy between the catalyst particles decides the reactor performance (mm and ms) (macroscopic kinetics). Pores, grains, droplets, and bubbles are the typical heterogeneous structures, which govern diffusion phenomena within each catalyst particle with dimensions in the μm range and time scales in the μs range (mesoscopic level). Enzymes, metal-organic molecules, clusters and surface patches with nm dimensions are the locations where individual molecule conversions take place which require typically ns for the completion of individual reaction cycles. Surface diffusion of pre-adsorbed species and of atoms constituting the active sites are the microscopic transport phenomena, which decisively affect the course of heterogeneous catalytic reactions. At still smaller scales in space (pm) and time (ps to fs) the elementary step reactions occur, which are required to convert reactant into product molecules (microscopic level) (Fig. 1.1).

Fig. 1.2 shows a flow chart for the combinatorial nature of the present catalytic science for the rational way towards the synthesis of a better heterogeneous catalyst [4]. Obviously, catalysis encompasses number of other subjects, including physics, physical chemistry, solid-state/materials chemistry, surface science, theoretical chemistry and chemical engineering. Catalysis researchers need to know the above subjects as well.

1.3. Model Studies using Metal Single Crystals

Surface science explores the elementary reaction steps involved in the reaction with various reaction dynamics on the '*metal single crystal surfaces*' representing a real industrial catalyst to understand a given chemical process. These surface science experiments are called model experiments, and in these studies, a well- defined, single-

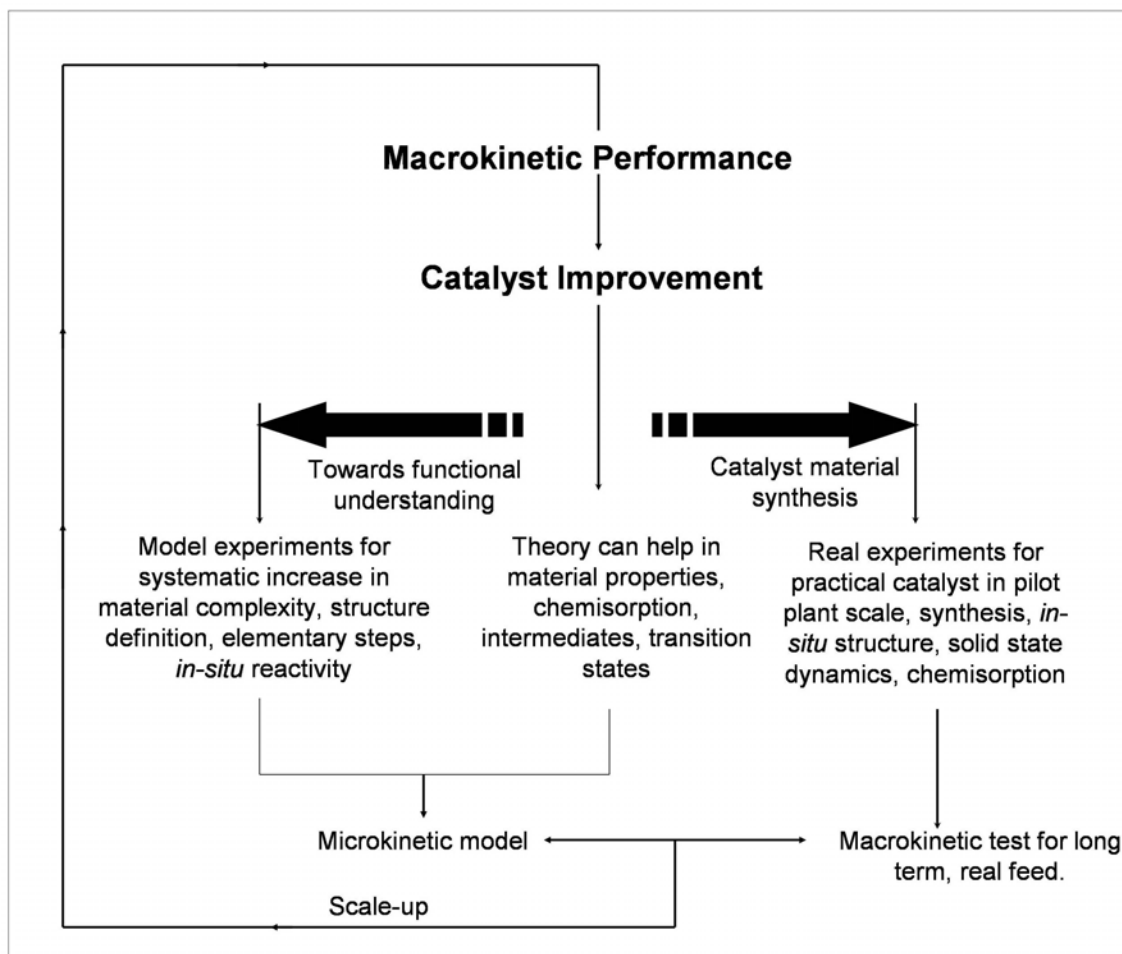


Fig. 1.2. Rough flow chart of a rational way towards a better heterogeneous catalyst for a given process. (Adapted from [3])

crystal plane is used to model a site or set of sites expected to exist on a real-world high-surface-area catalysts [5]. Though a clean surface of a practical catalyst may be prepared with less contamination, it usually contains large surface defects, kinks etc. The catalytic processes occurring in those models are still complicated to understand even with the advantage of simplicity in their structure compared to the real-world catalysts. Some of the chemical processes are found to be sensitive to the structure of the plane of the catalyst surface and the same can be understood with the help of model experiments [6]. In fact, Boudart [7] first coined the phrase ‘surface-sensitive / surface-insensitive reactions’ for this effect on catalyst surfaces.

Industrial catalysts (for any catalytic process) contain a set of different planar sites on their surface. TOF* for the same process is likely to be different from different facets, especially if the reaction is structure sensitive. This also causes the basis for *material gap*, which will be discussed later. Nonetheless, for a structure-insensitive reaction for e.g., steady-state specific methanation TOFs (methane molecules/site/sec) measured on the close-packed Ni(111) and more open Ni(100) surfaces [5,8] were found to be strikingly similar with respect to the specific rates and activation energies. A recent report claimed that the methane combustion on Pd is insensitive to structure [9]. Furthermore, the single-crystal results were virtually identical to the data acquired from the alumina-supported nickel catalysts [8]. These extraordinary similarities in kinetic data taken under nearly identical conditions demonstrated clearly that there is no significant variation in the specific reaction rate or the activation energy in changing from a catalyst consisting of small metal particles to one composed of a bulk single-crystal. Hence, these studies provided convincing evidence that the methanation reaction was indeed quite insensitive to the surface structure and established the appropriateness of using single-crystals to model this reaction. Although the kinetic measurements from these model studies for a structure-sensitive reaction can be transferred to the real catalytic system to some extent, it is completely transferred in the structure-insensitive reactions.

The effect of alkali metal promoters, like potassium [10], or an inhibitor, like sulfur [11-13], can be introduced as an impurity to the single crystal surfaces in a controlled fashion, and their effects on a given chemical process can be observed clearly. For example, adsorbed potassium causes a marked increase in the rate of CO dissociation on a Ni(100) surface [14]. The catalytic activity decreases substantially by the addition of electronegative species such as sulfur, as an inhibitor. In fact these effects are well recognized, but poorly understood in the industrial catalysis. Goodman et al [11-13] measured the rates of CO methanation as a function of S and P coverage over Ni(100) surface, and the results show a non-linear relationship between S coverage and the methanation rate. A sharp decrease in catalytic activity is observed at low S coverages, and the poisoning effects of S are rapidly maximized in their studies. Such is the case for the attenuation of the methanation activity by S for alumina-supported nickel catalysts

*Turn-over frequency (TOF) is defined as the number of product molecules formed per surface site per unit time.

[14]. Model catalyst approach has been effectively used to study structure sensitivity, effects of promoters/inhibitors on activity, and mixed-metal catalysis [6].

In general, model studies using metal single crystals provide important information like reaction mechanism, rate determining step (RDS), nature of the adsorbed species, etc. One more advantage of using metal single crystals as model catalysts should be mentioned here. In the study of CO oxidation on Ru surfaces, Ertl et al, [15,16] found that excitation with *femtosecond infrared laser pulses* in the pre-adsorbed CO and oxygen species on Ru(0001) single crystal surface enables the formation of CO₂; but mere conventional heating of the same Ru surface leads exclusively to the desorption of CO. In contrast, the desorption is caused by coupling of the adsorbate to the phonon bath of the Ru substrate, whereas the oxidation reaction is initiated by hot substrate electrons, as evidenced by the observed sub-picosecond reaction dynamics, which can only be observed as metal single crystals as model catalyst. Further activity/selectivity information obtained at UHV conditions may not be extended or correlated to that at high pressure, due to very high surface coverage including weakly bound species.

1.4. Pressure and Material Gap Problems

Generally, industrial chemical process occurs in the pressure range of 1-20 atm. Hence the pressure difference between the UHV studies on model catalysts and the actual technical or real world reaction conditions is to the tune of 10-12 orders of magnitude and thus it makes the basis for '*pressure gap*'. Highly complex real-world catalyst to that of relatively simple model catalysts forms the basis for '*material gap*'.

1.4.1. The Material Gap:

Single crystals of transition metals were utilized as model systems in heterogeneous catalysis because the surface structure was well defined and relatively easy to study its effect on fundamental parameters of catalysis such as, adsorption, reaction and desorption phenomena. They have a very low surface area of the order of <1 cm² oriented in some particular crystalline facet; however, they could not be able to simulate the most complicated, highly dispersed, high surface area (up to few hundred m²/g) catalyst systems used presently in the real-world. This makes one of the frequently asked questions on '*materials gap*' problem in the field of heterogeneous catalysis. The

effect of promoters and poisons on adsorption and catalytic activity was elucidated by depositing atoms such as K, Na, S, Cl etc. (i.e. complexity of the catalyst is increased) which may either directly influence the surface structure of a catalyst or/and modify the bonding of reactants and/or products [17-22]. In spite of the above material gap problems, single-crystal studies have thus greatly contributed to a better understanding of the catalytic phenomena at a molecular level, which is not possible with complex catalysts. Scientists try to overcome the material gap problem by systematically increasing the complexity of catalysts, i.e. metals deposited on a metal-oxide support in different sizes [23-36]. Somorjai et al prepared a 3-D model catalyst that has the surface area equivalent to the real-world catalysts ($\sim 100 \text{ m}^2/\text{g}$) [33-34]. Somorjai demonstrated the usefulness of the model studies in catalysis in a recent review article [28] (see, Fig 1.3). In any case, model studies using metal single crystals are necessary, particularly when a complex catalytic reaction is employed [37] or a new *in-situ* technique is applied [38].

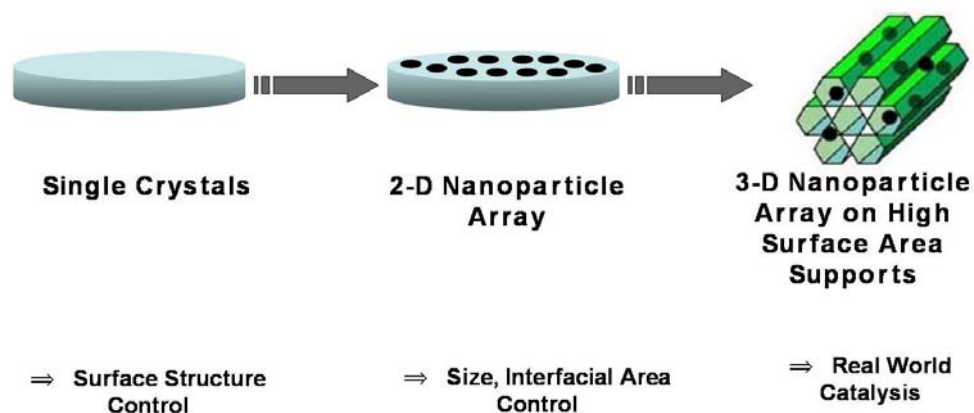


Fig. 1.3. The catalytic information gathered from model systems can be transferred to the more complex real world industrial catalysts. (Adapted from [29])

1.4.2. The Pressure Gap:

The pressure gap problem is tackled recently with the help of moderate to high-pressure in-situ spectroscopic techniques. The surface spectroscopic techniques widely applied at present can be applied to UHV / moderate / high pressure conditions. Using those techniques (SFG, PM-IRAS, etc), few groups [39-47] have studied catalytic processes at high / moderate pressure conditions. Nonetheless, the above moderate and

high pressure conditions were applied mostly in specially designed (mostly home-built) instruments; this indicates a considerably progress in this field of research.

Very recently, XPS is also extended to high pressure conditions. Possibility to measure XPS spectra at high pressure still exists from the fact that the mean free path of photoelectrons at a pressure of ~ 1 mbar is several millimeters. This means that to avoid weakening of the XPS signal, the mean-free path of photoelectrons in the high-pressure zone should be as large as possible, and the pressure gap between the high-pressure and vacuum zone as large as possible [38,48-51]. The pressure and material gap problems are thus overcome by using a complex model catalyst with high-pressure *in-situ* characterization techniques. Molecular beam technique, through which the pressure gap problem can be tackled to some extent, is described in the next section, with reported literature.

1.5. Molecular Beam Technique for Kinetic Studies

A molecular beam is a directed and spatially defined flux of molecules [52]. Molecular beams are used to find out the kinetic parameters and sticking coefficients of the gas molecules on solid surfaces. King and Wells [53] used successfully this technique for calculating the sticking coefficient of N_2 on tungsten crystal surfaces. In general molecular beam scattering experiments give detailed information about the first step toward a chemical reaction on surfaces. Beams with enhanced population of specific quantum states make an even more detailed analysis possible. Adsorption on surfaces can be studied very well using beam methods, especially in the case of activated processes. Beams allow the study of chemical reactions on surfaces, and in particular, where the products are directly ejected into the gas phase, or where reactions take place upon impact [54].

Molecular beam instrument (MBI) has several advantages over conventional UHV catalysis experiments and they are listed below [54-57]: a) High surface coverage can be achieved in the molecular beam technique. b) Molecular beams can be characterized to give single collision conditions compared to the conventional UHV catalysis experiments in which the whole chamber is filled with the gas(es) of interest to certain pressure. c) A pressure difference up to 10^5 Torr occurs between the pressure on

the sample surface and the background in these experiments and thus it bridges the gap between UHV high-pressure studies to some extent. d) Competitive adsorption of two different species can be identified. e) Details about the microkinetic details of the reactions and mechanistic studies of the reactions with the help of a MBI. f) Transient as well as steady state kinetics of the surface reactions can be studied.

1.5.1. Advantages of Molecular Beam Studies:

A kinetic measurement employing molecular beams inherently represents a single scattering experiment, i.e., molecules in the beam interact only once with the sample surface. Molecular beams are ideally suited for the study of surface kinetics on model systems; they allow for great control of the parameters that define the conditions of the reaction. Collimation, which makes the molecular beam, defines the directionality of it with respect to the surface plane. Additional control can be achieved on the energy of the reactants, both on their kinetic energy and on the energies of the different internal degrees of freedom with supersonic expansion. The details of the outgoing reactants can be characterized by angle-resolved, time-of-flight and spectroscopy-based detection [58]. Kinetic experiments with molecular beams can be easily carried out isothermally and, in some cases, isosterically as well.

Most of the past work on surface reactions with molecular beams has been performed using supersonic expansions, and the high energies of the molecules from those sources impinging on the surface make the extrapolation of the results to realistic catalytic conditions less than straightforward. Low-energy or effusive beams are perhaps more appropriate for the emulation of catalytic processes, which are used in our studies.

Libuda et al, [54] combined both the molecular beam approach with IR detection of surface species for complex supported model systems to tackle both pressure and material gap. The advantages of the combined approach of supported complex model with molecular beams are summarized in comparison with other kinetic probes as follows:

1. In an experiment, where there is only a single interaction of the reactant molecule with the surface, one can effectively “count” the surface events, i.e., determine absolute probabilities for different reactive and non-reactive surface events.

2. The possibilities to perform fast flux modulations are available, as diffusion, viscous flow, or pumping issues does not interfere much in the kinetic measurements. This allows one to perform fast and precise studies of transient processes.
3. In contrast to temperature programmed studies, molecular beam experiments can be performed under isothermal conditions, simplifying the analysis of the kinetics.
4. A large degree of control over the properties of the impinging molecules is provided, such as, e.g., their kinetic energy, the angle of incidence or their internal energy. This enables us to perform studies of the dynamics of the gas-surface interaction.
5. Molecular beam experiment is performed at low background pressure, which suppresses background reactions and enables to investigate the dynamic properties of the desorbing/scattered products and reactants, such as their angular distribution and kinetic energy. Besides studying the reaction potential energy surface (PES), such experiments may potentially be employed to probe site or facet specific kinetics on a heterogeneous surface.

In general the MBI bridges the gap between ideal conditions employed in surface science and the real world high pressure catalysis. (See Fig. 1.4)

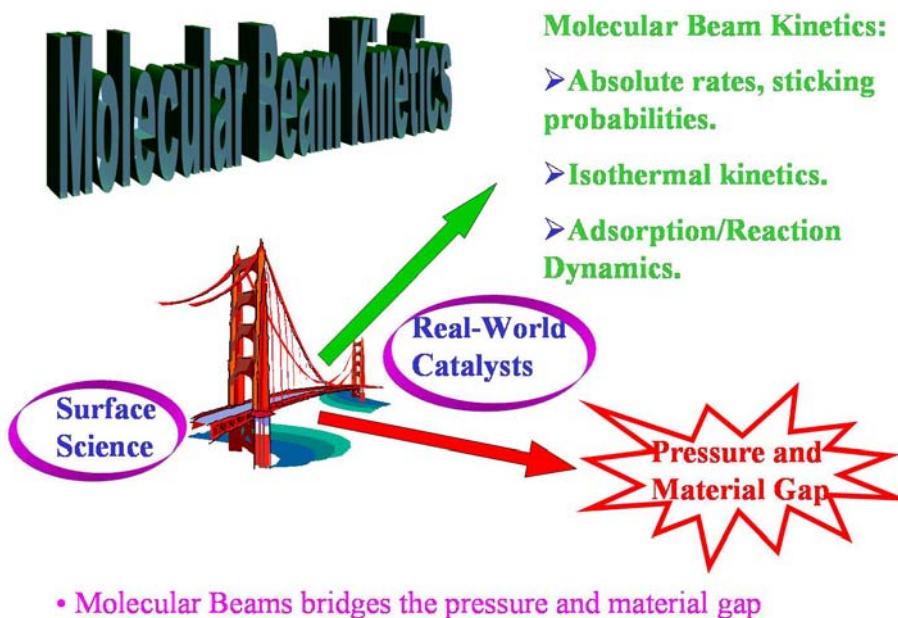


Fig. 1.4. Molecular beam kinetics – bridges the gap between surface science and catalysis.

Molecular beams have some other advantages; variation of the beam modulation frequency and surface temperature allows the parameterization of the rate-determining step or several sequential or parallel branches if they are moderately competitive. The effective pressures, although low, can be varied from 10^{-11} to 10^{-9} Torr if necessary to help identify the molecularity of intermediate steps. A specific advantage over thermal desorption studies is that in molecular beam reaction products are not the result of integrating over the changing thermal and coverage history that eventually leads to desorption in the former. In addition to the kinetic and mechanistic characterization of reactions on and with surfaces, dynamic details of the adsorption and desorption steps can be pursued by variation of the incident angle, velocity, internal energy, and identification of the same properties of the desorbing species with variation of the orientation and structure of the substrate. [54]

One of the areas of surface chemistry where molecular beam work has contributed greatly is the activation of stable molecules by surfaces [57]. Extensive work has been performed to elucidate the mechanism of alkane activation by metals. It has also been shown that the critical factor for alkane activation is the efficiency with which energy is transferred from the translational and internal degrees of freedom of the gas molecules to the particular C-H bond to be cleaved; the energy stored by the surface is often of little importance for this process [59-60].

Molecular beam work has also helped significantly in developing an understanding of the kinetics of adsorption [61-63]. From the kinetic point of view, adsorption is often described in terms of sticking coefficients (s), i.e., in terms of the probability of a molecule impinging on a surface to get adsorbed instead of scattering back into the gas phase. These sticking probabilities have commonly been measured by a method pioneered simultaneously by King and Wells [53] and Madey [63], which relies on reflectivity measurements of molecular beams directed at solid surfaces. Eq.1.2. helps in calculating s , where, f is the fraction of the collimated beam intercepted by the crystal surface, $\Delta P(t)$ is the difference between equilibrium and transient partial pressures, $P_{eq}(t)$ is the equilibrium pressure and $P_{base}(t)$ is the base pressure of the beam gas [64].

$$s(t) = \frac{1}{f} \frac{\Delta P(t)}{P_{eq}(t) - P_{base}(t)} \quad (1.2)$$

Therefore the molecular beam set-up can be used to measure adsorption probabilities. Molecular beam techniques can also be used to follow the transient kinetic behavior of adsorption systems around equilibrium. Ideally, kinetic measurements should be performed under both isothermal and isosteric conditions in order to separate the effects exerted by temperature and coverage on the overall kinetics of reaction.

Catalysis often involves two or more reactants. Accordingly, the kinetics of adsorption of catalytic reactants needs to be determined under competitive conditions. This is easily accomplished by using mixed molecular beams [65-72]. It is important to realize that the kinetics of adsorption of a given reactant can be deeply affected by competition with other adsorbates [67-69].

The kinetics of reactive adsorption can also be studied with molecular beams, in particular when the products desorb from the surface in the steady-state rate of the reaction. These changes are reversible, so restoration of the exposure of the crystal to the molecular beam results in the recuperation of the signals seen before the beam was blocked. Also, the transient response right after the blocking and unblocking of the beam provides some insight into the mechanism of reaction [67-69].

1.5.2. Deviations from Conventional Kinetic Theories and Limitations of the Technique:

The kinetic results from molecular beam technique shows significant deviations from the conventional kinetic theories [68]. In particular, it has been observed that neighboring adsorbates modify the energetics of surface reaction in ways not explained by macroscopic kinetic models. Free-energy barriers associated with transition state theory, which is the origin of chemical kinetics, can be expanded to include coverage-dependent terms. Changes in surface concentrations also lead to changes in adsorption geometries, and even to different adsorbate-surface bonding.

In general, molecular beam studies are restricted to the regime of low pressure kinetics in that they cannot provide effective pressures at the crystal surface higher than 10^{-2} Torr/s or usually 10^{-4} - 10^{-5} Torr for favorable geometries [73]. In addition, their advantages generally apply to reactions with reasonably high probabilities (10^{-4} or greater) that consist of only a few competitive branches (see 74, 75 for respective exceptions).

1.6. Present Status of NO Reduction on Pd(111) Surface and Scope of the Thesis

1.6.1. The Catalytic Converter:

In the last two decades increasing governmental regulations all over the world have stimulated tremendous growth in the research on environmental catalysis and green chemistry [76-80]. In particular, the automotive catalyst technology has improved, assisted by better petrochemical refining to yield cleaner fuels. Improvements in internal combustion engines and the above developments have led to fuel-efficient vehicles. The present technology of three-way catalytic (TWC) converters [76-77] meets the requirements of oxidation of CO. Figure 1.5 (right side image) shows an example for the structure of a commercial heterogeneous catalyst used in automobile exhaust emission control (TWC) processes. These catalysts are typically composed of a monolithic (or honeycomb) ceramic substrate, that exhibit equally sized and parallel channels (required for effective mass transport) with square shaped pores as shown in figure 1.5.

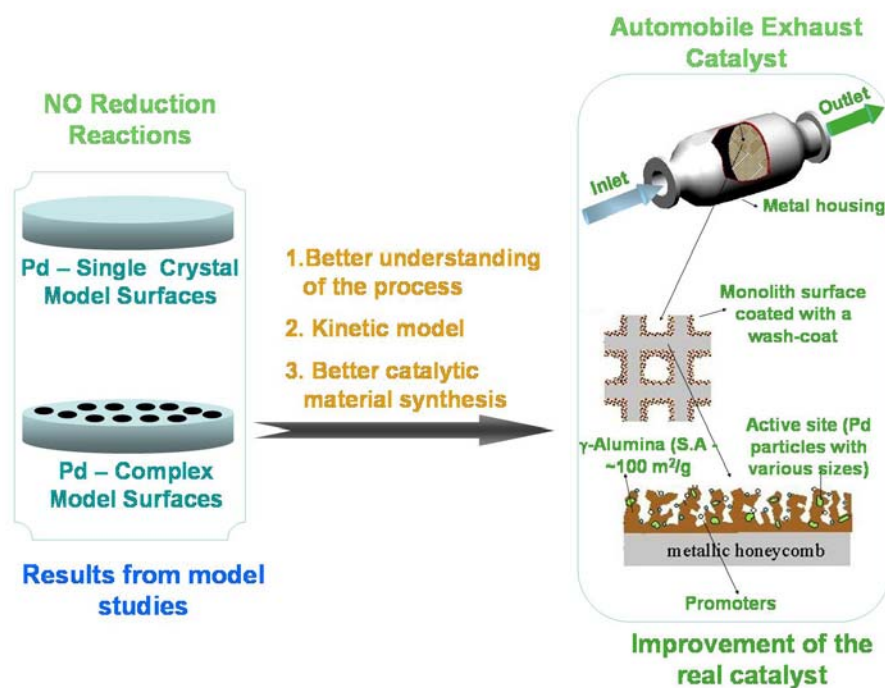


Fig.1.5. The goal and role of the present study

This monolith structure has an advantage of smaller pressure drop in exhaust system though it is expensive than pellet substrates. These ceramic monoliths have low surface

areas ($\sim 0.5 \text{ m}^2/\text{g}$) thus they need to be coated with a high surface area ($\sim 100 \text{ m}^2/\text{g}$) catalytic support such as $\gamma\text{-Al}_2\text{O}_3$, a *catalyzed wash-coat*, which is impregnated with the catalytically active sites (Pd, Pt, etc.) and promoters (CeO_2 , BaO, Na, K etc.) [76-78]. More problematic is the oxidation of nonvolatile organic species to CO_2 and, in particular, the reduction of NO to N_2 , especially under the highly oxidizing exhaust gas conditions of fuel-efficient lean-burn engines [81]. Although Rh is very active for NO reduction under fuel-rich conditions, this is not the case under net oxidizing conditions, since the excess oxygen inhibits the NO reduction activity of Rh by oxidizing it. Palladium has been suggested as an alternative active element for NO reduction due to its NO dissociation capacity and its stability under high temperature and oxidizing conditions [82-84].

There were few new technologies [85-86] introduced in the past decade, like NO_x storage or zeolite based catalysts, which provided different insights into the NO reduction. However, regarding long-term stability, low and high-temperature NO reduction is still a challenge [81]. The above points clearly indicate that there is an urgent need to develop catalysts for NO reduction under net oxidizing conditions. In this respect, obtaining molecular-level insights into underlying catalysis aspects of NO reduction is a major challenge for current research.

1.6.2. Nitric Oxide (NO) Reduction Reactions on Palladium – Structure of the Thesis:

Pd has not been subjected to intense research and its capability for NO reduction reactions is not fully understood, unlike Rh [66-68,87-90]. However, in the recent past, there are still considerable numbers of reports available on the NO reduction over Pd-based catalysts on different faces of single crystals and a variety of supported systems [91-109]. Despite that, there is a lack of fundamental understanding of NO reduction reactions on Pd surfaces. NO adsorption and dissociation on Pd(111) presented in this thesis (**Chapter 3**) focuses on fundamental kinetic aspects under isothermal conditions in Molecular Beam Instrument (MBI) developed in our laboratory (**Chapter 2**). Details of the fabrication of MBI and the calculation of important parameters like sticking coefficients (s), surface coverages, etc. are described in **Chapter 2**. Our studies on

NO/Pd(111) show that some inherent NO dissociation activity exists on Pd(111) surfaces, and the same can be observed clearly in the transient state.

The kinetics of NO+CO reaction on Pd(111) is presented in. The reactivity of Pd(111) surfaces for NO + CO reactions at different temperatures and beam compositions have been investigated systematically. Both steady state (SS) kinetics as well as transient state kinetics were analyzed. In **Chapter 4**, the results on the reaction kinetics at low and high temperatures and on the competitive adsorption of NO and CO at temperatures between 375 and 475 K were presented.

A revisit on the isothermal kinetics of the CO+O₂ reaction on Pd(111) (**Chapter 5**) explores many details of the reaction which are not addressed in the previous studies. From our present studies of CO+O₂ reaction on Pd(111) surfaces under broad range of conditions, it is clearly demonstrated that direct CO adsorption is feasible with significant s at high temperatures >500 K on oxygen-covered Pd(111) surfaces under SS conditions, and hence no significant oxygen poisoning was observed. However, some time delay in starting the CO₂ production and reaching the SS is observed; the above delay also decreases with increasing oxygen content and instantaneous CO₂ production is observed with O₂-rich beams. Some of the results were possible exclusively due to the employment of MBI techniques, without which we might not have observed the above results.

Our study, presented in **Chapter 6**, explores the influence of oxygen on NO+CO reaction on Pd(111) surfaces. CO₂ production increases with increasing oxygen content in the beam and whereas N₂ production decreases; however, N₂O production remains almost same at temperatures 475 K and 525 K. Beam-switching experiments carried out with oxygen-rich and oxygen-poor beams suggest a fast oscillation between the above two conditions would enable us to better manage the NO reduction. This is mainly due to large NO-dissociation in the transient state on relatively oxygen-free Pd(111) surface, that results from earlier exposure of oxygen-poor (or fuel-rich) beam composition. This dissertation work thus helps in better understanding of the deNO_x processes on Pd(111) surfaces. (Figure 1.5).

Chapter 2

*Fabrication of an Effusive MBI**

“A simple molecular beam instrument (MBI) was fabricated for measuring the fundamental parameters in catalysis such as, sticking coefficients, transient and steady state kinetics and reaction mechanism of gas/vapor phase reactions on metal surfaces. Important aspects of MBI fabrication are given in detail.”

* Thirunavukkarasu, K., Gopinath, C.S., communicated to J. Chem. Sciences, 2006.

Fabrication of Molecular Beam Instrument (MBI) for Kinetic Studies

2.1. Introduction

A simple molecular beam instrument was designed from our laboratory basically to carry out gas/vapor phase heterogeneous catalysis reactions on any metal surfaces. As explained in the previous chapter, one can get lot of kinetic information from molecular beam techniques. Some of the advantages are listed below: the measurement of sticking coefficients (s) of a particular gas species on metal surfaces under variety of conditions including in gas mixtures, competitive adsorption of two species in a mixed molecular beam, transient differential coverages, rate of the reaction in the transient state as well as under steady state conditions, mechanistic aspects of a surface reaction like whether the adsorption is precursor mediated or a simple Langmuir type, a qualitative idea on surface composition, distinguishing between Langmuir-Hinshelwood or Eley-Rideal mechanisms etc. Various important factors involved in the fabrication were taken into consideration during the designing of the UHV chamber and the doser set-up.

2.2. Design Considerations of MBI Chamber

Schematic representation of MBI, CAD diagrams from two different views and a recent photograph of MBI are given in Figures 2.1, 2.2, and 2.3 respectively. A 12 L capacity stainless steel UHV chamber houses all necessary accessories to create molecular beam and evacuated with a 210 L/s turbo-molecular drag pump (Pfeiffer, TMU261) to a base pressure of about 3×10^{-10} Torr. MBI is equipped with a molecular beam doser setup, which is described in the next section and a sputter ion gun (AG5000, VG Scientific) placed exactly opposite to each other at 180° apart (Figures 2.1, 2.2 and 2.3). There are four more cylindrical ports at 45° angle to the central horizontal axis going through Pd(111) sample and turbo pump of MBI; a view-port and an alternate gas leaking source are attached (not seen in Fig. 2.2 and 2.3).

An xyz-manipulator with a rotary platform for mounting the Pd(111) sample on a power-thermocouple feed-through (Caburn, 30 A-DC and 5 KV) is placed perpendicular to the doser and sputter ion set-up so that the sample can be moved in all three direction

and rotated 360°. The above feed-through is connected to liquid nitrogen well. Thus the crystal can be cooled to about 100 K with liquid nitrogen or resistively heated to 1373 K

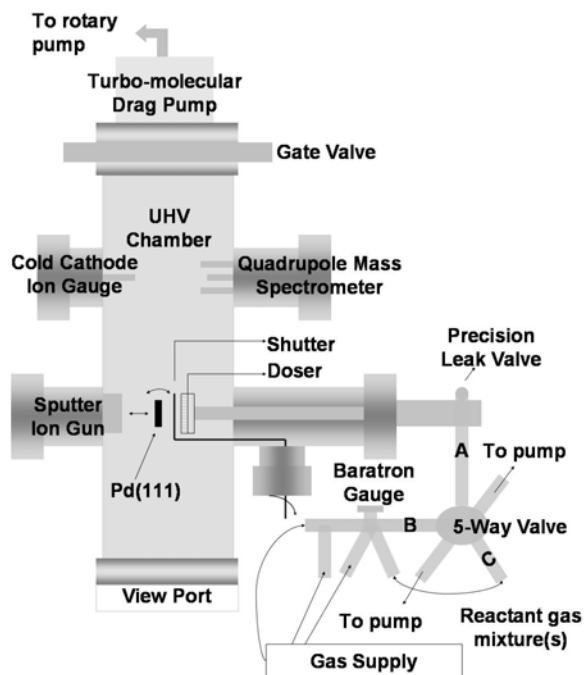


Figure 2.1. Schematic representation of the MBI.

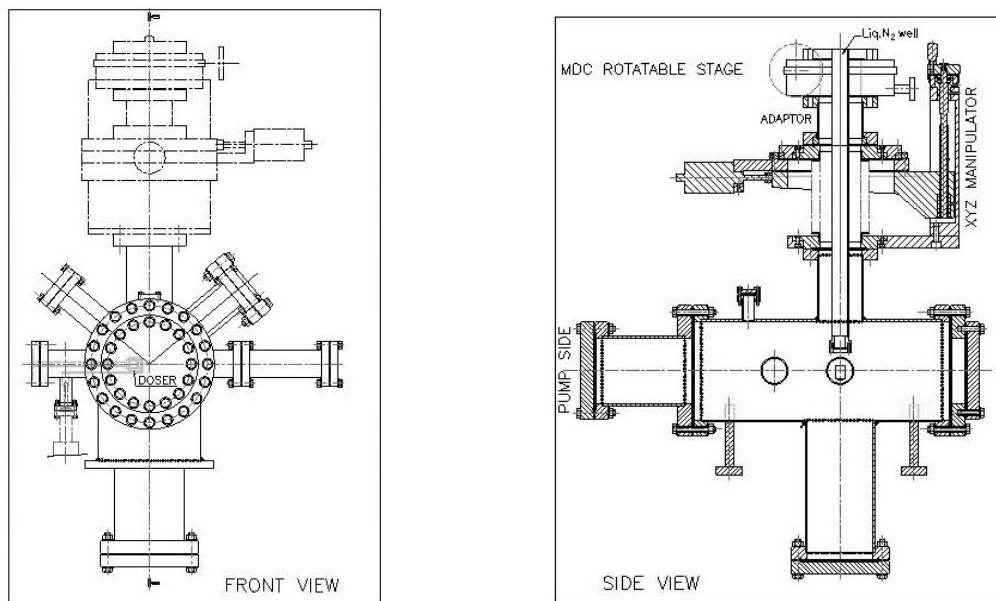


Figure 2.2. AutoCAD diagrams of the basic UHV chamber.



Figure 2.3. A recent photograph of MBI fabricated at National Chemical Laboratory, Pune.

by a temperature controller capable of maintaining any temperature within $\pm 2\text{K}$. A stationary quadrupole mass spectrometer (Pfeiffer, Prisma QMS 200M3), which can detect gas phase species, up to 300 amu and a cold cathode ion gauge (Pfeiffer, IKR270) for measuring the chamber pressure are connected opposite to each other and away from the beam doser. The mass spectrometer is kept out of the line-of-sight of the Pd(111) sample to avoid any angular desorption effects. Thus both the QMS and cold cathode ion gauge were kept at the same distance from turbo pump to minimize the difference between the total pressure readings. The Pd(111) single crystal sample was mounted by spot-welding a 0.5 mm thick tantalum wire on the backside of the crystal and connected to a pair of copper rods, which in turn were connected to the above power-thermocouple feedthrough. A K-type thermocouple was welded on the periphery of the crystal and to the thermocouple leads of the feed-through. The present set-up is based on the extension of the King and Well's method. [53]

2.3. Design Considerations of the Doser Assembly

Clausing's classic work on 1932 [110] introduced the details of molecular flow in a capillary tube. Low energy molecular beams can be created by an array of these microcapillary tubes.[52] Collimated gas beams are the main part of many important experimental techniques in molecular physics, mechanism of chemical reactions, many spectroscopic techniques, surface science and epitaxial growth of crystals.[111] Particularly molecular beams are extensively used in surface science studies.[23-25,37,53,54-57,103-105,112-113]

Molecular beam doser consists of a multichannel array of capillary disk with open segment of disk diameter to the sample (10 mm) is larger than that of the sample (dia = 8 mm). An important concept in describing the quality of a doser, the enhancement factor (E), which is the ratio between the true flux at the sample and the gas flux at pressure P, is calculated by the following expression.[114]

$$E = 1 + \left[\frac{fS}{k_B T (1 - fs) v_c A} \right] \quad (2.1)$$

where, v_c is the velocity of the gas molecules, $v_c = (2\pi mk_B T)^{\frac{1}{2}}$, f is the fraction of beam intercepted by the sample, S is the pumping speed, k_B Boltzmann constant, T is the temperature of the gas molecules, s is the sticking probability of the molecules, A is the surface area of the sample, and m is the mass of the gas molecules. Aspect ratio calculation of microcapillaries, which is capillary length (L) to diameter (a) ratio, decides the beam profiles. For microcapillary beam doser with an aspect ratio >40 , there would be no considerable beam profile changes except a reduction in conductance with increasing ratio. In the present case we have employed an aspect ratio of 100. In fact, Zaera et al [115] showed that the flattening of the beam profile was widely spread for a microcapillary with $a = 10 \mu\text{m}$ than that of a larger diameter ($a=50 \mu\text{m}$) with same lengths of capillary ($L = 2 \text{ mm}$) but a reduction in conductance was observed with $a=10 \mu\text{m}$ capillary array and good in beam quality. Indeed the present design provides uniform flux on the overall surface of the metal substrate of 8mm diameter.

The molecular beam doser, which is connected at present, consists of a 13 mm disk multichannel array made up of microcapillary glass tubes of 1 mm in length and 10

μm in diameter each (Collimated Holes Inc.). The doser is attached through a threaded cap and head with teflon O-rings. It is to be mentioned that the open portion of the above microcapillary is only 10 mm, due to the above design in holding the capillary.

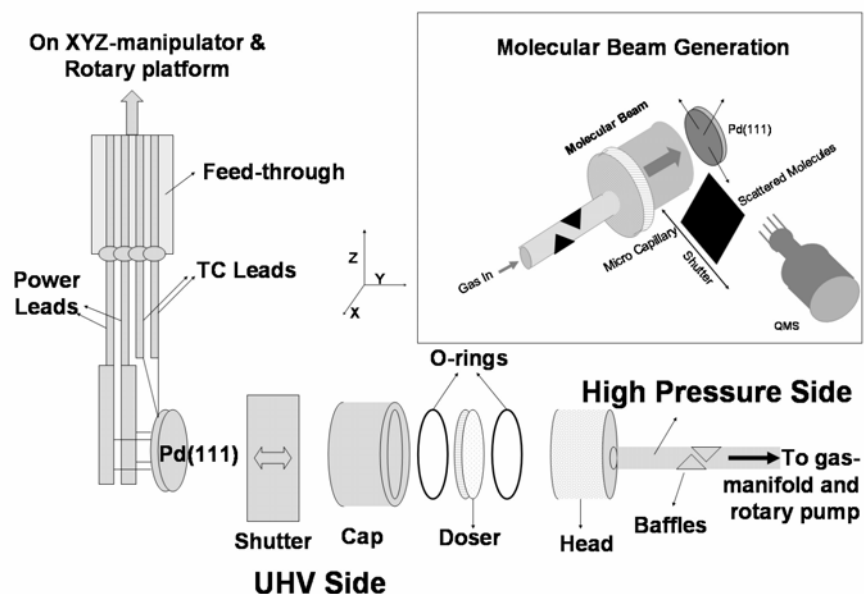


Figure 2.4. Schematics of doser assembly of MBI and the inset show the generation of molecular beam.

A quarter inch tube (OD) of 15 cm in length with baffles (shown in figure 2.4) to avoid the gas acquiring the shape of the tube is attached with the beam-doser head. Thus a minimum dead volume and a minimum gas load can be maintained in the present set-up compared to a recently reported beam doser [116]. A laterally movable stainless steel shutter, which is manually operated, is placed between the microcapillary doser and the Pd(111) crystal in order to interrupt the beam at will (Fig. 2.4 inset). Hence we could maintain a minimum of 5 mm doser to sample distance in our present setup, which gives an enhancement factor (E) of ~ 12 [114] and $\sim 45\%$ fraction of the beam (f) impinges on the surface. Cyclohexane condensation was performed at 125 K (Fig. 2.5) for the calculation of f value in eq. 1.2 and 2.1, the fraction of the beam intercepted by Pd(111), which is also an important factor for calculating the adsorbate coverage at time, t. [64]

$$\theta(t) = \frac{N(t)}{A} = \frac{1}{A} \int_0^t [\alpha \Delta P(\tau) + \beta s(\tau) P(\tau)] dt \quad (2.2)$$

where $N(t)$ is the number of adsorbate molecules, A is the surface atom density of the Pd(111) sample (surface atom density of Pd = $7.8 \times 10^{14} \text{ cm}^{-2}$), α , β are constants and independent of beam flux, sample-to-surface distance and surface temperature.

Calculated values for α and β are 2.99×10^6 molecules/g and 1.76×10^5 molecules/g respectively for our present set-up. The pumping rate is determined by means of the following equation. [117]

$$P = P_o \exp \left[- \left(\frac{\Lambda RT}{V} \right) t \right] \quad (2.3)$$

where P , P_o , Λ and V here represent the pumping rate, pumping coefficient, pumping constant and volume of the chamber, respectively.

The gas-flux in the molecular beam is determined and controlled by the precision leak-valve opening and the backing gas pressure in the gas-manifold. The gas flux is set by setting both the precision leak valve, and the backing gas pressure in volume B (Fig. 2.1), which is measured by a MKS Baratron pressure gauge initially calibrated against the

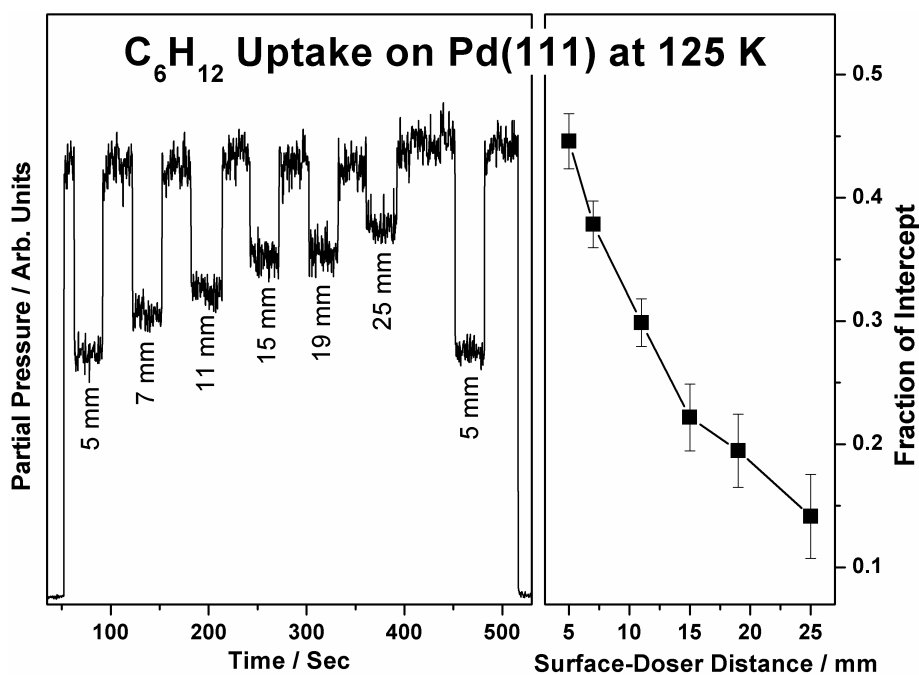


Figure 2.5. Cyclohexane uptake/condensation on Pd(111) surface as a function of distance between the doser assembly and the crystal surface at 125 K.

equilibrium vapor pressure of water at different temperatures. For flux dependent measurements, normally the backing pressure varied and the precision leak valve-opening kept at a predetermined position.

The metal substrate, an 8 mm diameter Pd single crystal cut in the (111) direction was used as supplied (Metal Crystals and Oxides Ltd., Cambridge), was mounted by the method described above. The crystal is cleaned *in-situ* by a combination of argon ion sputter-anneal cycles at 1000 K in oxygen atmosphere and oxygen treatments at 1000 K followed by flashing to 1200 K before each experiment as described by Ramsier et al. [95-96] The cleanliness of the sample was verified by recording standard temperature programmed desorption (TPD) measurements after adsorption of NO or CO and reproducible CO oxidation kinetics. The cleanliness of the Pd(111) surface was further checked by AES and XPS in another UHV chamber. There were no Si, S and P impurities detected on Pd(111).

2.4. Coverage Calculations - CO Adsorption on Pd(111) Surface at 300 K

Typical coverage calculation from the molecular beam data is given below with an example. Indeed, sticking coefficient calculation was already described in sec.1.5.1 and it will not be repeated here. CO adsorption was performed at different temperatures and a typical coverage calculation is shown through the 300 K data (Fig. 2.6a) and to check the validity of the above equations and performance of the MBI fabricated: At time $t = 10$ s, the CO beam was allowed to enter the UHV chamber. With the shutter blocking the crystal, there is, however, no direct exposure to the CO beam. After few seconds, at $t = 15$ s, the shutter was removed to allow the beam to directly impinge on the Pd(111) surface. An instantaneous decrease in the partial pressure of CO can be noticed as a result of CO adsorption from the beam. This adsorption in the transient state continues until the surface is saturated with CO (around $t \sim 33$ s). The geometrical arrangement in our MBI, as described in the earlier sections, is such that about 25% of the beam is intercepted by the crystal. This is mainly to ensure a uniform beam profile over the entire crystal surface. CO adsorption was turned off at $t = 60$ s, and the sticking probabilities (s) and coverages (θ) of CO with respect to time and plotted in Figure 2.6b and c, respectively by following the procedure described below [64]:

The method followed to analyze the experimental data obtained (Figure 2.6a) using the present setup described above will be discussed in this section. Liu et al [64] extended the previous methods, originally developed by Madey [63], in order to include the contribution of adsorption from the background gases to the sticking coefficient measurements. According to Madey's [63] derivation (eq. 1.2), and as shown in Figure 2.6a, $P(t)$ denotes the CO partial pressure measured experimentally, $P_{eq}(t)$ represents the CO partial pressure expected if the direct beam were blocked throughout dosing (CO was dosed without opening the shutter at the same sample temperature, shown as open circles in figure 2.6a), $P_{base}(t)$ is the original base pressure (best linear fit), and f is the fraction of

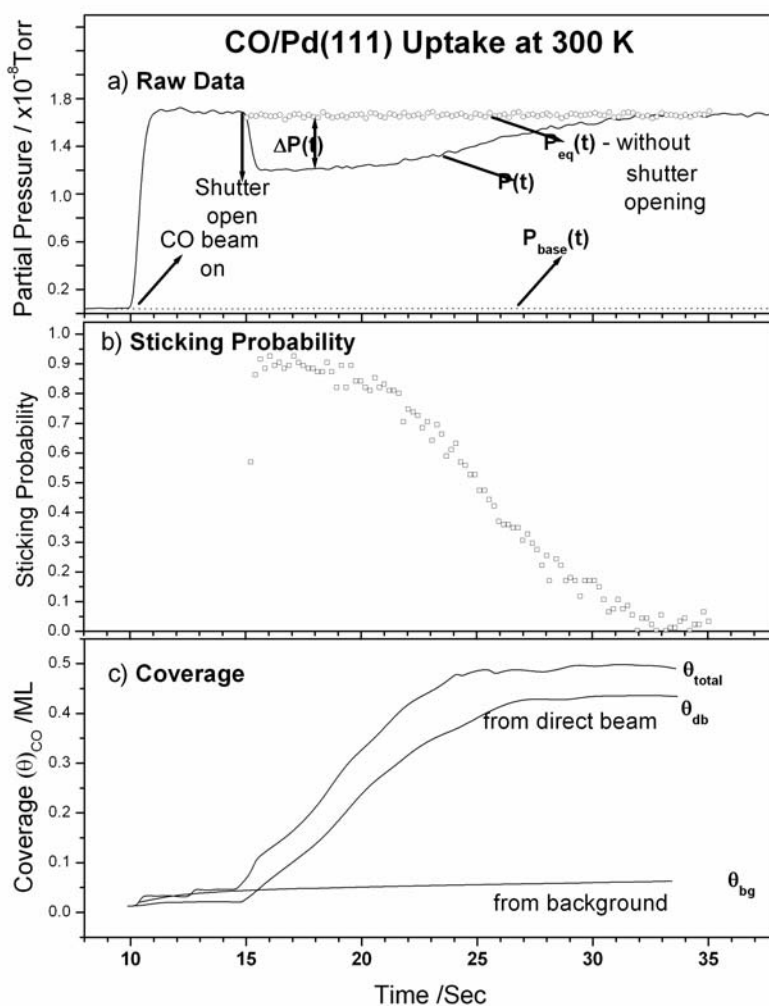


Figure 2.6. (a) Adsorption of CO on Pd(111) surface at 300 K, (b) Sticking probability vs time, calculated from CO adsorption using the formula, eq. 1.2., (c) Total CO surface coverage (θ_{total}) vs time and contributions from direct CO beam (θ_{db}) and the background gases (θ_{bg}) calculated from eq. 2.2.

impinging molecules intercepted by the Pd(111) surface (determined experimentally by cyclohexane adsorption, as given in sec. 2.3). Figure 2.6b shows the time dependence of the sticking probability for CO on Pd(111) at 300 K calculated by applying eq 1.2, to the CO adsorption data in Figure 2.6a.

The temporal evolution of the surface coverage is estimated by integration of the adsorption rates. The rate for direct adsorption from the molecular beam, $dN_{db}(t)/dt$, is given by,

$$\frac{dN_{db}(t)}{dt} = \alpha [P_{eq}(t) - P(t)] = \alpha \Delta P(t) \quad (2.4)$$

The total number of molecules adsorbed on the surface from the direct incident beam, $N_{db}(t)$, is then given by

$$N_{db}(t) = \alpha \int_0^t [P_{eq}(t) - P(t)] dt = \alpha \int_0^t \Delta P(t) dt \quad (2.5)$$

The rate for background adsorption $dN_{bg}(t)/dt$, on the other hand, is proportional to the CO partial pressure in the vacuum chamber, $P(t)$ and to the sticking probability at the corresponding coverage:

$$\frac{dN_{bg}(t)}{dt} = \beta s(t)P(t) \quad (2.6)$$

As described earlier, α , β are constants and independent of beam flux, sample-to-surface distance and surface temperature. The number of molecules adsorbed on the surface from the background gases, $N_{bg}(t)$, is given by,

$$N_{bg}(t) = \beta \left[\int_0^{t_i} s(t)P(t) dt \right] \quad (2.7)$$

$$N_{bg}(t) \approx \beta \left[\int_0^{t_i} s_0 P(t) dt + \int_{t_i}^t s(t)P(t) dt \right]$$

The initial sticking probability s_0 was used in this expression for times before $t = t_i$, the shutter removal time, because $s(t)$ can only be evaluated after time t_i . The total adsorption before shutter removal amounts to less than 10% of saturation in all cases and hence the approximation in eq 2.7 is justified.

The time dependence of the total CO adsorbed on the surface, $N(t)$, is then,

$$N(t) = N_{db}(t) + N_{bg}(t) \quad (2.8)$$

and the absolute adsorbate coverage at time t , $\theta(t)$, is given by, eq. 2.2. The values of α and β were obtained from the cyclohexane uptake calibration experiments and applied. The time dependence of the direct, background, and total CO coverages for the data given in Figure 2.6a, is calculated by using eqs. 2.2, 2.5, and 2.7. Coverages in figure 2.6 are reported in monolayers, ML, defined as the number of adsorbed molecules per platinum surface atom. A saturation coverage of 0.5 ML was reported for CO adsorption on Pd(111) surface at 300 K [118]. Initial sticking probability of ~ 0.96 was observed for this case, which is in good agreement with ref [118].

2.5. Summary

A simple molecular beam instrument (MBI) was fabricated successfully at National Chemical Laboratory, Pune, as the first phase of the dissertation work presented. The performance of MBI was verified with CO adsorption at 300 K and cyclohexane adsorption at 125 K. A good agreement with the standard value of initial sticking coefficient of CO (s_{CO}) available in the literature confirms the good performance of MBI.

Chapter 3

*NO Adsorption and Decomposition on Pd(111) Surfaces**

“The kinetics of NO adsorption and dissociation on Pd(111) surface and the NO sticking coefficient (s_{NO}) were probed by isothermal kinetic measurements between 300 and 525 K. NO dissociation and N_2 productions were observed in the transient state from 425 K and above on Pd(111) surfaces with selective nitrogen production. Maximum nitrogen production was observed between 475 and 500 K. It was found that, at low temperatures, between 300 and 350 K, molecular adsorption occurs with a constant initial s_{NO} of 0.5 until the Pd(111) surface is covered to about 70-80% by NO. Then s_{NO} rapidly decreases with further increasing NO coverage, indicating typical precursor kinetics. The dynamic adsorption-desorption equilibrium on Pd(111) was probed in modulated beam experiments below 500 K. CO titration experiments after NO dosing indicate the diffusion of oxygen into the subsurface regions and beginning surface oxidation at ≥ 475 K. Finally, the results with respect to the rate-limiting character of the different elementary steps of the reaction system were discussed.”

* Thirunavukkarasu, K., Thirumorthy, K., Libuda, J., Gopinath, C.S., *J. Phys. Chem. B.*, **2005**, 109, 13283, and Thirunavukkarasu, K., Nagarajan, S., Gopinath, C.S., S.D. Prasad, *in preparation*.

NO Adsorption and Decomposition on Pd(111) Surfaces

3.1. Introduction

In the last two decades increasing governmental regulations all over the world have stimulated tremendous growth in the research on environmental catalysis and green chemistry. Especially the automotive catalyst technology has improved, assisted by better petrochemical refining to yield cleaner fuels. Improvements in internal combustion engines and the above developments have led to fuel-efficient vehicles. The present technology of three way catalytic converters meets the requirements of oxidation of CO. Although Rh is very active for NO reduction under fuel-rich conditions, this is not the case under net oxidizing conditions, since the excess oxygen inhibits the NO reduction activity of Rh by oxidizing it. Pd is also added to the catalytic converters as one of the active metal for NO reduction for the last few years; however the mechanistic details of deNO_x reactions on Pd are not fully understood yet. Unlike Rh, [66-68,87-90] Pd has not been subjected to intense research with respect to its capability for NO reduction. However, there are considerable amount of reports available on the NO reduction over Pd-based catalysts on different faces of single crystals and a variety of supported systems [91-109] in the recent past. Despite that, there is a lack of fundamental understanding of NO reduction on the Pd surfaces. This chapter on NO adsorption and dissociation on Pd(111) focuses on fundamental kinetic aspects under isothermal conditions in the MBI. [64,119-122]

It was suggested that NO dissociates only at defect sites on Pd(111) without significant inherent activity on Pd(111); [92-98] nonetheless, there are reports [69,100-106,108-109] on the steady-state NO dissociation to N₂ and N₂O on Pd(111) as well as on supported Pd particles with reductants, like CO and H₂, indicating inherent catalytic activity toward NO dissociation. Our present studies show that an inherent NO dissociation activity exists on Pd(111) surfaces, and the same can be observed clearly in the transient state.

3.2. Experimental Procedure

The NO gas-flux in the molecular beam (F_{NO}) is determined and controlled by the precision leak-valve opening and the backing gas pressure in the gas-manifold. A laterally movable stainless steel shutter was placed between the microcapillary doser and the Pd(111) crystal in order to interrupt the beam when desired (refer Figure 2.3 inset). The Pd(111) crystal surface was cleaned as described by Ramsier et al.[95-96] The procedure involves Ar^+ sputtering at 1000 K in a partial pressure of oxygen (4×10^{-8} Torr) for 60 min, followed by annealing for 30 min at 1000 K in 2×10^{-7} Torr of oxygen, and, finally, flashing to 1200 K in a vacuum. This cycle was repeated several times, testing the cleanliness of the surface by monitoring CO and CO_2 during high-temperature flashing after oxygen adsorption at room temperature. Room temperature NO adsorption and subsequent TPD experiments were also carried out, and the results are in good agreement with results reported earlier, [92-96] ensuring surface cleanliness of Pd(111). However with subsequent NO dosing experiments, especially at high temperatures (above 500K), small amounts of N_2 and CO were observed during high temperature flashing, possibly indicating the subsurface diffusion of N and O atoms at high temperatures. Hence, after each set of high-temperature experiments the surface was cleaned by above Ar^+ sputtering procedure. For the present chapter, NO/Pd(111) studies between 300 and 525 K are reported. ^{15}NO (Air gas, 99% isotopically pure), ^{14}NO , CO (99.9%), and ^{13}CO (Isotec) were used without any further purification. It is to be noted that the ^{15}NO contains about 1% of unlabeled ^{14}NO . The purpose of using ^{13}CO and ^{15}NO is two-fold: First it allows a clear identification of the possible products such as $^{13}\text{CO}_2$ (amu 45) and $^{15}\text{N}_2\text{O}$ (amu 46). In addition, these species can be distinguished from common background signals like $^{12}\text{CO}_2$ (amu 44). The second factor is related to the ^{13}CO employed to minimize the interference between background ^{12}CO and the main product of N_2 in the NO dissociation reaction. However, ^{14}NO (amu 30) present in the ^{15}NO interferes with the identification of $^{15}\text{N}_2$ (amu 30), and most of the experiments reported here are carried out with ^{14}NO . However, cross-reference experiments were carried out with ^{15}NO too. Small amounts of ^{13}CO were present in the MBI chamber, adsorbing especially below 400 K. However, the adsorbed ^{13}CO does not interfere our experiments since CO is displaced by NO in the transient state of the subsequent experiments and can

be detected easily. [69] Several test experiments have been carried out initially to probe all possible products of NO decomposition, including N₂O and NO₂ under a variety of experimental conditions. Apart from nitrogen and nitrous oxide, no other nitrogen containing products were produced under any conditions. The mass spectrometer intensity was calibrated for NO by measuring the uptake on clean Pd(111) at 300 K, assuming a saturation coverage of 0.33 monolayers (ML) following Bertolo et al. [93-94] Different parameters (s_{NO} , θ_{NO}) were calculated by following the procedures given in Chapter 2.

3.3. Results and Discussion

3.3.1. General Considerations:

The experimental procedure followed in a typical molecular beam dosing experiment for the present chapter is explained in Figure 3.1. For all experiments, the clean Pd(111) metal surface was kept at constant temperature and exposed to an effusive ¹⁴N¹⁵O molecular beam. All relevant gas-phase species formed are detected by QMS as a function of time. Figure 3.1 shows a typical set of kinetic data recorded during ¹⁴N¹⁵O exposure of Pd(111) at 465 K: At time $t = 5$ s, the NO beam was allowed to enter the UHV chamber (Figure 2.3, inset). With the shutter blocking the crystal, there is, however, no direct exposure to the ¹⁴N¹⁵O beam. Nonetheless, a small amount of ¹⁴N¹⁵O adsorption from the background cannot be prevented. After few seconds, at $t = 10$ s, the shutter was removed to allow the beam to directly impinge on the Pd(111) surface. An instantaneous decrease in the partial pressure of ¹⁴N¹⁵O for few seconds can be noticed as a result of ¹⁴N¹⁵O adsorption from the beam. This adsorption in the transient state continues until the surface is saturated with ¹⁴N¹⁵O. The geometrical arrangements in our MBI [70] is such that about 25% of the beam is intercepted by the crystal and, hence, the drop in NO pressure upon shutter removal is relatively shallow; this is mainly to ensure an uniform beam profile over the entire crystal surface. A clear N₂ and N₂O production in the transient state begins around $t = 15$ s can be seen, indicating the dissociation of ¹⁴N¹⁵O on the Pd(111) surface. Nitrogen desorption is evident at other temperatures also (Figure 3.3). However, the amount of ¹⁴N₂O desorption is comparatively much lower than that of

N_2 . Amu 12 was also followed in all the experiments to ensure that there is no contribution from CO and CO_2 .

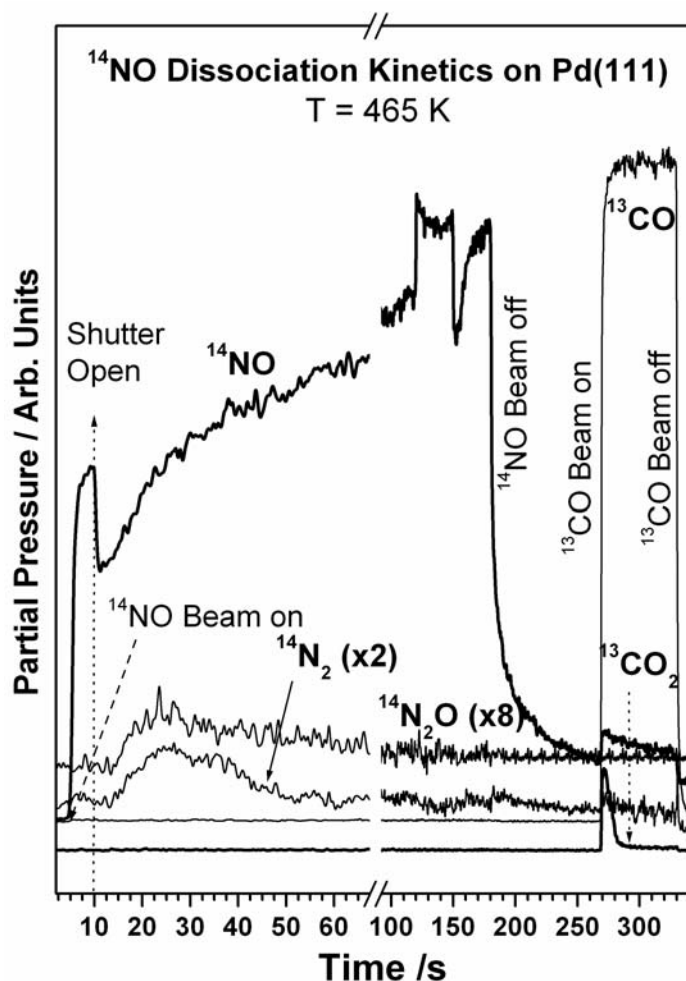


Figure 3.1. Experimental data from a typical isothermal kinetic test described in the section 3.3.1 carried out with ^{14}NO at 465 K. Subsequently the surface oxygen, due to the dissociation of ^{14}NO , was titrated with ^{13}CO beam at the same temperature.

The partial pressure of the ^{14}NO increases up to a new steady-state value, due to adsorption on UHV chamber walls; [66-67] however, it does not represent any change in the molecular beam characteristics. ^{14}NO adsorption was continued for at least 60 s before any steady-state measurements were made. Upon reaching the steady-state, the beam was blocked for about 30 s. During the beam blocking period in the steady state, an increase in the partial pressure of ^{14}NO (Figure 3.1) was observed clearly. Moreover, the sudden increase in the ^{14}NO partial pressure in the steady state upon closing the shutter can be attributed to the immediate desorption of ^{14}NO , since the substrate temperature is

close to the NO desorption maximum of 500 K. [92-96] This result shows that there is a substantial ^{14}NO steady-state coverage established throughout the reaction period. N_2 and N_2O desorption stops completely within a minute of starting of NO dosing and there is no change in the partial pressure of N_2 and N_2O in the steady-state indicating that the NO dissociation activity does not sustain on its own. This is attributed to poisoning by dissociated atomic species, mainly oxygen atoms. It is also to be noted that the NO uptake after shutter removal in the steady state is nearly the same as that of NO uptake on clean Pd(111) in the transient state. This indicates that almost all nitrogen and NO desorb during the beam blocking period and the NO and nitrogen coverages are low.

A subsequent TPD shows no NO and a small nitrogen coverage. This is further supported by TPD results (in Figures 3.5). After turning off the NO beam, the ^{13}CO beam was switched on at $t = 270$ s. and constant temperature in order to titrate the surface oxygen species produced by NO dissociation. A clear production of $^{13}\text{CO}_2$ indicates the NO dissociation on Pd(111). The above CO dosing was carried out also to minimize the diffusion of oxygen into the subsurface and the bulk region. Finally, the ^{13}CO beam was shut off, and the chamber background pressure was allowed to return to normal before TPD experiments were performed at a heating rate of 5 K/s. The TPD results indicate a strongly temperature-dependent coverage of NO and small amount of nitrogen (Figure 3.5). As there is no desorption of nitrogen-related products above 550 K, the TPD experiments were stopped at 650 K. Subsequently, the Pd(111) crystal was flashed to 1000 K before the next dosing experiment.

3.3.2. Temperature-Dependent NO Adsorption and Dissociation on Pd(111):

Figure 3.2 shows the temperature dependence of ^{14}NO adsorption on Pd(111) between 300 and 525 K at a constant $F_{\text{NO}} = 0.05$ ML/s. NO beam was turned on at $t = 7$ s followed by the shutter opening at $t = 10$ s; there is a clear decrease in the ^{14}NO partial pressure due to ^{14}NO adsorption on the Pd(111) surface at the shutter removal point. A number of reference experiments were made, in which the shutter was not at all opened and the data were used as background for those experiments reported in the manuscript for all the calculation purposes. One such reference experiment is shown in Figure 3.2 at 300 K.

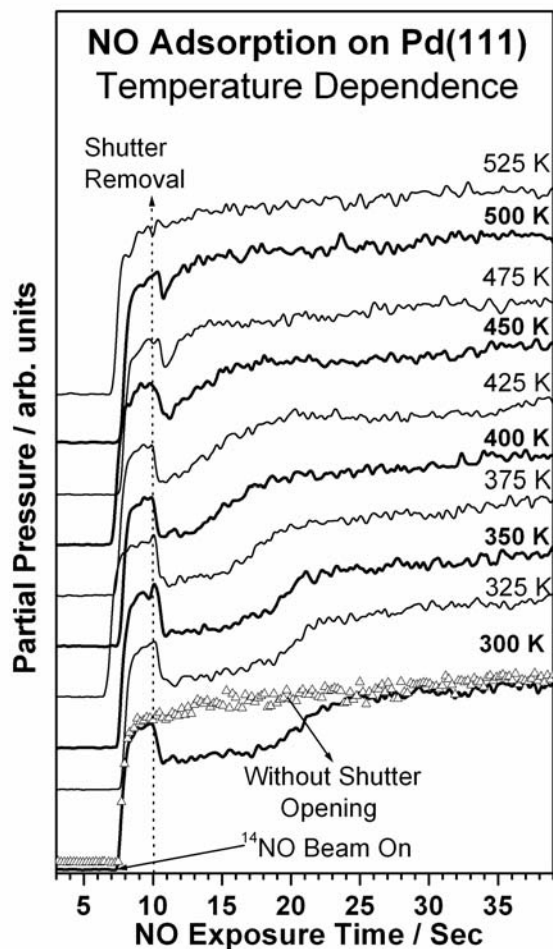


Figure 3.2. Temperature dependence of ^{14}NO adsorption on Pd(111) in the transient state on clean metal surface. Scattered data points (open triangles) shown for 300 K are from the experiment carried out without opening the shutter to use as standard for background subtraction. Reference data has been shifted vertically for clarity.

It is to be noted here that the above procedure is reliable than fitting with an exponential or quadratic equations. However, some background adsorption (about 5%) cannot be avoided, [64,70] and to reduce that contribution, a minimum time gap (2-3 s) was kept between the beam on and the shutter removal time. Further, the uniform beam profile over the crystal surface also ensures the pressure on the crystal surface is much higher than the background.

At temperatures below 400 K, ^{14}NO was continuously adsorbed at the same rate for a few seconds, before a gradual decrease occurs due to the surface reaching the saturation NO coverage (θ_{NO}) around $t = 20$ s. At and above 400 K, there is a gradually

decreasing total NO adsorption capacity compared to the experiments between 300 and 350 K. The decreasing saturation coverage with increasing temperature is due to a reduction of the number of vacant sites, as a result of NO dissociation to N and O atomic species. It should also be noted that the initial NO adsorption probability remains constant immediately after the shutter removal at reaction temperatures between 300 and 425 K. The corresponding changes in the amu 28 and 44 traces (due to $^{14}\text{N}_2$ and $^{14}\text{N}_2\text{O}$) (Figure 3.3) provide a hint that, at least in part, the reduction in θ_{NO} above 400 K is due to NO dissociation. There is a decrease in the initial and overall ^{14}NO adsorption capacity above 450 K and no ^{14}NO adsorption could be directly detected through pressure change at 525 K.

As far as product desorption is concerned, two temperature regimes can be observed in Figure 3.3: (i) NO adsorption without formation of any nitrogen containing products below 400 K and (ii) simultaneous N_2 and N_2O production at ≥ 425 K. Above 400 K, the formation of N_2 and N_2O production becomes evident from the results shown in Figure 3.3. The reference experiments mentioned above, without removing the shutter, showed no considerable products formation is attributed to the low NO coverage under these conditions.

It is interesting to compare the different kinetics of N_2 desorption and NO uptake. Indeed, a remarkable feature is the temporal behavior of the N_2 and N_2O production between 425 and 500 K with a time delay observed for the onset of N_2 and N_2O production, although NO uptake is observed at $t = 10$ s. This delay indicates the buildup of some nitrogen coverage. A finite time delay of about 6-7 s before the onset of N_2 and N_2O production at 425 K decreases with increasing temperature (solid arrows in Figure 3.3). At 525 K, N_2 formation appears almost simultaneously with NO uptake upon shutter removal. Moreover, there is hardly any N_2O formation. These observations can be interpreted in terms of an increasing NO dissociation probability, leading to a decreasing time gap between shutter removal and the onset of N_2 and N_2O desorption at high temperatures. The above observations point toward the fact that N_2 and N_2O desorption could be diffusion-controlled. In this case, the NO adsorption and dissociation steps could be faster than the production of N_2 and N_2O , under the above experimental conditions.

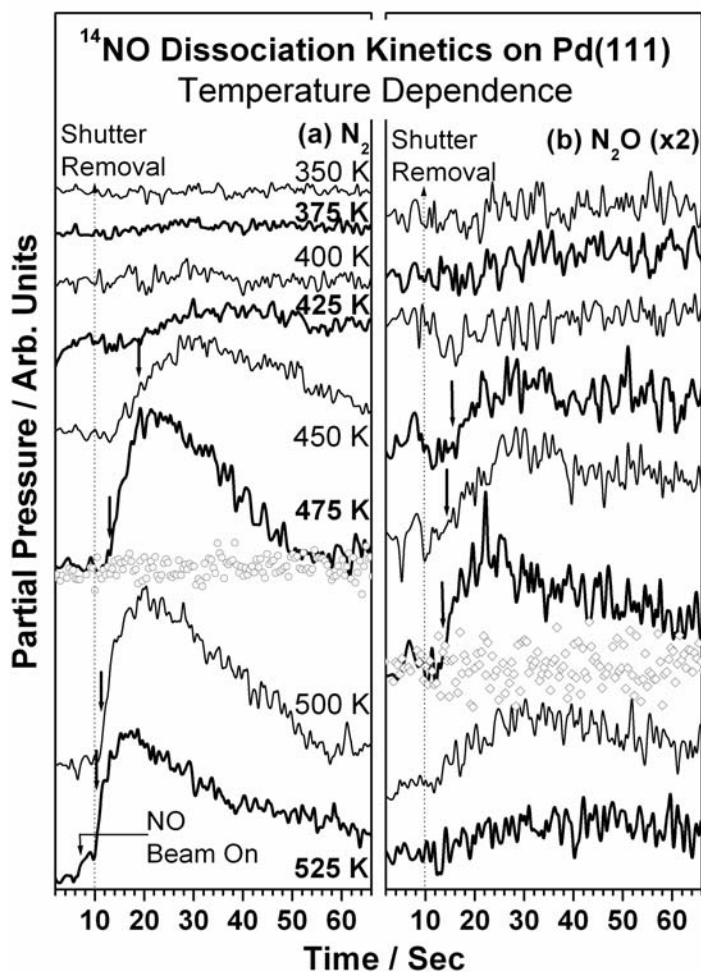


Figure 3.3. (a) N_2 and (b) N_2O production from Pd(111) surface due to NO dosing at different temperatures. Note the maximum N_2O production at 475 K and N_2 between 475 and 500 K. Solid arrows indicate the on-set of products desorption. Scattered data points shown for 475 K are from the experiment carried out without opening the shutter.

Between 475 and 500 K, maximum nitrogen production can be clearly seen after shutter removal, indicating the fast dissociation of ^{14}NO to a comparatively large extent. The total nitrogen formation rate goes through a maximum between 475 and 500 K, and at >500 K, a reduction in the reaction rate is observed. At 525 K, the nitrogen desorption continues for little longer than a minute. However a small amount of CO production is also inferred (through amu 12), possibly due to the interaction between mobile oxygen in the bulk/subsurface and carbon in bulk, along with N_2 . At temperatures higher than 525 K, the CO production increases significantly and, hence, reliable NO dissociation experiments could not be performed. It is to be noted here that the oxygen migration and

hence considerable concentration of oxygen in the subsurface reported recently by Leisenberger et al. [123] is in line with our observation.

A careful analysis of the products desorption traces in Figure 3.3 leads to the following four points: (a) There is a sudden rise in the N_2 and N_2O production rate between 425 and 500 K, but after a time delay; the decreasing time delay with increasing temperature indicates a decrease in initial nitrogen buildup. (b) The slope of the leading edge of the N_2 (and N_2O) traces increases steeply with increasing temperature from 425 to 525 K. Also, a partial N_2 production through an N_2O intermediate cannot be excluded on the basis of the experiments. (c) A clear decrease in N_2O production at >475 K with no N_2O at 525 K indicates, again a change in overall kinetics and mechanism. (d) The selectivity for N_2 production is 5-10 times higher than for N_2O , depending on the temperature. In this respect, the presence of coadsorbed oxygen due to NO dissociation can be expected to be an important factor. However, it is difficult to quantify this effect, especially due to the onset of subsurface diffusion and possible surface oxidation around 475 K (see next section). Also on rhodium surfaces, it has been confirmed that coadsorption of oxygen and nitrogen leads to N_2 desorption at lower temperatures as compared to N_2 desorption from the N-only containing Rh surfaces. [66-67,124-126] The effect was attributed to repulsive interactions between N and O atoms on the surface. Indeed, oxygen pre-dosage was shown to completely inhibit NO dissociation, [91] indicating that similar effect may be operative on Pd(111). Another interesting aspect is the dynamic NO adsorption-desorption behavior observed on the Pd(111) surface in the steady-state. Although N_2 and N_2O desorption stops in the transient state, NO adsorption-desorption continues, as long as the NO beam is maintained for the reaction temperatures below 500 K. Remarkably, the extent of NO adsorption in the steady-state after shutter removal at $t = 150$ s is similar to that of the NO uptake on clean Pd(111) surface at the beginning (see Figure 3.1). Similar observations were made down to 350 K (data not shown). This directly suggests that the oxygen and nitrogen coverage due to NO dissociation does not affect the NO adsorption in a significant manner, and hence, it might not play any important role in the overall kinetics of NO dissociation, at least below 500 K. This is in sharp contrast to the NO dissociation behavior on supported Pd particles studied recently. [108,109] The complete loss of the NO adsorption capacity in

the latter case at temperatures above 375 K supports the hypothesis that NO dissociation on the particles is strongly dominated by defect sites. At $T = 500$ K on Pd(111), the steady-state NO coverage in the dynamic adsorption-desorption equilibrium decreases drastically, indicating fast desorption. Furthermore, it is likely that the substantial drop in N_2O production above 500 K is related to the rapidly decreasing NO coverage in this temperature region (see section 3.6).

3.3.3. Surface Oxygen Coverage and Oxygen Diffusion into Subsurface/Bulk:

Figure 3.4 shows the results on the surface oxygen titration with ^{13}CO beam after the NO adsorption experiments, as explained in Figure 3.1. CO dosing was carried out at the same reaction temperature as that of NO adsorption. $^{13}CO_2$ production was observed at temperatures between 400 and 475 K. However, CO_2 desorption decreases sharply at 500 K and no CO_2 was observed at 525 K, despite nitrogen desorption observed in the transient state, shown in Figure 3.3. This is attributed mainly to subsurface diffusion of oxygen and surface oxidation of Pd(111). As noted earlier, there is a small amount of ^{12}CO production along with N_2 at 525 K in the NO adsorption experiments. Further, there is some carbon dioxide formation while flashing to 1000 K, after reaction. Above observations supports the hypothesis of oxygen diffusion into the subsurface. Desorption of no or very small amount of molecular oxygen above 700 K in TPD [98,99] due to NO dissociation on a variety of Pd surfaces, including Pd(311) where NO dissociation is largest, unambiguously hints the disappearance of oxygen from the surface and it has been attributed to oxygen diffusion and supports our above conclusion. Leisenberger et al. [123] observed oxygen diffusion into the near surface region at 523 K and in good agreement with our results.

Recently, surface oxide formation on Pd(111) has been investigated experimentally in great detail. [127-134] Also, the oxidation of Pd surfaces has been investigated theoretically [131] and shows that subsurface oxygen is just a precursor to surface oxidation. Decreasing the CO_2 signal at 500 K in our results may also be due to a reduced reaction probability of CO and the inability to strongly adsorb CO due to the oxidized palladium surface. It is to be noted that the more oxidized Pd surface and PdO are unreactive toward CO, as found by Zhang and Altmann.[128-130] Indeed the amount of CO_2 desorption at 475 K is somewhat lower than that at 450 K, indicating that surface

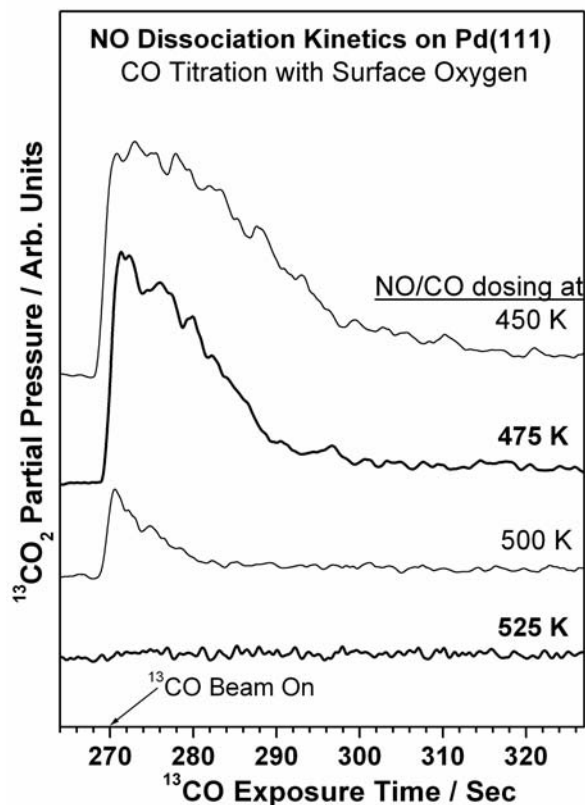


Figure 3.4. Surface oxygen due to NO dissociation on Pd(111) is titrated with ^{13}CO beam at the same NO adsorption temperatures. Note the decrease in oxygen coverage ≥ 500 K is attributed to diffusion of oxygen into subsurface.

oxidation may begin around 475 K, in accordance with adsorption studies on Pd(111) at elevated temperatures. [127-130] The complex interaction of the Pd surfaces with oxygen significantly complicates the kinetic analysis, especially at temperatures above 475 K. However, sustainable CO_2 production in NO + CO reactions on Pd(111) up to 625 K [69,101] suggests that surface oxide formation and subsurface diffusion may be strongly suppressed in the presence of CO as a reducing agent.

3.3.4. Temperature-Programmed Desorption Studies of NO/Pd(111):

Figure 3.5 shows the TPD of NO and N_2 species recorded after the above dosing experiments. No significant N_2O was observed. NO desorbs between 450 and 550 K, in good agreement with the earlier TPD results.[91-97] Gradual decrease in the quantity of NO desorbed is observed in the TPD from the NO dosing experiments conducted above 300 K (not shown). Between 300 and 325 K, no change in NO coverage was observed in

TPD (as well as NO uptake in dosing) experiments, suggesting that the γ -saturation coverage [91-97] is retained. However, the NO yield in TPD decreases linearly from 0.33

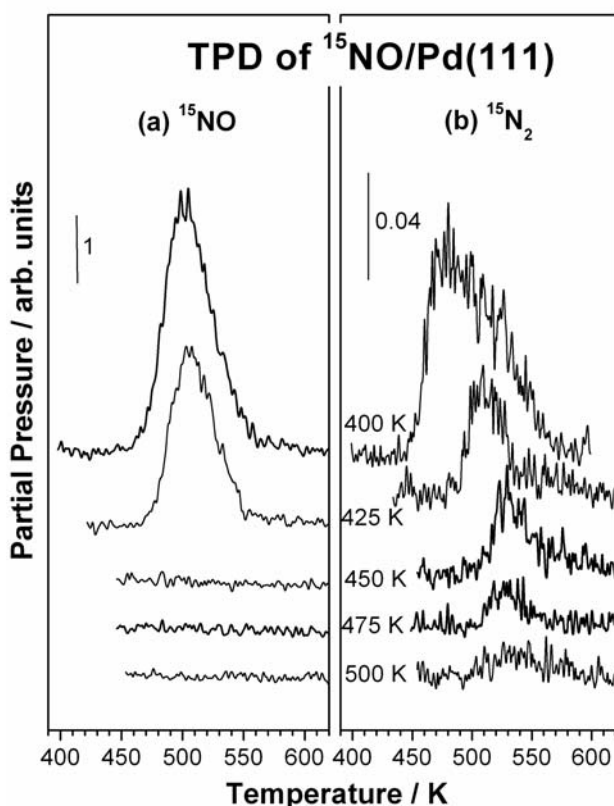


Figure 3.5. Representative results from the temperature-programmed desorption (TPD) at a heating rate of 5 K/s carried out after the experiments described in Figures 3.2 and 3.3. NO dosing temperatures are given.

to 0 ML between 300 and 325 and 450 K dosing temperatures, respectively. Nonetheless, the temperature-dependent NO dosing experiments indicate NO uptake on the surface at adsorption temperature <500 K. It may be recalled here that the NO uptake on clean Pd(111) at the beginning of the experiment as well as in the steady-state after temporary blocking is almost the same (Figure 3.1 - note the change in x -axis scale after the break). This shows that there is complete desorption of NO with no beam at temperatures >425 K on the time scale of the experiment.

TPD results display a decrease in nitrogen desorption, suggesting that the atomic nitrogen coverage decreases with increasing temperature. However, the nitrogen coverage seen on Pd(111) in the TPD is ≈ 0.06 ML and comparable to that of nitrogen coverage observed after NO + CO reaction on Pd(111). [69] Nonetheless, the nitrogen

coverage is much lower than that observed on Rh(111) [66,125] after NO and/or NO + CO reactions.

3.3.5. Sticking Coefficient of NO on Pd(111):

Figure 3.6 shows the temperature and θ_{NO} dependence of s_{NO} on Pd(111), by adopting the method employed in refs 63-64, 114 and 135. Briefly, s_{NO} is directly proportional to the change in pressure due to NO uptake on Pd(111) after shutter removal with respect to the total pressure if there was no adsorption. Furthermore, $s_{\text{NO}}(0.5)$ is

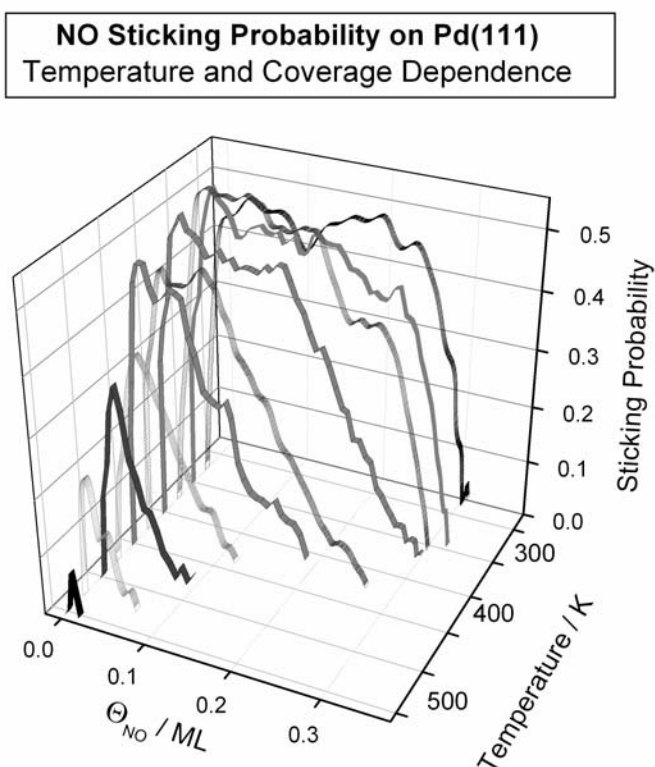


Figure 3.6. Temperature dependence of θ_{NO} coverage and sticking coefficient calculated from the NO uptake data in Figure 3.2. Note the same initial sticking coefficient is maintained between 300 and 425 K up to about 80% of saturation coverage for adsorption temperatures at 300 and 325 K.

inversely proportional to the fraction of the beam intercepted, which is 0.25 in the present case. Estimated error margin of s_{NO} values from the uptake measurements is up to 5% and should be considered for any purpose. A time evolution of s_{NO} was calculated first from the experimental data, given in Figure 3.2, and converted in terms of increasing θ_{NO} . The initial s_{NO} is constant between 300 and 425 K and decreases at temperatures higher

than 425 K. A maximum of $s_{\text{NO}} = 0.5$ was observed at low temperatures between 300 and 350 K on clean Pd(111) up to 70-80% of the saturation coverage. This behavior is typical of precursor-mediated adsorption. At high temperature, the plateau becomes smaller due to faster desorption and phenomenologically a description of s_{NO} on the basis of a Langmuir model becomes more appropriate. Very similar trend in s_{NO} on Pd(110) surface was reported by Sharpe and Bowker [99] and indicates the lifetime of chemisorbed NO species decreases linearly with increasing temperature on Pd(111) and Pd(110).

3.3.6. Reaction Mechanism:

The isothermal experimental results in MBI provide some new insights into the mechanism for the thermal dissociation of NO on Pd(111) surfaces. Earlier reports [18,25] suggested the main elementary steps of the reaction in this system are:



Although the above mechanism may appear simple, there are few complications that have not been resolved until now. In particular, TPD experiments show weakly and strongly adsorbed nitrogen peaks at 450 K and between 545 and 595 K, respectively, by Goodman et al.; [101,102] however only a minor N_2 peak at 500 K were observed by several other groups. [91,95-96,100] TPD results of Nakamura et al. [98] and Wickham et al. [136] show no evidence of NO dissociation on Pd(111). In contrast, pronounced N_2 desorption was observed at 670 K by Conrad et al. [92] Sugai et al. [97] also shows through Auger electron spectroscopy that surface-bound N remains on the surface as high as 700 K. Although present isothermal experiments may not be compared directly to the earlier TPD results due to the different reaction conditions in a molecular beam setup, certain valid conclusions may be derived as discussed in the following.

Our present results shows that, indeed, there is NO dissociation activity on Pd(111), which leads to dominant production of N_2 and minor N_2O production between 400 and 500 K and exclusive N_2 production above 500 K. Nevertheless, some NO

dissociation activity is possible from the defect sites (step sites) and cannot be ruled out. A substantial NO coverage on Pd(111) is observed between 400 and 500 K in the dynamic adsorption-desorption equilibrium and it is not strongly affected by the presence of N and O atomic species. This result is in general agreement with the observation of comparable coverages of NO coverage via high-resolution electron energy loss spectroscopy measurements by Ramsier et al. [95-96] This suggest that the NO adsorption [eq 1] cannot be the rate-determining step (RDS), at least below 500 K. Post-adsorption TPD experiments shows that there is only one N₂ desorption peak with a peak maximum around 500-530 K and in good agreement with majority of earlier reports.[91,95-96,100] New observation of nitrogen desorption show some delay with respect to NO uptake, indicating that atomic nitrogen recombination to gaseous N₂ could have large degree of rate control. The delay in the nitrogen desorption below 500 K may also be explained in terms of the necessity of a critical surface N concentration before their average inter-atomic distances are short enough, so that they can interact to form N₂ molecule. Nonetheless, repulsions among the dissociated atomic species lowers desorption barrier as well as the strength of adsorption and hence it should also be taken into account. However, as the temperature increases the diffusion rate of atomic nitrogen also increases and hence a decrease in the initial delay as well as N-buildup and instant N₂ production can be observed at 500-525 K. In fact, the common leading edge of the isothermal kinetic runs, below 525 K, is expected for a two-dimensional diffusion-limited reaction. [137] Similar results of a time gap between NO uptake and nitrogen formation and the repulsive interactions between the atomic species has been observed and reported on Pd(110), [99] Rh(110), [39] and Rh(111) [66-67,125] surfaces. Furthermore, on the basis of the observation of a significant NO coverage and nitrogen buildup it can also not be excluded that the N₂ formation, at least in part, might be through an N₂O intermediate also. Indeed, a similar slope in the leading edges of N₂ and N₂O desorption kinetics supports this view; nonetheless, further support is necessary. The small nitrogen coverage observed in the TPD after reactions above 425 K indicates that the oxygen could exert repulsive interactions with nitrogen, providing an additional driving force for N₂ desorption. Nevertheless, the high rate of subsurface diffusion of oxygen and surface oxide formation around 525 K may change the nature of the surface and affect the overall

kinetics. As the nitrogen coverage decreases drastically $>500\text{K}$ along with an increase in NO desorption rate, both nitrogen recombination and adsorption are not expected to contribute substantially to the rate control. However, NO dissociation might play a significant role toward the overall kinetics at temperatures higher than 525 K.

Indeed, fast CO_2 production below 525 K in NO + CO reactions on Pd(111) supports the relatively fast NO dissociation. [68] The complete stopping of NO dissociation in the steady-state is attributed to the sizable oxygen coverage observed through CO titration and it is in correspondence with the observation of Schmick et al. [91] and Henry et al. [103-105] that coadsorbed oxygen inhibits NO dissociation. Also on supported Pd particles, we have recently observed large oxygen coverages after NO dissociation, together with small amounts of N adsorbed at specific sites on the particles. [108,109]

3.4. Summary

MBI is employed to probe NO adsorption and its dissociation on Pd(111) surface through isothermal kinetic experiments between 300 and 525 K. Molecular NO adsorption was observed $\leq 400\text{ K}$. The adsorption kinetics indicate that NO dissociation starts on Pd(111) surfaces at around 400 K. NO dissociation to N_2 and N_2O was observed clearly in the transient state at temperatures $\geq 425\text{ K}$. Major amounts of N_2 desorption were found along with a minor amount of N_2O desorption, in agreement with earlier results from TPD. The decrease in the time delay between N_2 desorption onset and the shutter removal at increasing temperature suggests that nitrogen formation occurs through a diffusion-controlled mechanism and it could be partly rate limiting, at least below 500 K. The rate of N_2 formation does not follow that of NO uptake. The adsorption - desorption equilibrium of NO is established in the presence of NO-beam, indicating substantial NO-coverages below 500 K. Oxygen diffusion into the sub-surface sites and surface oxide formation starts around 475 K and increases significantly above 525 K. Sticking coefficient measurements show $s = 0.5$ for NO adsorption between 300 and 350 K up to high coverage, indicating the precursor mediated adsorption. s_{NO} decreases with increasing coverage and temperature. The present molecular beam experiments on NO dissociation throw more light than the earlier conventional TPD experiments.

Chapter 4

*NO + CO Reaction on Pd(111) Surfaces**

“NO reduction with CO on the Pd(111) surface was studied under isothermal conditions as a function of temperature, NO:CO beam composition, and beam flux. Systematic experiments were performed under transient and steady state conditions. Displacement of adsorbed CO by NO in the transient state of the reaction was observed at temperatures between 375 and 475 K for all of the NO:CO compositions studied. NO accumulation occurs on Pd(111) surface under steady state conditions, below 475 K, due to stronger chemisorption of NO. The steady state reaction rates attain a maximum at about 475 K, nearly independent of beam composition. N₂ was found to be the major product of the reduction, along with a minor production of N₂O. The production of N₂ and N₂O indicates molecular and dissociative adsorption of NO on Pd(111) at temperatures up to 525 K. Post-reaction TPD measurements were performed in order to determine the nitrogen coverage under steady-state conditions. Finally, the results are discussed with respect to the rate-controlling character of the different elementary steps of the reaction system.”

* Thirunavukkarasu, K., Thirumoorthy, K., Libuda, J., Gopinath, C.S., *J. Phys. Chem. B.*, **2005**, 109, 13272.

NO + CO Reaction on Pd(111) Surfaces

4.1. Introduction

The overall NO + CO reaction in TWC is known and almost a complete microscopic understanding of the elementary reaction steps is in place for Rh. [66-68,87-90] However, Pd has not been subjected, like Rh, to detailed studies and microscopic understanding is far from clear. Further, NO_x reduction performance at low temperatures and resistance to oxidation of the metal particles at high temperatures has led to an increased interest in Pd. [80] Recent reports on Pd-CeO₂ and Pd-Rh-CeO₂ show similar or even superior catalytic performance over the conventional Rh-Pt-CeO₂. [79] In addition to the above, a few new technologies were introduced in the last decade such as NO_x storage and zeolite based catalysts in order to tackle NO_x abatement. [85,138-140] Nonetheless, stability problems associated with NO_x storage and the inability of zeolites to cause NO reduction in the presence of water vapor [81] are problems faced in real applications.

A number of groups [93-94,96,98-99,101-105,107-110,141-147] have studied deNO_x reactions with CO or H₂ as the reductant on Pd single crystals, Pd on supports and powder catalysts. Still, the kinetics of the reaction is not fully understood. Infrared reflection absorption spectroscopy (IRAS) and high-resolution electron energy loss spectroscopy (HREELS) have been employed to study NO adsorption and its co-adsorption with CO on Pd(100) and Pd(111) single crystals.[101,102] Goodman and coworkers found that the closely packed Pd(111) surface was significantly more active than the relatively more open Pd(100) surface for the NO + CO reaction, [101,102] in spite of the fact that the latter has a higher NO dissociation activity. This effect was attributed to the strong bonding of a fraction of the N_{ads} on Pd(100), leading to partial poisoning of the surface.[101] Also, the N₂/N₂O product ratio was found to depend on the crystallographic orientation, with lower selectivity for N₂ on Pd(111) than on Pd(100). In more recent work, high N₂O/N₂ product ratios were observed on the Pd(111) surface at elevated pressures. [102] Some differences remain between the TPD results reported by Goodman et al. [101] on Pd(111) and Pd(100) and those reported by other groups, [93-94,96,98,148] in particular, with respect to N₂ desorption above 550 K.

Well-shaped Pd nanoclusters supported on MgO, with Pd(111) and Pd(100) facets, were employed in NO dissociation studies by Henry et al. [103-105] Relatively high reaction rates were observed on Pd(111) facets, in good agreement with ref. [101]. Particle size dependent effects were interpreted mainly in terms of the morphology of the particles, which expose different fractions of (111) and (100) facets. [103-105] Recent micro-kinetic simulations of the molecular beam experiments show that there are many open questions concerning the reaction kinetics, even for simple single crystal surfaces. [105] From the above it is clear that there is a need for detailed and quantitative kinetic measurements on Pd single crystal surfaces under well-controlled conditions.

The reactivity of Pd(111) surfaces for NO+CO reactions at different temperatures and beam compositions have been investigated systematically. We have employed molecular beam methods, which have enabled us to perform kinetic experiments in a quantitative and well-controlled fashion, both under steady state and under transient conditions. In this chapter we present results on the reaction kinetics at low and high temperatures and on the competitive adsorption of NO and CO at temperatures between 375 and 475 K.

4.2. Experimental

The doser assembly, aiming directly at the Pd(111) crystal surface, is connected to a gas manifold unit and the beam flux is set both by filling the manifold unit to a specified pressure and by fixing the precision leak valve to a predetermined position. 0.1 ML/s total flux of the NO + CO mixture ($F_{\text{NO+CO}}$) with a desired composition was used in all the experiments reported here unless otherwise specified. A movable stainless steel shutter is placed between the sample and the doser to block or unblock the beam when desired. The geometrical arrangement in our MBI is such that about 25% of the beam is intercepted by the crystal and, hence, the drop in the reactants pressure upon shutter removal is relatively shallow this is mainly to ensure a uniform beam profile over the entire crystal surface. [70,148]

^{15}NO (Air gas, 99% isotopically pure), CO and ^{13}CO (Isotec) were used without any further purification. It is to be noted that ^{15}NO contains about 1% of ^{14}NO (amu 30), which adds to the partial pressure of $^{15}\text{N}_2$ (amu 30) during measurements. Very small

amount of $^{15}\text{N}_2\text{O}$ (amu 46) ($\leq 0.1\%$) is also present; however it does not affect the measurements significantly since the amount is very small. However, ^{15}NO allows a clear identification of all the products of the reaction $^{15}\text{N}_2$ (amu 30), $^{15}\text{N}_2\text{O}$ (amu 46) and $^{12}\text{CO}_2$ (amu 44) along with the reactants, ^{15}NO (amu 31) and ^{12}CO (amu 28). It is observed that N_2O gives a key fragment ion N_2 to a large extent. The partial pressure values observed during the reaction for N_2O and N_2 were corrected for the above fragment contribution by following the procedure in ref. 149. The mass spectrometer intensities for ^{15}NO and CO were calibrated by measuring the NO and CO uptake on clean Pd(111) at 300 K separately, assuming a saturation coverage of 0.33 monolayer (ML) for NO following Bertolo et al.[93-94] and 0.50 ML for CO . [118] An exposure of 1 ML corresponds to 7.8×10^{14} molecules/cm². ^{15}NO and CO were exclusively used for all the experiments reported here. Hence, hereafter ^{15}NO would be simply noted as NO . Further, the rates calculated and given in Figures 4.9, 4.10 and 4.12 have an error margin of $\pm 10\%$.

4.3. Results

4.3.1. General Aspects on Catalytic Activity Measurements:

In all the isothermal experiments reported here, the clean Pd(111) sample was kept at a constant temperature and exposed to an effusive molecular beam of the reactant mixture of the desired composition. The partial pressures of all the relevant species were recorded as a function of time. A typical raw isothermal kinetic data of the reaction of ^{15}NO and CO with a beam composition of 1:2 at 475 K is presented in Figure 4.1a along with the TPD spectra recorded at a heating rate of 5 K/s (Figure 4.1b). The scattered data points for all the species were collected without opening the shutter in a separate experiment. The various steps in all the experiments are explained below with reference to the above data: (1) At $t = 5$ s a molecular beam of a mixture of the reactants ($\text{NO}:\text{CO} = 1:2$, $F_{\text{NO}+\text{CO}} = 0.10$ ML/s) was turned on; an immediate increase in NO and CO partial pressures could be seen. Some adsorption of the reactants from the “background” cannot be avoided at this stage. (2) At around $t = 8$ s the shutter was removed to allow the beam to interact directly with the Pd(111) surface kept at 475 K. An immediate decrease in the partial pressure of the reactants was observed indicating the adsorption of the reactants on the Pd(111) surface. A slow increase in NO partial pressure was due to decreasing

adsorption on the UHV chamber walls and does not indicate a change in the F_{NO} on Pd(111). An increase in the partial pressure of the products, $^{15}\text{N}_2$ (30 amu), CO_2 (44 amu)

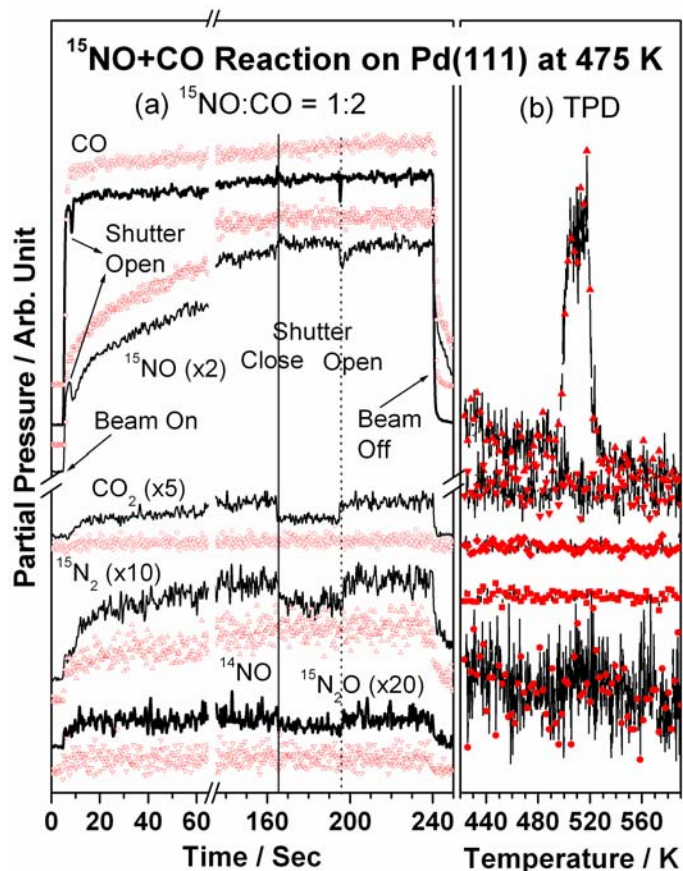


Figure 4.1. (a) Raw isothermal kinetic data of a typical molecular beam experiment conducted with (NO + CO)/Pd(111) system at 475 K for the beam composition of 1:2 NO:CO. (b) Temperature-programmed desorption recorded after the kinetic experiment. Scattered data points shown on left panel are from the experiment carried out without opening the shutter throughout the experiment to demonstrate the marginal effect due to background. Data points have been shifted vertically for clarity. An increase in the intensity of amu 30 in the above experiment is essentially due to ^{14}NO present in ^{15}NO .

and $^{15}\text{N}_2\text{O}$ (46 amu) were also observed. The changes observed from the point where the shutter is opened until the steady state is reached is termed as the transient state, and this normally takes up to 60 sec under the present experimental conditions. (3) In the steady state, the reaction rate was measured by blocking the beam deliberately for 30 s (between $t = 165\text{-}195$ s) with the shutter. An increase in the partial pressure of NO and a clear decrease in the partial pressures of N_2 and CO_2 were observed. A slight decrease in the partial pressure of N_2O was also observed. An increase in the partial pressure of NO

indicates its continuous uptake from the beam in the steady state; a sharp change in the CO partial pressure was observed only at the blocking and unblocking of the beam, but an overall increase was not observed during the beam blocking time. The measured changes in the partial pressures of CO₂, N₂, and N₂O allow us to directly determine the steady-state reaction rates. Additional kinetic information can be derived from the transient response (see section 4.3.2). A sharp decrease in the CO₂ partial pressure was observed when the beam was blocked, whereas a slow change in partial pressure was observed for the N₂ and N₂O. It is to be pointed out here that the change in the partial pressure of the reactants and the products has to be corrected for the background adsorption, during the period the beam was blocked in the steady state which is estimated to be around 10% for the adsorption processes in our system. (4) The shutter is opened again at $t = 195$ s. The pressure difference observed for the reactants and the products during beam blocking and unblocking provides the rate of the reaction, of course after initial calibration of all the relevant species. (5) At about $t = 240$ s, the beam was turned off to stop the reaction. After the pressure of the UHV chamber reached the initial background level, the sample was heated to 700 K at a heating rate of 5 K/s to record the TPD of all the relevant species. The coverage by the nitrogen atoms that remained on the Pd(111) surface was calculated by integrating the area of the N₂ desorption peak observed in the TPD, and oxygen coverage was measured through CO titration at 450 K. A systematic study of the NO + CO reaction kinetics on Pd(111) surfaces was carried out by following the above procedure as a function of temperature, NO:CO composition, and total beam flux.

During the reaction measurements, the total pressure in the chamber increases to about $(1-2) \times 10^{-8}$ Torr and that induces some additional adsorption/reaction apart from the direct beam onto Pd(111). As shown in Figure 1, the reactants pressure increase in the same manner, whether the beam was blocked or not, except while opening/closing the shutter. However, the products pressure increases marginally when the beam was fully blocked, as seen in the scattered data points due to the limited adsorption from the background. CO₂ shows an increase in pressure and displays that there is reaction to some extent due to background adsorption of NO + CO. In the case of ¹⁵N₂ (amu 30) a large increase in background pressure is mostly due to 1% ¹⁴NO (amu 30), as mentioned

earlier, in addition to some $^{15}\text{N}_2$. Indeed, at low temperature (375 K) measurements, where there is no effective reaction, show a very similar trend and supports the above increase in pressure is due to ^{14}NO . It was difficult to make out any contribution due to the very poor signal/noise associated with the data of $^{15}\text{N}_2\text{O}$ production from background. However, at the time of shutter opening/closing, a good change in partial pressure of all the products demonstrate that major contribution is due to molecular beam. Further, the extent of CO_2 production due to background adsorption is not more than 10% of the CO_2 produced from the direct beam. However, a similar measurement for $^{15}\text{N}_2$ was not reliable as the background is largely due to ^{14}NO . For the above reason, the background contribution is not included in the results reported. As shown in Figure 4.12 (vide infra) the partial pressure of different species were converted into reaction rates by calibration experiments for the reactants and products, following the procedure reported, [148] and no background contribution is included.

4.3.2. Transient Kinetics:

First, we focus on the transient regime of the reaction, immediately after impingement of the beam. A clean metal surface at the start of the reaction undergoes dynamic changes in surface composition of reactants and products as a function of time before it reaches the steady state, where there is no change in surface composition of reactants as long as the reaction conditions are not perturbed. It is important to note that the sticking coefficients of the reactants NO and CO may drastically change as a function of temperature and coverage in the transient region.

4.3.2.1. Displacement of CO by NO:

The displacement of a chemisorbed species by another adsorbing species has been suggested and observed by few groups [67,69,101,142,150] in various catalytic reactions. Figure 4.2 shows the direct displacement of CO_{ads} by NO at (a) 375 K and (b) 475 K for the NO:CO compositions of 2:1, 1:1, and 1:2. The $F_{\text{NO+CO}}$ used in Figure 4.2b is (0.3 ML/S) thrice that used in the experiments of Figure 4.2a (0.1 ML/S). Reference experiments were also carried out without opening the shutter, and the data collected were used for background subtraction from the data of the relevant experiments. One such reference experiment is plotted in Figure 4.2a for 2:1 NO:CO beam composition. The trends of NO adsorption (Figure 4.2) follow the expected behavior at all the

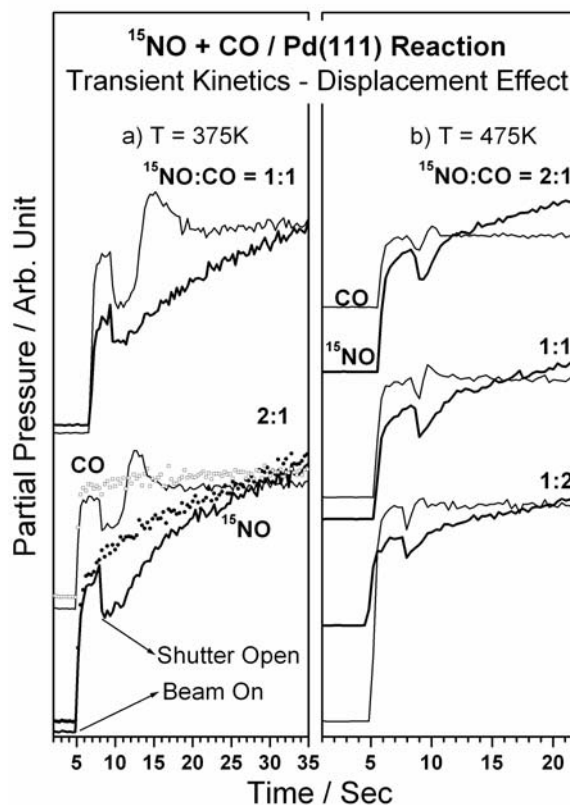


Figure 4.2. Displacement of CO by NO during the initial adsorption of the reactants on clean Pd(111) surface at (a) 375 and (b) 475 K for the NO:CO beam compositions 2:1, 1:1, and 1:2. The $F_{\text{NO+CO}}$ used in panel b is thrice that of panel a, and displacement effect was not clear at lower flux at 475 K. Scattered data points shown on left panel for 2:1 beam are from the experiment carried out without opening the shutter to use as standard for background subtraction. Similar experiments were carried out for other experiments.

temperatures and compositions. An initial drop in the partial pressure is observed upon shutter removal due to initial uptake on Pd(111) and a subsequent asymptotic approach to the steady state. The time evolution of partial pressure of CO is more complex. An immediate drop in the partial pressure upon unblocking the beam was observed, followed by an increase in partial pressure after few seconds. Finally, the steady-state level is reached. It indicates that a large amount of CO is displaced by NO because of its preferential adsorption on Pd(111) compared to CO. This effect was observed for all beam compositions at 375 K. For CO-rich beam compositions the process is slower since the CO displacement is directly proportional to F_{NO} . Generally as the beam becomes richer in CO (and hence poor in NO), the displacement of CO molecules takes a longer time and the displacement signals becomes weak to be observed. It is also to be noted

that the CO displacement effect decreased with decreasing $F_{\text{NO+CO}}$; the extent of CO displacement was marginal at a $F_{\text{NO+CO}} = 0.1$ ML/s at 475 K for the beam compositions shown in Figure 4.2b. At temperatures >525 K the displacement effect was very poor or not observed due to the very small steady state coverage of the reactants, particularly CO. [151] However at temperatures <525 K, this effect was observed clearly and the surface ratio of the reactants changed in the transient state until it reached the steady state. It is also clear from these observations that the adsorption of NO on Pd(111) is dominating and hence an enrichment of NO over CO occurs compared to the gas phase. A similar effect has already been observed on Rh(111). [67]

Figure 4.3 shows the coverages of NO_{ads} , CO_{ads} , and CO_{des} and the difference between CO_{ads} and CO_{des} on Pd(111) in the transient state for all the NO:CO

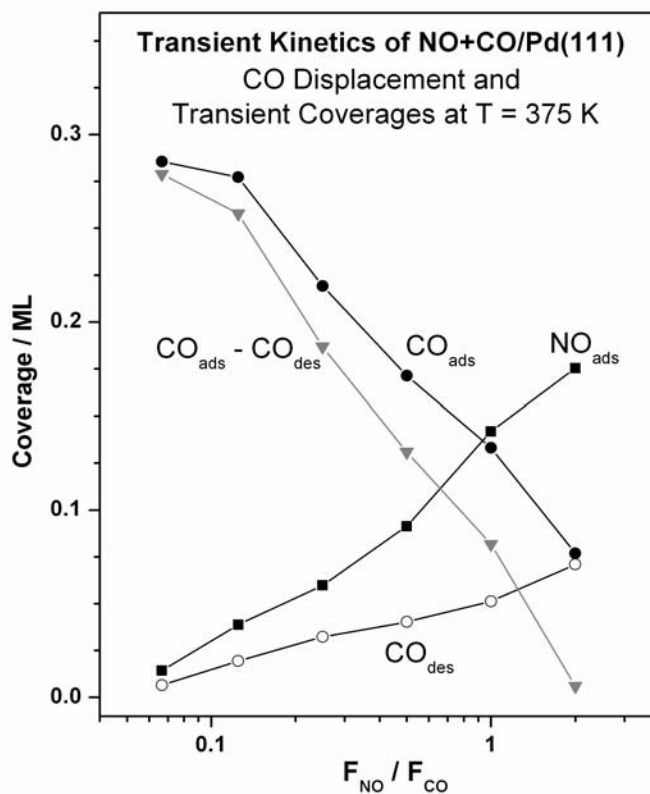


Figure 4.3. Coverage of NO and CO in the transient state on NO + CO (1:1)/Pd(111) system at 375 K. NO_{ads} , CO_{ads} , and CO_{des} correspond to the coverage of NO and CO immediately after shutter removal and coverage of desorbed CO in the transient state, respectively. The difference between $\text{CO}_{\text{ads}} - \text{CO}_{\text{des}}$ gives qualitative CO-coverage on the surface at the end of transient state. It is to be noted that the surface is increasingly poisoned by CO with CO-rich beams and an almost exclusively NO-covered surface occurs for a 2:1 NO:CO beam.

compositions at 375 K. The above coverages were obtained by integrating the area of the adsorption and desorption in the transient state (Figure 4.2). NO_{ads} decreases linearly as the beam becomes CO-rich. Initial CO_{ads} also increases with the CO-rich beams. However the amount of CO_{des} indicates that the CO displacement is very strong for NO-rich beams and gradually decreases as the beam becomes richer in CO. Only minor CO-displacement was observed for 1:15 NO:CO beam. The present results reveal a clear difference between surface and beam compositions the surface accumulating NO.

Figure 4.4 shows the transient state kinetics of CO_2 and N_2 evolution at 475 K for two NO:CO compositions, namely, 1:4 and 1:8. CO_2 production shows a transient kinetics depending on NO:CO beam composition. At high F_{NO} (with 2:1 of NO:CO, data not shown), the CO_2 production rate is low and it increases with increasing F_{CO} up to 1:4 NO:CO. A further increase in F_{CO} leads to a decrease in the CO_2 formation rate, likely due to CO poisoning of the surface. Generally, the N_2 production reaches the steady state within a minute; however the CO_2 production reaches the steady state slowly in about 2 min. This delay occurs especially with NO:CO compositions (1:1 to 1:8) that exhibit a high rate of CO_2 production. However such a delay does not occur with NO- or CO-rich beams since the CO displacement effect is observed too fast or too slow and hence the poisoning of the surface with NO or CO, respectively. With a 1:15 NO:CO composition, the CO_2 production reaches a steady-state quickly within 20 s after shutter removal and the rate is limited by CO-poisoning. A close look at the transient state in Figure 4.4 shows a jump in CO_2 production at the point of shutter opening and some delay in N_2 production. Further, the change in CO_2 partial pressure for beam blocking at $t = 75$ s shows a considerably smaller change in rate and a slower CO_2 decay when compared to the sharp changes at $t = 165$ s. However, the change in nitrogen partial pressure is similar at both beam blockings. We attribute this delay, at least in part, to the CO displacement effect and a continuous change in surface composition until it reached the steady-state. Nonetheless, the above observation has to be treated with care due to the low signal-to-noise ratio for the N_2 signal. A slower response of the N_2 signal would indicate that the N_2 recombination step has some significant degree of rate control. Spectroscopic and structural investigations could throw more light on the changes that might be occurring on the surface under reaction conditions.

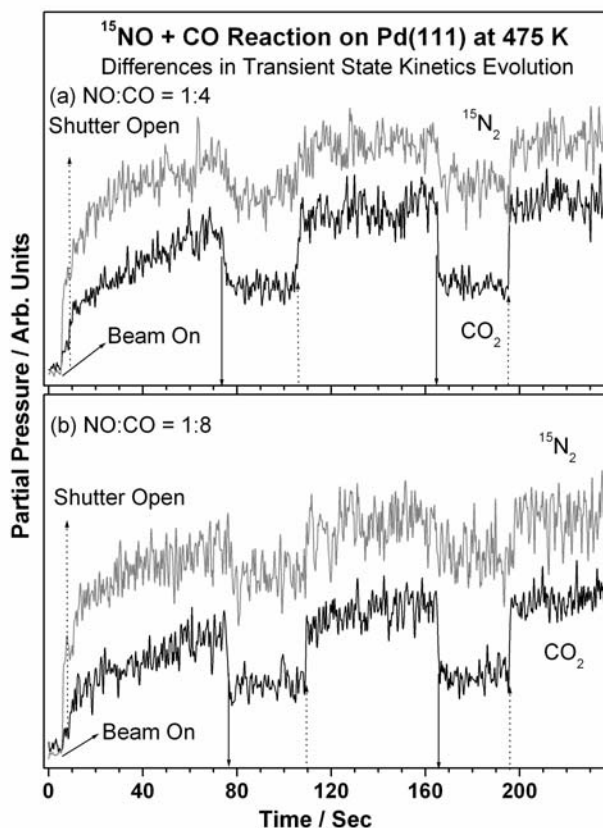


Figure 4.4. Time evolution of the partial pressure of the products $^{15}\text{N}_2$ and CO_2 in the transient state for NO:CO beam compositions of (a) 1:4 and (b) 1:8 at 475 K. It is to be noted that the partial pressure of CO_2 reaches steady-state slowly than N_2 and it is attributed, at least in part, to CO poisoning and CO displacement by NO. The change in CO_2 partial pressure for beam blocking is considerably lower in the transient state than in the steady state.

4.3.2.2. Restart Experiments:

Restart experiments were performed in order to identify differences in the transient state due to accumulation of surface species, produced during the reaction. Figure 4.5 shows the transient state kinetics of CO_2 and N_2 evolution at 475 K for two NO:CO compositions, namely, 1:4 and 1:8. CO_2 production shows a transient kinetics depending on NO:CO beam composition. At high F_{NO} (with 2:1 of NO:CO data not shown), the CO_2 production rate is low and it increases with increasing F_{CO} up to 1:4 NO:CO. Figure 4.5 shows such an example, where clean Pd(111) interacted with 1:1 NO:CO beam ($F_{\text{NO+CO}} = 0.25$ ML/s) for about 120 s (in Figure 4.5a) before the molecular beam was turned off. After the partial pressures of all the species reached their background level the reaction was repeated without any further cleaning of the Pd(111)

surface and the result is shown in Figure 4.5b. A decrease in the partial pressure due to adsorption of NO and CO and the displacement effect in the transient state was observed on clean and restart experiments. The partial pressures for N₂ and N₂O increased to the steady state value gradually without any significant change in both the clean and restart experiments. However, a considerable increase in the CO₂ formation was observed in the restart experiments. Even before the shutter removal a small but considerable CO₂ production started as soon as the molecular beam was turned on due to the reaction of the background CO on the Pd(111) surface. After shutter removal, a further rise in the CO₂ production was observed compared to the clean surface. This immediate production of

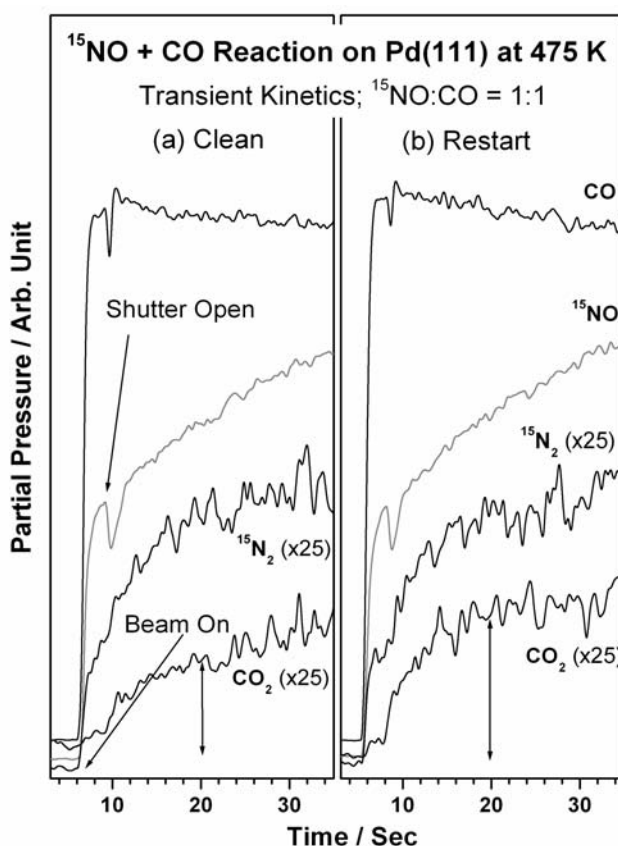


Figure 4.5. Isothermal kinetic experiments carried out with a 1:1 NO: CO beam at 475 K on (a) clean Pd(111) and (b) on the Pd-surface after reaction a, but without any cleaning. An enhancement in CO₂ production could be seen in the transient state indicates that some amount of oxygen available.

CO₂ was more pronounced for NO-rich beams. However, the rate of formation of CO₂ remained unchanged in the steady state for clean and restart experiments. The displacement of CO by NO also decreased significantly in the restart experiments. This

effect is attributed to the additional CO₂ production due to reaction with surface oxygen in the restart experiment. CO₂ production was instantaneous in restart experiment compared to the clean surface. It indicates that some oxygen atoms remain on the surface at the end of the first reaction on clean Pd(111). Furthermore, the restart experiments indicate that the production of N₂ and N₂O does not need any threshold coverage as on Rh(111) surface. [67]

4.3.3. Steady-State Kinetics:

4.3.3.1. Temperature Dependence:

Figure 4.6 shows the temperature dependence of molecular beam kinetics in the steady state for the production of N₂, N₂O, and CO₂ for 1:4 NO:CO beam compositions. No NO+CO reaction on Pd(111) could be observed within the detection limits of our experiment up to 425 and >625 K. The active temperature window for NO reduction lies

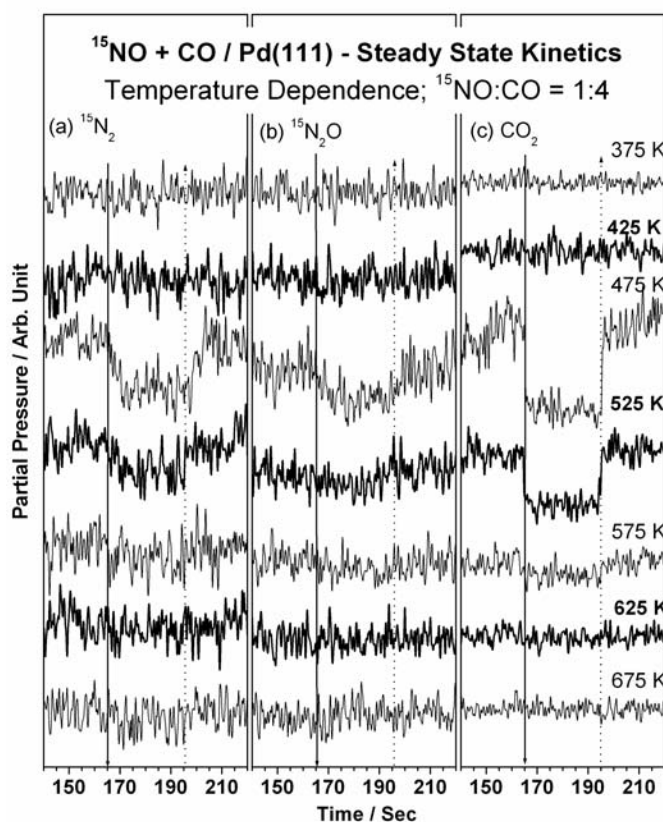


Figure 4.6. Steady-state kinetics of isothermal experiments as a function of temperature with a 1:4 NO:CO composition and time evolution of the partial pressure of the products (a) N₂, (b) N₂O, and (c) CO₂. Dotted and solid arrows indicate the closing and opening of the shutter.

between 425 and 575 K with a maximum steady-state rate at 475 K. The N₂O production rate is about an order of magnitude lower than that of N₂ production. For >525 K, the rate slowly decreases and no N₂O production was observed. The differences in response of the partial pressures of the product species for shutter opening/closing to the new steady state should be noticed, particularly between 475 and 525 K. The partial pressure of CO₂ responds immediately to modulation, whereas the N₂ partial pressures displayed a slow response on beam blocking and unblocking indicating that nitrogen recombination might be the rate determining step (RDS). However, the low signal-to-noise ratio associated with N₂O makes deriving any meaningful conclusions difficult. However, >525 K, CO₂, and N₂ formation undergo fast changes on beam modulation.

4.3.3.2. Composition Dependence:

Figure 4.7 shows the dependence of the steady-state kinetics on the NO:CO beam composition at 475 K for compositions ranging from 2:1 to 1:15 of NO:CO. When the beam is rich in NO (for instance, 2:1 NO:CO), the rate of the overall reaction is low compared to other beam compositions even at a high surface temperature. As the beam is made richer in CO, the NO + CO steady-state reaction rate increases until it reaches a maximum of 1:4 NO:CO composition. The N₂O production rate reaches its maximum at the beam composition of 1:2 NO:CO and not for the NO rich beams. This clearly indicates that the surface composition established for 1:2 of NO:CO beam composition induces more N₂O production than the NO-rich beam compositions. N₂O production decreases slowly as the beam becomes richer in CO. N₂ and CO₂ production rates decrease on either side of 1:4 NO:CO composition. From Figures 4.6 and 4.7, it is observed that the maximum in NO + CO reaction rate occurs at 475 K for the composition of 1:4 NO:CO with a minor production of N₂O.

4.3.3.3. Flux Dependence:

Figure 4.8 shows the flux dependence of the NO + CO reaction on Pd(111) at 475 K for 1:4 NO:CO for the total fluxes ranging from $F_{\text{NO+CO}} = 0.01$ to 0.25 ML/s. The rates of production of the major products N₂ and CO₂ along with N₂O increase linearly with increasing total beam flux and indicate a first order dependence on F_{NO} . The studies on flux dependence clearly show the slow change in the partial pressure of N₂ for beam

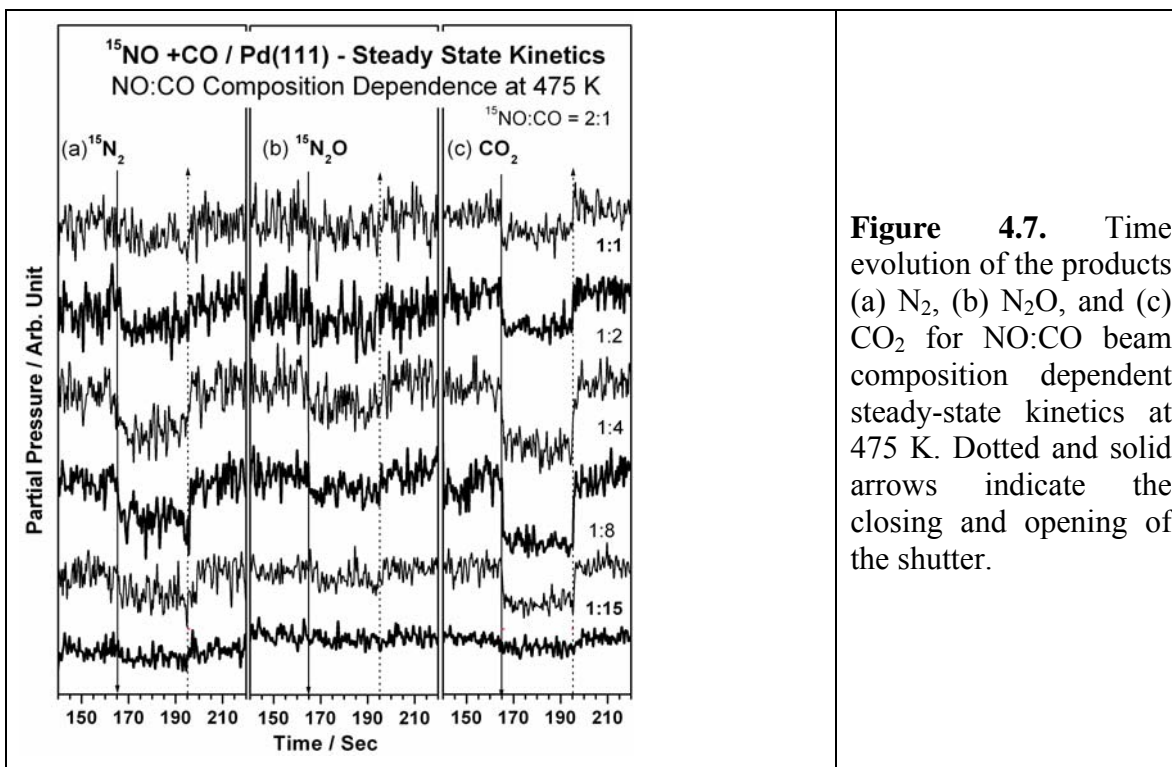


Figure 4.7. Time evolution of the products (a) N₂, (b) N₂O, and (c) CO₂ for NO:CO beam composition dependent steady-state kinetics at 475 K. Dotted and solid arrows indicate the closing and opening of the shutter.

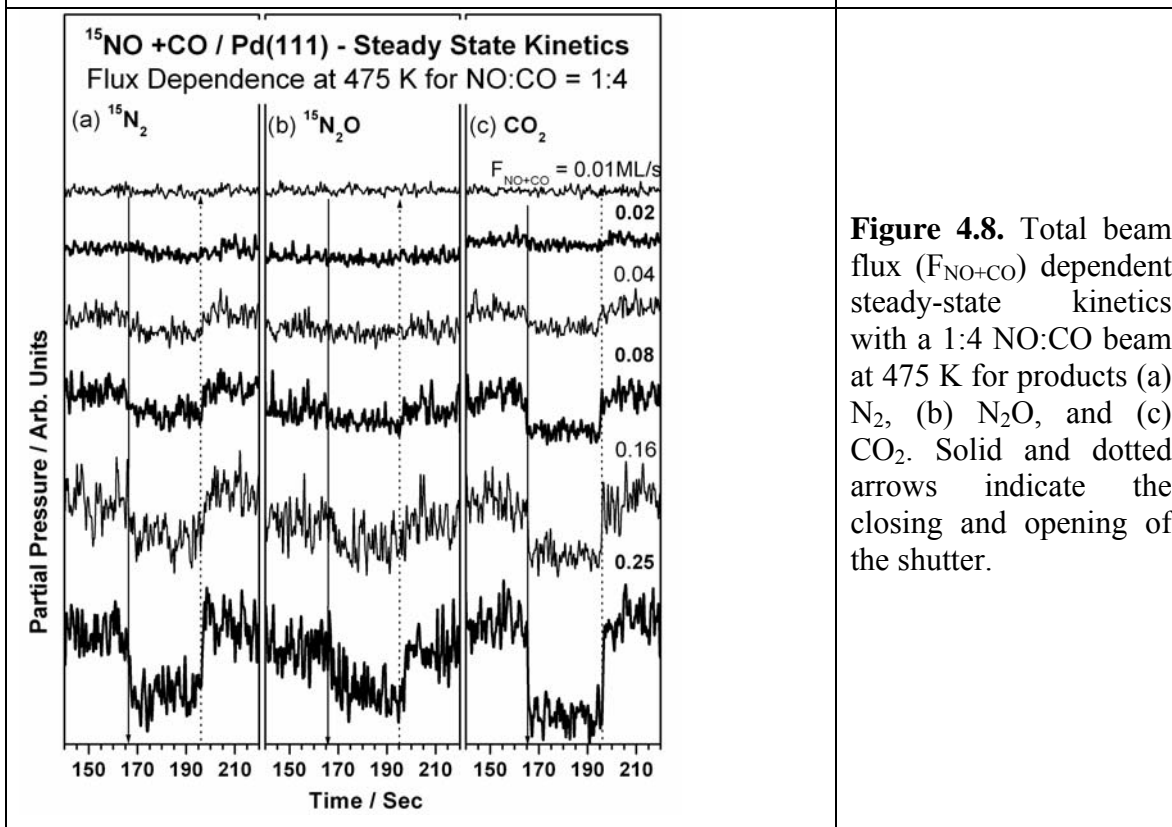


Figure 4.8. Total beam flux (F_{NO+CO}) dependent steady-state kinetics with a 1:4 NO:CO beam at 475 K for products (a) N₂, (b) N₂O, and (c) CO₂. Solid and dotted arrows indicate the closing and opening of the shutter.

blocking and unblocking and suggest that nitrogen formation could be the RDS for the NO + CO reaction on Pd(111) surfaces below 500 K and for $F_{\text{NO+CO}} = 0.16$ ML/ s. Further, at a high flux ($F_{\text{NO+CO}} = 0.25$ ML/s), N₂ production also shows fast changes on beam blocking and unblocking, suggesting that there may be a contribution from other reaction steps to the RDS as well.

4.3.3.4. Steady-State Reaction Rates:

Figure 4.9 shows the rate of formation of all the three products namely, (a) N₂, (b) N₂O, and (c) CO₂ measured in the steady-state at a total flux of 0.25 ML/s. All beam compositions show a reaction maximum at 475 K. At the reaction temperature of 475 K and the 1:4 NO:CO composition, a maximum in productivity is observed for the major products N₂ and CO₂ and the production maximum for N₂O is observed for a 1:2 NO:CO beam. There is a general broadening of the temperature range in which the rate is considerable relative to the maximum rate as the beam becomes richer in CO.

$$R(\text{CO}_2) = 2R(\text{N}_2) + R(\text{N}_2\text{O}) \quad [4.1]$$

The above steady-state rate data is plotted in Figure 4.10 in a modified and different manner for (a) CO₂ and (b) 2R(N₂) + R(N₂O) to clearly see the rate dependence on composition and to see the consistency in the experimental data through eq 4.1. A good overall correspondence is observed between the rate of CO oxidation and nitrogen containing product formation suggesting that the data is self-consistent within the error limit. This figure also confirms that the maximum in the reaction rate is observed for a NO:CO ratio of 1:4. All the NO:CO compositions shows a reaction maximum at 475 K.

4.3.3.5. Temperature-Programmed Desorption (TPD) Studies:

TPD experiments were performed to measure the surface nitrogen left after the NO + CO reaction on Pd(111) surface at a heating rate of 5 K/s. Two TPD results recorded after the 1:4 NO:CO reaction at (a) 475 and (b) 525 K are given in Figure 4.11. Both experiments show nitrogen desorption around 500 K in a single peak. Generally, TPD results from the surfaces that are exposed to a beam of any composition at $T > 525$ K show only low oxygen coverage after the reaction

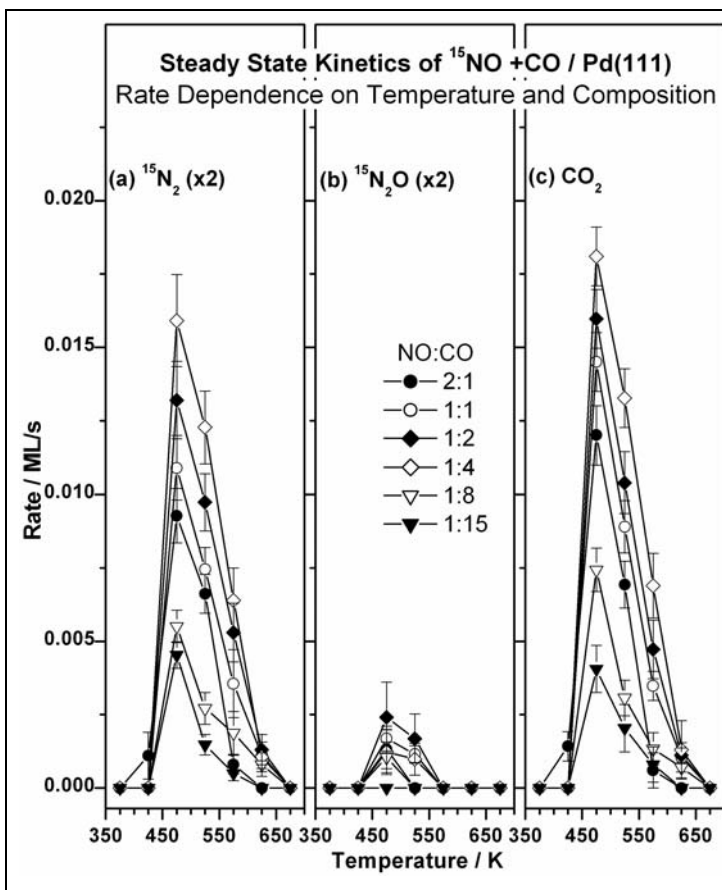


Figure 4.9. Steady-state rate of production of (a) N_2 , (b) N_2O , and (c) CO_2 are given for all NO:CO compositions and reaction temperatures. Maximum rate was observed at 475 K for all NO:CO beam compositions.

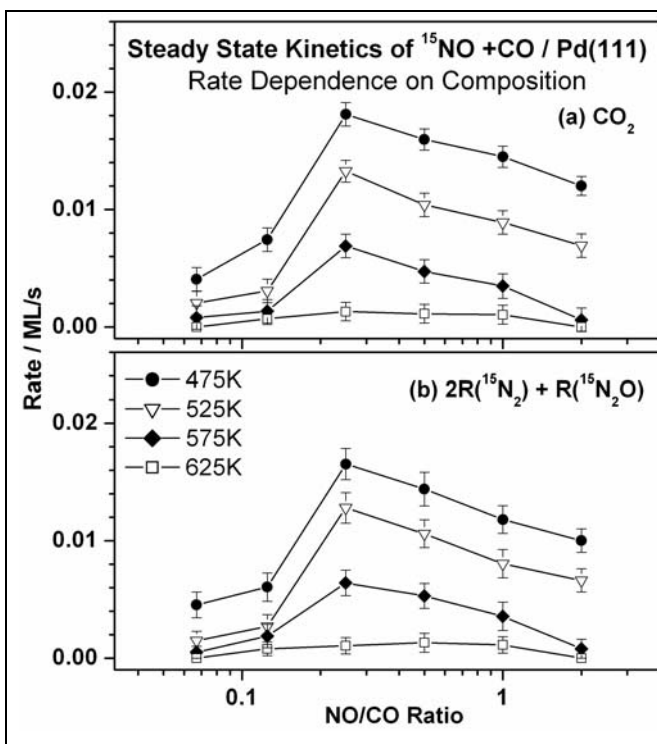


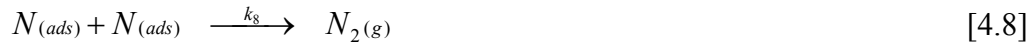
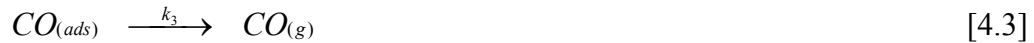
Figure 4.10. Steady-state rate dependence on the beam composition at four temperatures for (a) CO_2 and (b) $2R(N_2) + R(N_2O)$.

However, the coverage of oxygen measured through CO-titration varies from one experiment to another. This effect may be attributed to subsurface and bulk diffusion, [123] which makes the reliable estimation of oxygen coverage difficult. At 475 and 525 K, a small coverage of nitrogen is also observed for all beam compositions and θ_N is <0.05 ML. At lower reaction temperatures (375 and 425 K) the desorption of all the products and reactants is seen. Large amounts of NO (>0.18 ML) or CO (>0.25 ML) are desorbed from surfaces that are exposed to NO-rich (2:1 and 1:1 NO:CO) or CO-rich (1:8 and 1:15 NO: CO) beams at 375 K, respectively, indicating surface poisoning, as observed in the transient coverage results (Figure 3).

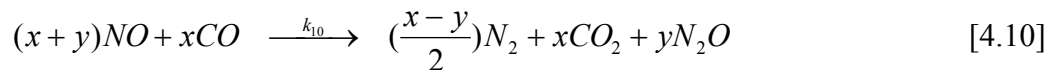
4.4. Discussion

4.4.1. Reaction Mechanism:

The isothermal kinetic data obtained provide some new insights on the mechanism of the NO + CO reaction on Pd surfaces. The following elementary surface reactions are considered for the overall NO + CO reaction on Pd(111) surfaces:



The overall reaction is



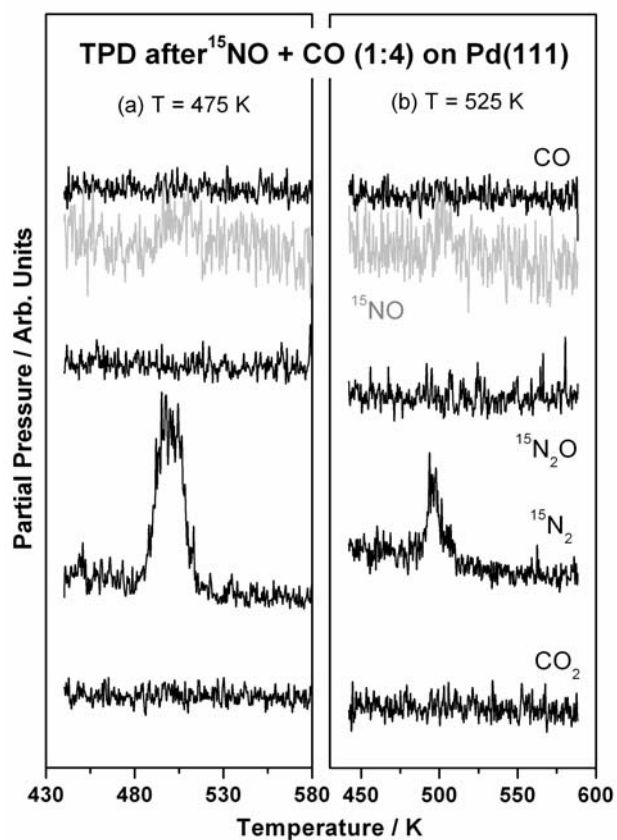


Figure 4.11. TPD recorded after the NO + CO reaction with 1:4 beam composition at (a) 475 and (b) 525 K. The nitrogen coverage decreases with increasing temperature and no nitrogen coverage is observed at reactions temperatures $>525 \text{ K}$.

One of the important controversies in the literature with respect to the NO + CO reaction mechanism relates to the reaction RDS. [101,105,146] Our kinetic results clearly show that the CO_2 production is fast compared to N_2 and/or N_2O production under the present experimental conditions. This also suggests that the NO adsorption and its dissociation cannot be the RDS, at least in the low-temperature regime, $<525 \text{ K}$. This leaves eq 4.8 or 4.9 to be possible RDS. The low signal-to-noise ratio associated with N_2O makes deriving any meaningful conclusions difficult. Further, N_2O being a minor product in the parallel pathway for both N_2 and N_2O formation, it is ruled out that N_2O formation can be the RDS. A slow change in partial pressure of N_2 was observed below 525 K for the beam blocking in the steady-state of NO + CO reactions under most of the conditions; however, high flux ($F_{\text{NO+CO}} = 0.25 \text{ ML/s}$) measurements (Figure 4.8) shows

the fast changes in N₂ production for beam blocking. It is likely that also the other steps (in particular NO dissociation) have some degree of rate control >525 K (as indicated by the linear flux dependence of the reaction rate in Figure 4.8). This suggests that the N₂ formation from the recombination of N atoms below 525 K might be controlling the overall reaction; however the NO dissociation also has some degree of rate control as indicated above. Above 525 K, CO₂ as well as N₂ formation shows fast changes for beam blocking and unblocking. Furthermore, the rate of desorption of reactants species is faster than the adsorption and NO dissociation, and hence, a decrease in overall NO + CO rate for >525 K is observed. In the high-temperature regime, it is expected that the degree of rate control by NO dissociation increases and the degree of rate control of the other steps decreases.

Another piece of evidence to support the reaction mechanism suggested above, as well as to calculate the reaction stoichiometry, is given in Figure 4.12. The rate of adsorption of NO and the rate of formation of various products in the steady-state is shown for 1:4 NO:CO beam composition at a surface temperature of 475 K in Figure 4.12. It is to be noted that the rate of NO adsorption (0.018 ML/s) in the steady state is equal to that of the sum of either CO₂ (0.0181 ML/s) and N₂O production (0.0006 ML/s) or 2N₂ (0.016 ML/s) and 2N₂O (0.0012 ML/s) production, within the error limit (10%). The above result suggests that about 90% of adsorbed NO dissociates and the remaining amount is adsorbed in the molecular state. At temperatures higher than 525 K, a ratio of 1:1 for CO₂: ½ N₂ is observed suggests that the rate of NO-uptake is equal to that of CO₂ or ½ N₂ production. The above two stoichiometries, below and above 525 K, were found to hold good for all the reaction conditions employed in our experiments.

4.4.2. Steady-State Kinetics:

Under steady-state conditions, the rate of all the elementary processes should be equal. However, the recombination of N + N is considered as the RDS due to the low rate constant values. Alternatively, the rates of other elementary processes compensate under steady-state conditions through changes in the respective surface coverage. [66] From the above discussion and the arguments of section 4.1, the rate expression for CO₂ is derived from the surface coverage of the different adsorbates.

$$R(\text{CO}_2) = k_7\theta_{\text{CO}}\theta_{\text{O}} \quad [4.11]$$

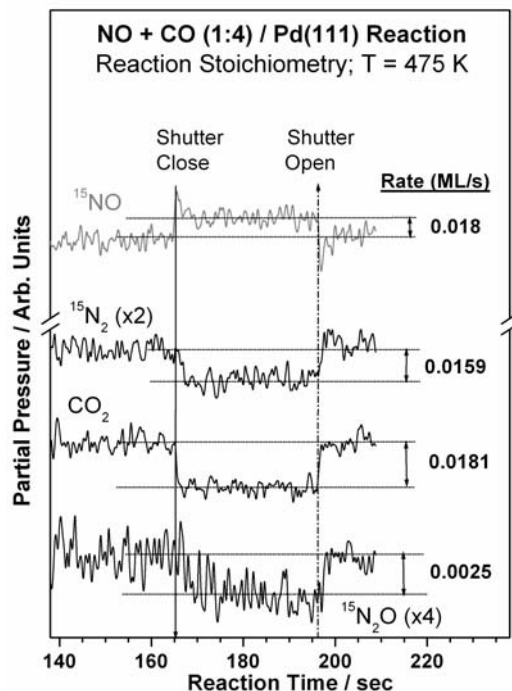


Figure 4.12. Steady-state reaction rates for the NO uptake and N₂, N₂O, and CO₂ production at 475 K with 1:4 NO:CO beam on the Pd(111) surface. The absolute values of the rate were calculated and given for NO and all the products. It is to be noted that the stoichiometry observed in all the experiments changes at temperatures above 525 K, as there is no N₂O production and a 1:1 ratio of CO₂: ½ N₂ is observed.

It is clear that the oxygen for CO oxidation is provided exclusively by NO dissociation, and hence, θ_O entirely depends on eq 4.6. It is also well-known that k_7 is a function of surface coverages. Furthermore, θ_O and $R(\text{CO}_2)$ also depend on the F_{NO} as given in eqs 4.12 and 4.13:

$$\theta_O = \frac{k_6 \theta_{\text{NO}} \theta_{\text{vac}}}{k_7 \theta_{\text{CO}}} = \frac{k_6 \theta_{\text{vac}}}{k_7} \frac{s_{\text{NO}}^0}{k_5 + k_6 \theta_{\text{vac}}} \frac{\theta_{\text{vac}}}{\theta_{\text{CO}}} F_{\text{NO}} \quad [4.12]$$

and hence

$$R(\text{CO}_2) = \frac{k_6}{k_5 + k_6 \theta_{\text{vac}}} \theta_{\text{vac}}^2 s_{\text{NO}}^0 F_{\text{NO}} \quad [4.13]$$

The s_{NO} changes with temperature and the surface coverage and hence the number of vacant sites too. This also directly affects the proportionality in eq 4.13. Nitrogen atoms also desorb as N₂ around 500 K creating more vacant sites. This hints at a high rate constant for CO₂ production and hence fast changes in the steady-state kinetics.

The CO molecules in the 1:2 and 1:4 of NO:CO compositions remove the dissociated O atoms effectively from the surfaces, especially around 500 K, thereby increasing the reaction rate and the number of vacant sites. This helps in turn a larger dissociation of NO. However, at >500 K, s_{NO} and s_{CO} decrease very much and lead to a number of vacant sites; NO and CO desorption rates may play a significant role increasingly at higher temperatures. [103-105,146]

In the CO-rich beam (1:15 of NO:CO) the NO + CO reaction is not effective under the present experimental conditions. This is attributed to a CO poisoning effect at <500 K and fast desorption of NO at >500 K. Contrarily, in NO-rich beams (2:1 NO:CO) the dissociated O and N atoms hinder the further adsorption of reactants in the steady state by occupying the sites. CO displacement by NO also leads to a low θ_{CO} and hence a low overall rate. No reactivity is observed at >625 K on Pd(111), compared to the reported reactivity of NO + CO reaction on powder and model supported Pd-catalysts. [101,103] Henry et al. [103] invoked the reverse spillover effect from the support to the metal on Pd/MgO, which helps to move $\text{NO}_{\text{ads}}/\text{MgO}$ to Pd and cause its dissociation at temperatures as high as 723 K and sustain the NO + CO reaction. This explains the high-temperature activity of Pd for the NO + CO reaction and its application in TWC.

Present TPD measurements after the reaction at temperatures ≥ 525 K reveal no θ_{N} and/or θ_{NO} on Pd(111) and indicates that no stabilized NO molecules are present, in contradiction to ref 101. Adsorption of NO/Pd(111) [148] also shows no stabilized N adatoms and/or NO molecules and generally our results are in agreement with the TPD data reported by several groups. [93-96,98,100] Besides, a plot of the steady-state rate as a function of temperature on Pd/MgO [103] displays a volcano shape with a rate maximum between 475 and 525 K, which is in good agreement with the present results. However, a linear increase in rate with temperature up to 625 K on Pd(111) by Goodman et al. [101] is considerably different from our present results. It should be pointed out that reasons for the above discrepancy could be due to the differences between the present single scattering molecular beam experiments, and the batch mode reaction at high pressure ($P_{\text{NO}} = P_{\text{CO}} = 1$ Torr) employed to measure the rate by Goodman et al. [101] Batch reactor studies at high pressure cannot be directly comparable. Furthermore, the reaction mechanism at >500 K is also considerably different at high pressure and under

UHV conditions. At high pressure, high θ_{NO} observed leads to more N_2O ; [101-102] however, only N_2 was produced under UHV conditions in the present report and by Henry et al. [103,105]

4.4.3. A Comparison between (NO + CO)/Pd(111) and (NO+ CO)/Rh(111):

Rh surfaces show high catalytic activity for NO reduction, [76-78] and the NO + CO reaction on Rh(111) has been studied in detail by Zaera et al., [66-67,137,152-154] and Belton et al. [124] It is now worth comparing the activity of Pd(111) and Rh(111) for the NO + CO reaction. The important similarities and differences between the present results on (NO + CO)/Pd(111) obtained using a molecular beam setup and those reports on Rh(111) [66-67,137,152] are presented briefly below. The isothermal kinetic data presented in this work shows a significant reactivity on Pd(111) compared to Rh(111) for the NO + CO reaction. [66-67,137,152] A comparable catalytic activity of Pd(111) to the (NO + CO)/Rh(111) system [66] was observed in the steady state; however, only in the temperature window 425-575 K. However, Rh(111) is active in a wider temperature range from 450 to 900 K. [66] A considerable amount of N_2O production is directly observed on Pd(111) system, but no N_2O was observed directly on Rh(111) under UHV conditions.

The production of N_2 in the transient state is instantaneous on Pd(111) system; however, on Rh(111) system, [66-67,137,152] N_2 production starts only after the accumulation of a threshold coverage of adsorbed nitrogen on the surface which depends on the beam composition and surface temperature. On the basis of the spontaneity of N_2 production, it is clear that no threshold nitrogen coverage concept is operating on the Pd(111) system. At the same time in the (NO + CO)/Rh(111) system, CO_2 and N_2 are produced rapidly in the transient state at low (450-550 K) and high temperatures (>550 K), respectively, because of the immediate availability of surface oxygen or nitrogen atoms from the fast NO dissociation step. [67] This is mainly attributed to the relatively large and constant s_{NO} (~0.8) [137] on Rh(111). The value of s_{NO} is less than 0.5 above 400 K on Pd(111), and this limits the reaction to a large extent and a trend similar to that of Rh(111) is not observed. Additionally, the displacement of CO by NO was observed in the temperature range of 375-475 K in the transient state indicating that the lateral repulsive interactions of CO are more than NO [101] at least above 375 K.

The occurrence of a similar displacement effect on Rh(111) system has also been demonstrated. [67] Although not discussed due to the lack of direct evidence, the nitrogen formation through N₂O intermediate is not ruled out on Pd(111). However, Zaera and Gopinath [154] have published kinetic evidence for the formation of nitrogen through an N₂O intermediate on Rh(111). Loffreda et al., [143-145] have investigated the NO + CO reaction through theoretical calculations on (111) and (100) facets of Pd and Rh surfaces and found that NO dissociation was endothermic on Pd and exothermic on Rh at low coverages. In general, the above comparison indicates a good similarity in the activities of Pd and Rh, and more work needs to be carried out for full commercial exploitation of Pd.

4.5. Summary

A kinetic study on the NO + CO reaction on Pd(111) surfaces carried out at a wide range of temperature, beam composition and total flux is reported. The isothermal kinetic study of the NO + CO reaction on Pd(111) surfaces reveals significant and comparable catalytic activity as that of Rh(111) in the narrow temperature window 475-575 K. Detailed kinetic experiments and analysis suggests that N₂ formation limits the rate of the overall reaction below 525 K. However, the NO dissociation step contributes in a major way toward the RDS above 525 K. Direct displacement of CO_{ads} by NO was observed between 375 and 475 K and the transient state coverage calculations show that the surface composition was different from the NO:CO beam composition at low temperatures. The rate of NO + CO reaction increases linearly with increasing total beam flux and indicates a first order dependence on F_{NO} .

Irrespective of the NO:CO composition, a rate maximum always occurs at 475 K (or between 475 and 525 K) for all the beam compositions investigated. However, there is a broadening of the active rate regime from 475 to 525 K for 2:1 to 475-625 K for 1:4 NO:CO. The reaction rate is maximum for the 1:4 NO:CO beam composition among all the compositions studied. Both NO-rich and CO-rich beams show poor catalytic activity and is attributed to surface poisoning by those species.

Chapter 5

*CO + O₂ Reaction on Pd(111) Surfaces**

“CO oxidation on Pd(111) surfaces was revisited to explore the microkinetic details of the reaction, essentially due to the recent observations such as, surface oxide (Pd_xO_y) formation and oxygen diffusion into the sub-surface/bulk. The reaction was studied under wide range of conditions, such as CO:O₂ compositions ranging from 4:1 (CO-rich) to 1:20 (O₂-rich) between 375 K and 600 K, and oxygen-rich conditions are relevant to automobiles. Interesting results were observed for the transient state (TS) of the reaction. It is clearly demonstrated that direct CO adsorption is feasible with significant sticking coefficient at high temperatures (500 – 600 K) on oxygen-covered Pd(111) surfaces under steady-state (SS) conditions and hence no significant oxygen poisoning was observed. However, some time delay in starting the CO₂ production and reaching the SS is observed; the above delay also decreases with increasing oxygen content and instantaneous CO₂ production is observed with O₂-rich beams. CO adsorption characteristics shows some similarity in the two extreme conditions on clean Pd(111) between 375 and 450 K, and oxygen covered Pd(111) surface above ≥ 500 K. Low temperature regime (375 - 450 K) is dominated by CO-adsorption, especially with CO-rich beams. An intermediate temperature regime (450 - 525 K) generally exhibits high rate for all compositions. In the high temperature regime (≥ 525 K) overall CO₂ formation rate is controlled by CO-adsorption, in spite of a possible oxygen diffusion into the subsurface/bulk of Pd(111). Differential coverage calculated from the TS data clearly correlates with the fast reaching of SS with high rate regime when the above coverage is close to zero.”

* Thirunavukkarasu, K., Gopinath, C. S.- Two articles are in preparation.

CO + O₂ Reaction on Pd(111) Surfaces

5.1. Introduction

A detailed understanding of the catalytic processes is mandatory particularly to manipulate the catalytic activity in the desired direction. Especially, the dynamic changes in coverage on a catalyst surface during a heterogeneous catalytic process, especially in the transient state (TS), lead to enormous changes in the macroscopic kinetics. Bistability behavior associated with catalyst nanoparticles of intermediate size and higher ($\geq 6\text{nm}$) with the CO+O₂ reaction was recently addressed by Libuda et al [155] on Pd/Al₂O₃ system and it was shown that the coverage fluctuations on catalyst particles could change the macroscopic catalytic behavior. Indeed, not many studies have been carried out so far for the CO + O₂ reaction on Pd(111) surfaces [118,156-158]. Although the chemical reactivity of bulk or subsurface oxygen was indicated in few studies, it has not been addressed in detail for the above reaction [158]. Nonetheless, high reactivity of oxygen on Pd surface, oxygen diffusion into bulk and formation of surface palladium oxides have been reported in the recent past by few research groups [123,127-134,159-166] In fact Engel and Ertl [118] had earlier studied CO + O₂ reaction on Pd(111) surfaces by molecular beams, and it was well established that the CO oxidation reaction on Pd(111) surface occur through Langmuir-Hinshelwood mechanism, and not through Eley-Redeal mechanism. They successfully elucidated the reaction mechanism for the first time through atomic elementary steps for the reaction on Pt group metals [167]. There are a significant number of reports on CO+O₂/Pd system dealing with sticking coefficients, TS and SS kinetics, IR spectroscopy etc [147,166-177].

Recent developments in the understanding of Pd(111) surfaces, particularly its interaction with oxygen and formation of 2-D surface oxides and their decomposition, subsurface diffusion, bulk oxide formation and segregation of oxygen species upon heating rekindled the necessity of a better understanding of the CO oxidation on palladium surfaces. The oscillatory nature of the CO oxidation reaction on platinum group metals is yet to be resolved and this might be partly due to not so clear understanding of oxygen interaction with palladium surfaces [177]. Reports in the last six

years on this topic have thrown some light on the understanding [123,127-134,159-164]. Furthermore it is important in pollution control processes particularly in three-way catalytic converters fitted in automobiles, since Pd-only catalytic converters are in use for the last few years, [79-80] and in power generation centers. Hence a revisit on CO oxidation on Pd(111) surface was made with molecular beams under isothermal conditions. Molecular beam (MB) studies coupled with temperature programmed desorption (TPD) results provide valid information on the kinetics of a particular process. From our present studies of CO+O₂ reaction on Pd(111) surfaces under a broad conditions, it is clearly demonstrated that direct CO adsorption is feasible with significant sticking coefficient at high temperatures (550 – 600 K) on oxygen-covered Pd(111) surfaces under SS conditions, and hence no significant oxygen poisoning was observed. However, some time delay in starting the CO₂ production and reaching the SS is observed; the above delay also decreases with increasing oxygen content and instantaneous CO₂ production is observed with O₂-rich beams. The above delay is due to preferential oxygen adsorption from the CO+O₂ beams. Some of our results were possible exclusively due to the employment of molecular beam techniques, without which we might not have observed the above results.

5.2. Experimental

The Pd(111) sample was cleaned by Ar⁺ sputtering in the presence of an oxygen atmosphere as described in earlier chapters. [95-96] CO (99.99%), and O₂ (99.9 %) were used without any further purification. 0.04 ML/s total flux of the CO + O₂ mixture ($F_{\text{CO+O}_2}$) with a desired composition was used in all the experiments reported here unless otherwise specified. The mass spectrometer intensities for CO and O₂ were calibrated by measuring the CO and O₂ uptake on clean Pd(111) at 300 K separately, assuming a saturation coverage of 0.50 monolayer (ML) for CO and 0.25 ML for O₂ following Engel and Ertl. [118] An exposure of 1 ML corresponds to 7.8×10^{14} molecules/cm². Further, the steady-state rates given in the figure 5.14 have $\pm 5\%$ error margin.

5.3. Results

5.3.1. Typical Isothermal Kinetic Measurements:

All the results reported in this manuscript were carried out in the following typical procedure and an example is given in Figure 5.1. For all experiments Pd(111) was kept at a constant temperature and exposed to CO+O₂ beam of desired composition. The partial pressure of all the relevant species was recorded as a function of time. Figure 5.1 shows a typical raw kinetic data obtained by exposing 1:2 CO:O₂ beam on clean Pd(111) surface kept at 400 K. A series of actions were taken during these experiments are given below: (1) 1:2 CO:O₂ beam was turned on at $t = 10$ s, after recording the background intensity of the relevant mass species for a short while. At this point reactant molecules (CO and O₂) are scattered in the UHV chamber. An immediate increase in the partial pressures of CO and O₂ could be clearly seen and their partial pressure values increase up to a new steady-state value. It is to be noted that the partial pressure of CO₂ does increase at this point due to the reaction between the background reactants on Pd(111) surface. This represents a maximum of 4% of the total rate and not included in the data analysis. (2) Around $t = 15$ s the shutter, till then blocking the beam from impinging the Pd(111) surface directly, was removed to allow for direct adsorption of reactants on the surface. A decrease in the partial pressure of the reactants was observed and along with a slow increase in the CO₂ partial pressure. This stage is termed as the transient state (TS) and will be discussed in detail later. A careful look at the CO₂ evolution data exhibit about 2 s delay in starting the CO₂ production, although CO and O₂ adsorbs at the point of shutter removal. (3) The CO+O₂/Pd(111) system is allowed to evolve until a steady state (SS) is reached, which normally occurs somewhere between 0 and 30 s after shutter removal; in the present example in Figure 5.1 SS reaches around $t = 25$ s (10 s after shutter opening). Obviously the rate of adsorption of reactants and desorption of products does not change with time in SS. (4) In the SS the MB was deliberately blocked between $t = 60 - 90$ s to measure the steady state rate of the reaction. There is a clear increase in the partial pressure of CO and O₂ and a drop in CO₂ partial pressure. A new SS reaches in few seconds after blocking the beam. It is to be noted that the partial pressure of CO increases above the new SS, but no such change in O₂, indicating some CO desorption at the point of beam blocking. Similarly, CO₂ partial pressure reaches the new SS after a delay of about 7-8 s

and there is a slow decay in the partial pressure is observed. Indeed, the above observation of slow CO₂ decay and CO desorption in the SS varies with reaction temperatures and beam compositions. (5) After about 30 s from the blocking of the beam, the shutter was removed again at $t = 90$ s and again the reaction is allowed to return to the earlier SS mentioned in point 3.

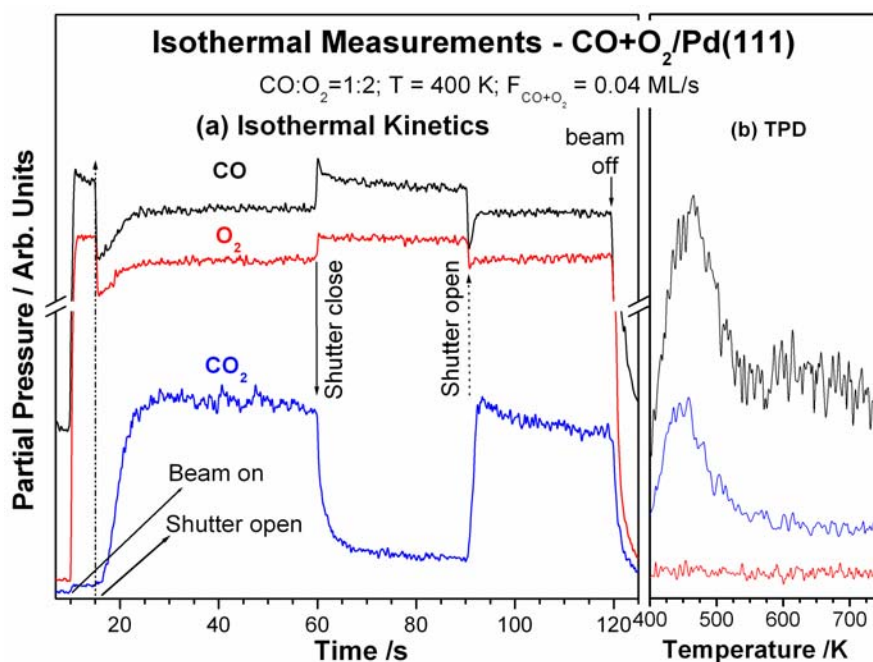


Figure 5.1 (a) A typical raw kinetic data measured under isothermal condition. An effusive 1:2 CO:O₂ molecular beam was directed onto Pd(111) surface kept at 400 K and the relevant mass species (CO, O₂, CO₂) ($amu = 22$ followed, but not shown) were followed as a function of time. The beam was deliberately blocked in the steady state at $t = 60$ s and unblocked at $t = 90$ s to measure the rate of the reaction and shown by solid and dotted arrows, respectively. (b) TPD spectra for the relevant species in the CO+O₂ reaction after the above isothermal experiment at a heating rate of 10 K/s.

Again a clear adsorption of the reactants and a slow rise in the CO₂ production is observed, as in the TS, but at a lower level. The reaction was allowed for some more time under SS conditions and the beam was shut-off at $t = 120$ s. (6) Partial pressure of the reactants and the product reach their initial levels in few seconds and then the crystal temperature was ramped at a constant rate of 10 K/s to record TPD. The results from the TPD are shown in Figure 5.1b. A clear desorption of CO and CO₂ indicates the presence of reactants on the surface after the reaction. For reaction temperatures above 500 K there

is no CO/CO₂ desorption observed, since the desorption maximum is below 500 K and only oxygen desorption is observed, and that too with oxygen rich beams, at high temperatures (>650 K). The flux for all the mixed beams reported here was set to 0.04 ML/s except for flux dependent studies.

5.3.2. Adsorption of Oxygen on Pd(111) surface:

One of the main purposes of the present work is to understand the oxygen solubility and/or oxygen diffusion into the subsurface and bulk in Pd. It is important to know the extent of oxygen diffusivity in the Pd(111) before we present the results on CO+O₂ reaction. A set of experiments were carried out to saturate the Pd(111) surface with oxygen and titrate with CO. Adsorption of oxygen on Pd(111) was performed at different temperatures ranging from 400 K to 800 K at a constant flux (0.04 ML/s) followed by CO titration at oxygen adsorption temperature or at 500 K, whichever is minimum. Figure 5.2a shows the oxygen uptake on the Pd(111) surface. A careful look at the oxygen uptake at low temperatures and ≥ 700 K demonstrate a fact that oxygen uptake continues, at least at lower level, at high temperatures as long as the oxygen beam is present; however oxygen adsorption stops after the surface saturation at temperatures ≤ 500 K. The dashed line shown on some of the traces, which connect the O₂ partial pressure before opening the shutter and after reaching the SS, where there is no adsorption, demonstrate the above. A blind experiment carried out without removing the shutter shows the pressure trend as that of 400 K, except for oxygen uptake initially. The above points clearly indicate a non-zero and significant sticking coefficient (S) of oxygen ($\sim 0.03 - 0.001$) on fully O-covered Pd(111) surface at high temperatures. It is likely that the O₂ adsorption involves an activated stage. The above observations hints that there could be oxygen diffusion into the sub-surface or bulk Pd(111) and the same increases significantly at high temperatures (≥ 600 K) and hence a small, but observable s_0 . Our results are in agreement with Klotzer et al [164] and Leisenberger et al. [123]

After 100 Langmuirs of oxygen dosing, O₂ beam was shut off and evacuated to background level and CO titration was carried out. Upon CO titration on the O/Pd(111) surfaces, CO₂ was produced and the amount of CO₂ desorbed is given as I_{CO2} in Figure 5.2b. It is clear that I_{CO2} the same up to 450 K. At and above 500 K, the oxygen coverage measured through the CO titration decreases linearly with increasing temperature of

oxygen dosing up to 600 K. An order of magnitude difference in CO₂ desorption is observed for every hundred degree above 600 K up to 800 K. The above observations clearly demonstrate that under the present experimental conditions oxygen diffuses into the subsurface ≥ 500 K. Indeed, similar observation was made from our earlier studies on NO/Pd(111) ≥ 475 K, followed by CO titration [Section 3.3.3, 148].

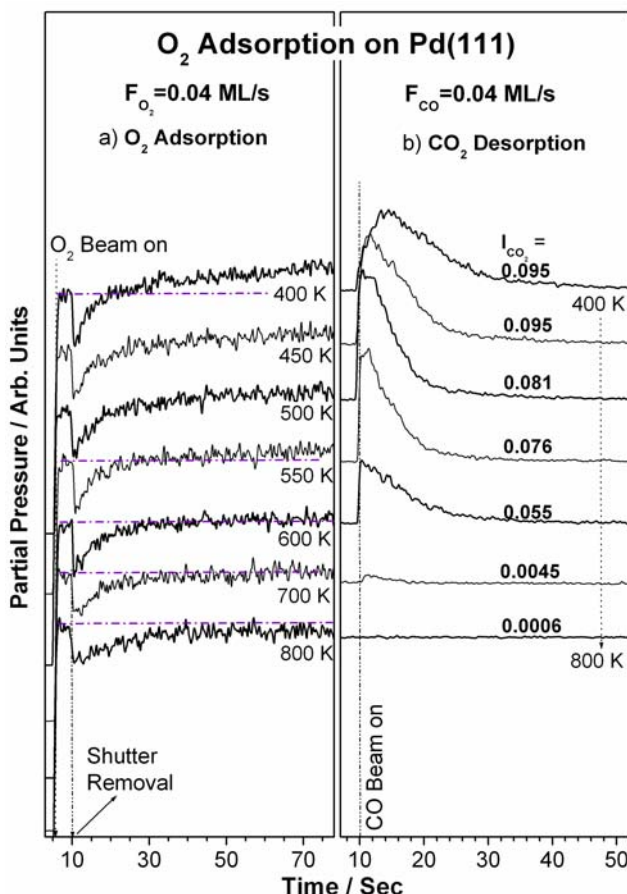


Figure 5.2: (a) Oxygen uptake from oxygen molecular beam on clean Pd(111) at different temperatures. (b) CO₂ desorption from the oxygen covered Pd(111) surface prepared above through CO-titration at the oxygen dosing temperature. Integrated CO₂ desorption is given. Note the decrease in CO₂ desorption ≥ 500 K and no CO₂ desorption at 800 K in spite of continuous oxygen uptake.

Our present result also agrees well with the result reported by Schlogl et al on oxygen disappearance on Pd(111) > 573 K [162-163]. Very small or no CO₂ production was observed ≥ 700 K due to dissolution of oxygen into the bulk at a relatively fast rate and/or due to oxygen desorption [160]. Due to the above observations and facts, we have set our reaction temperature window between 375 K and 600 K for the study of CO oxidation on

Pd(111) surface to minimize the complications that arise due to oxygen desorption or diffusion into the sub-surface and the bulk.

5.3.3. Transient Kinetics:

Transient state (TS) kinetic details of the CO+O₂ reaction on Pd(111) surface will be discussed in detail in the following sections, and it clearly demonstrates the dynamic behavior of adsorbate coverages and their effect on product formation. TS have been particularly important for CO oxidation reaction on Pd surfaces, particularly because of the fast desorption of CO₂ immediately after its formation on the surface. The trends in the changes in the partial pressure of all the relevant species after shutter opening gives original information on CO₂ formation.

5.3.3.1. Temperature Dependence:

Figure 5.3 shows the temperature dependence of reactants, CO and O₂, adsorption (a and b respectively) and product CO₂ desorption (c) with a CO:O₂ beam composition of 2:1 on Pd(111) surface. A careful analysis of all TS raw kinetic data indicates that there are three temperature regimes and the CO₂ desorption trend changes significantly in the above regimes. It is explained in detail with the results shown in Figure 5.3 for a 2:1 CO:O₂ composition. (1) Between 375 and 425 K: An unambiguous CO and O₂ adsorption was observed initially on Pd(111) at the point of shutter removal and adsorption continues depending on the CO₂ production rate. Indeed large CO adsorption is evident from the substantial CO uptake from the beam at lower temperatures. However, O₂ adsorption is not that high as that of CO. Continues CO and O₂ adsorption at $t > 40$ s marks the beginning of the steady state (SS) clearly above 400 K, albeit a low level changes in the steady-state partial pressure of CO and O₂. CO₂ desorption in the TS continues up to 40 s and thereafter reaches the SS. Nonetheless, compared to SS rate, an over production of CO₂ is observed after a few seconds (5 s at 375 K) delay. The above delay is with respect to the shutter removal time, where a clear adsorption of reactants seen. The above delay decreases with increasing substrate temperature. Further, the over-production of CO₂ also decreases with increasing temperature. (2) Between 450 and 525 K: Although a clear CO adsorption is seen at the point of shutter removal, a overall CO uptake directly from the beam decreases with increasing temperature. It is also clear that

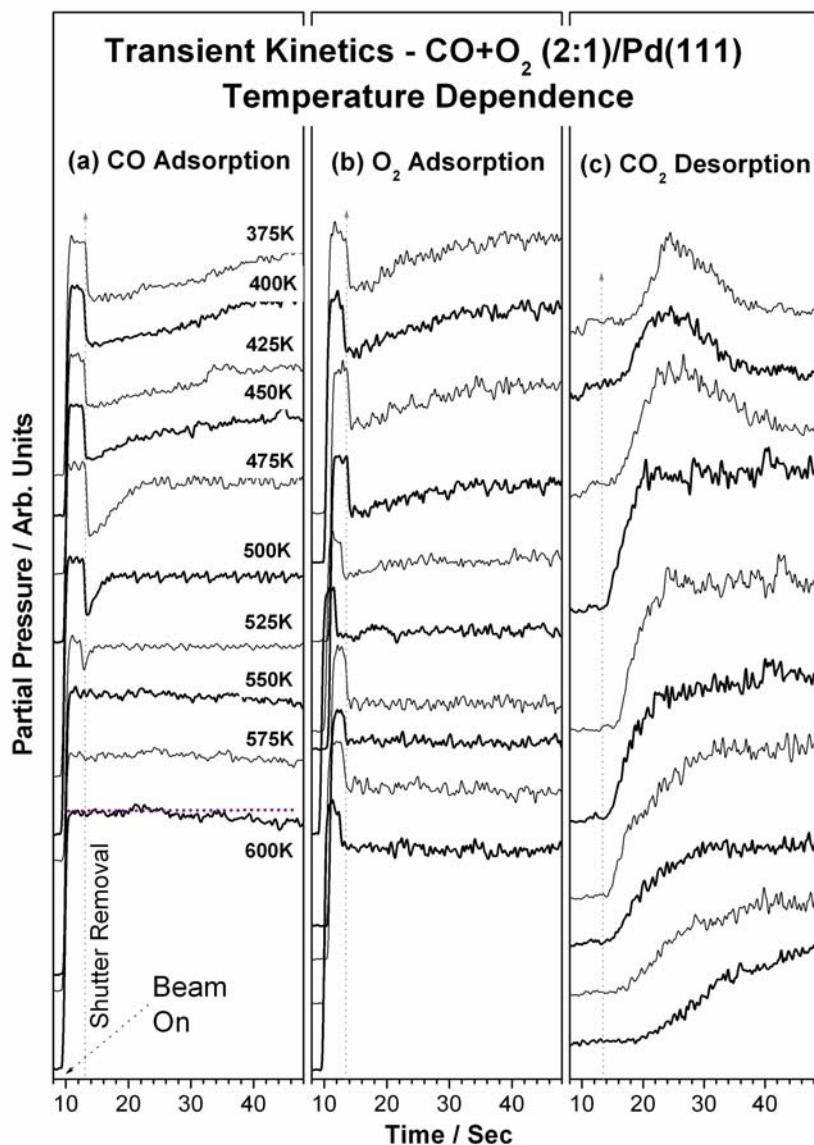


Figure 5.3: Time evolution of the partial pressures of (a) CO, (b) O₂, and (c) CO₂ during the transient state of the CO + O₂ (2:1) experiments on Pd(111) as a function of substrate temperature. Fast steady-state reached in the intermediate temperature regime of 450 to 500 K to be noted.

the rate of CO desorption increases above the CO desorption maximum at 450 K. On the contrary, O₂ adsorption increasingly dominates the Pd(111) surface, in spite of CO-rich beam composition (CO:O₂ = 2:1) employed. Indeed, same O₂ sticking coefficient is evident throughout the reaction at 525 K. CO₂ desorption reaches the SS slowly but directly after a delay of 7-8 seconds. It is to be noted that there is no over-production of CO₂ in the TS in this temperature regime. (3) Above 550 K: Apparently no CO

adsorption could be seen in the TS; however a decrease in CO partial pressure at higher time on stream (> 30 s), compared to initial, and hints a direct CO adsorption from the beam. A dotted line drawn on 600 K here demonstrates a significant CO adsorption at $t > 30$ s. Oxygen adsorption remains the same as observed above at 525 K. The TS rate slowly increases and reaches the SS after a time delay and the time delay increases with increasing temperature with respect to CO₂ production. Indeed, no CO₂ production was observed after the shutter removal till $t = 21$ s at 600 K; even after that the CO₂ rate increases very slowly and reaches its maximum rate around $t = 45$ s. Although there is delay observed in a similar fashion at low (375 K) and high temperature (600 K), it is obviously due to different reasons, such as CO poisoning and likely oxide (Pd_xO_y) formation, respectively. This will be discussed latter.

5.3.3.2. Beam Composition Dependence:

Figure 5.4 shows the CO:O₂ beam composition dependence of adsorption of CO and O₂ species and CO₂ desorption in the TS from Pd(111) surfaces at 425 K. Similar to the above temperature dependence description, there are three regimes are apparent, namely, (a) CO-rich, (b) stoichiometric, and (c) oxygen-rich regime. (a) CO-rich regime (CO:O₂ < 2:1): An enormous CO adsorption is clear from the CO pressure drop in the TS after shutter removal. Significant oxygen adsorption also is observed. A clear excess CO₂ over production is observed after a delay of few seconds, depending on the CO-content in the beam. (b) Stoichiometric regime (1:1 to 1:4): A significant amount of CO and oxygen adsorption is apparent in the TS upon shutter removal. In less than 20 s, ($t < 35$ s) adsorption of reactants species reaches a SS, where there is no change in adsorption characteristics. Indeed, almost the same oxygen adsorption continues with 1:1 composition indicating the sticking coefficient of oxygen remains the same throughout the reaction period. Oxygen (CO) adsorption in the TS continues to increase (decrease) with oxygen content in the beam. CO₂ production rises gradually and reaches the SS directly. Nonetheless, with increasing oxygen content in the beam, a slight over-production of CO₂ is observed. An unambiguous increase in slope of CO₂ leading edge in the TS demonstrates an increase in the rate with increasing oxygen content. (c) Oxygen rich regime ($\geq 1:7$): Large oxygen adsorption is restricted only to the TS and this trend increases with increasing oxygen content. Conversely, continuous CO adsorption is seen

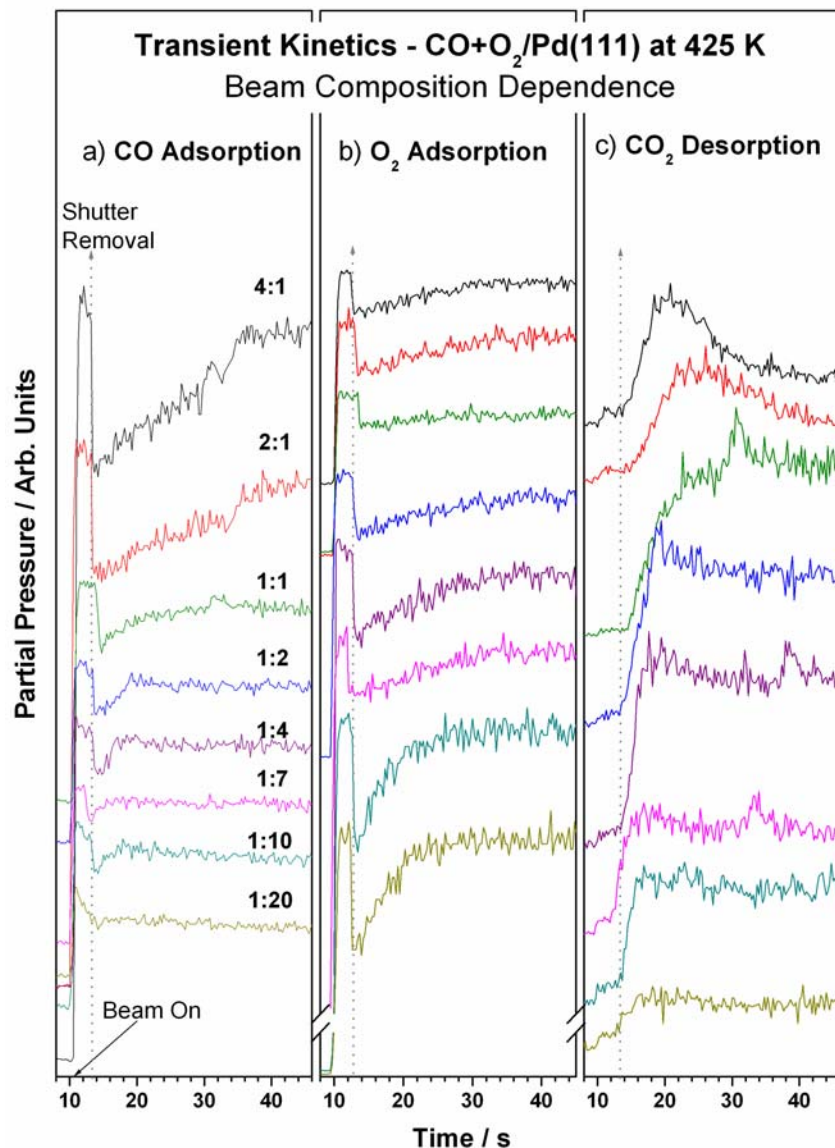


Figure 5.4: Time evolution of the partial pressures of (a) CO, (b) O₂, and (c) CO₂ during the transient state of the CO + O₂ reaction at 425 K on Pd(111) as a function of different ratios of CO:O₂. Fast steady-state reached in the intermediate beam compositions (1:1 to 1:10 CO:O₂) regime is to be noted.

for oxygen-rich beam (1:20) and this trend decreases with decreasing oxygen content. CO₂ production reaches the SS directly and quickly, although the overall rate decreases with increasing oxygen content. Although the 1:20 beam composition is oxygen rich, a considerable CO₂ production clearly exhibits a preferential CO-adsorption. A further analysis hints almost the same SS rate of CO₂ production for 4:1 and 1:20 hints that the

rate of adsorption of oxygen or CO poisoning, respectively, is similar. However, it is not that simple and different scenarios observed are explained in Figure 5.5 with CO₂ desorption in the TS at different temperatures.

Figure 5.5 gives an overall and better analysis of how the substrate temperature and CO:O₂ beam compositions influence the transient kinetics of CO+O₂ reaction on Pd(111) surface. Raw TS kinetic results are shown for representative beam compositions and temperatures in different regimes. Before we proceed further a brief definition is given here on what is CO₂ over-production and under-production observed in the TS, and indeed it is defined by Gopinath and Zaera [67]. It is basically to obtain the coverage differential parameter ($\Delta\Theta^{\text{TS}}$), and it is a difference between the experimental CO₂ yields and those expected if the reaction were to reach the SS immediately after the shutter removal without any transient state. No background contribution is considered here, however the trends in the data are expected to shed some light on the underlying surface changes, especially surface composition. More details about the calculations are given in [67].

It is clear from Figure 5.5, that over-production of CO₂ observed in the TS at 400 K with CO-rich beam (4:1) changes to under-production ≥ 475 K. Apart from the above, there is a time delay in the beginning of CO₂ production ≥ 475 K, after shutter removal, and it increases with increasing temperature (13 s at 600 K) with 4:1 beam. Oxygen adsorption increases with substrate temperature, in spite of the CO-rich composition (See Figure 5.8). An interesting observation to be highlighted here is the steady oxygen uptake from CO rich beams at >525 K; however a delay in the beginning of CO adsorption and this delay increases with temperature. This important observation clearly demonstrates that direct CO adsorption is feasible at high temperatures on oxygen covered surfaces with significantly high sticking coefficient and hence a reactive CO adsorption. It is reminded here that CO sticking coefficient decreases dramatically above the CO desorption maximum (450 K) on clean Pd(111) [118].

For the 1:2 composition, an under-production of CO₂ is observed at 400K; nonetheless at higher temperatures, CO₂ production reaches directly to SS. Although oxygen adsorption is high at high temperatures for 1:2, competing CO adsorption also could be seen and this fact supports the reaching of an instantaneous SS (See Figures 5.7

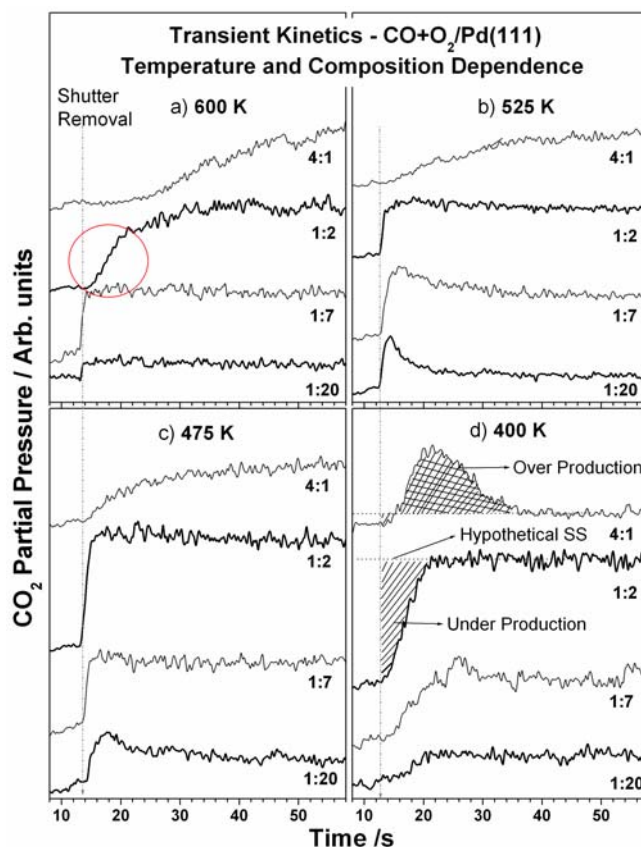


Figure 5.5: Temperature dependence of the CO₂ desorption in the transient state for four representative beam compositions at (a) 600 K, (b) 525 K, (c) 475 K and (d) 400 K. Hatched and cross-hatched areas indicate the under-production and over-production of CO₂ in the transient state. Hypothetical steady-state indicated by a dotted line helps to calculate the above quantities to know the change in surface composition.

and 5.8). This clearly indicates the surface adsorbate stoichiometry might be close to the expected ratio of CO:O = 1:1 under the above conditions. When the CO:O₂ beam becomes significantly oxygen-rich (1:7), almost the same observations were made as that of 1:2 beam. Two exceptions to be noted are a slight over-production of CO₂ at a temperature regime around 525 K, and an instantaneous CO₂ production even at 600 K. It is to be noted that a clear and continuous CO adsorption observed after shutter opening indicates the favorable conditions for high CO₂ rate regime extends to high temperatures with oxygen-rich beams. The trend observed with highly oxygen rich beam (1:20) is similar to that of 1:7 beam composition. However a slight over-production of CO₂ at >450 K and a direct SS observed at the point of shutter removal at T = 600 K, as in 1:7. It is to be noted that as the oxygen content increases in the beam, an overall decrease in

CO₂ rate is observed and it is partially due to decreasing F_{CO}. Nonetheless, an important conclusion is made here on using excess oxygen in the beam. No oxygen poisoning seems to occur or hamper the reaction, at least under the above conditions employed in our studies up to 600 K. Although there are some indications of oxygen poisoning only in the TS under certain conditions, a slow recovery in the TS to high rate SS regime suggests that in the presence of sufficient CO flux, oxygen poisoning does not prolong and it undergoes dynamic changes (Figure 5.5d).

5.3.3.3. CO+O Coverage Differential ($\Delta\Theta^{\text{TS}}$):

The transient differential coverages ($\Delta\Theta^{\text{TS}}$) for CO₂ production were calculated for all the beam compositions and reaction temperatures studied and given in Figure 5.6 as a function of (a) temperature and (b) beam composition. Estimated errors involved in these results vary between 5-15%; and the error is less when $\Delta\Theta^{\text{TS}}$ is highly positive or negative (most/least CO₂ produced in the TS), and high when $\Delta\Theta^{\text{TS}}$ is close to zero. It is very well known that CO₂ desorption is instantaneous [118] and hence the coverage calculated above is the sum of the equal amount of CO and O coverages. Hence for desorption of every CO₂ molecule there will be two vacant sites available for further reaction and hence the $\Delta\Theta^{\text{TS}}$ values measured through the method described above is multiplied by a factor two and given in y-axis on Figure 5.6a. Further the above coverage does not include non-reacting CO and O species. In Figure 5.6, positive and negative values indicate an over-production and under-production of CO₂, respectively, in the TS. CO-rich compositions (4:1, 2:1 and 1:1) produce excess CO₂ of the order of $\Delta\Theta^{\text{TS}} = 0.035$ ML and it decreases with increasing temperature. A glance at the CO and O₂ uptake under the above conditions (shown in Figures. 5.7 and 5.8) indicate the surface is still dominated by adsorbed CO at T <500 K. At T >500 K an under production of CO₂ was observed up to the tune of $\Delta\Theta^{\text{TS}} = - 0.12$ ML depending on the beam composition and temperature. For oxygen rich beams (1:20, 1:10 and 1:7) the above trend changes almost in an opposite manner, but the extent of $\Delta\Theta^{\text{TS}}$ is not that high as in the above case. $\Delta\Theta^{\text{TS}}$ varies from -0.035 ML at 375 K to 0.04 ML on the high temperature side depending on the CO:O₂ composition. Above observations in CO and O₂ rich beams suggests the changes, especially the surface composition, occurring on the Pd(111) surfaces also reverses from CO-rich to oxygen-rich beam compositions. Nonetheless, for

intermediate beam compositions (1:2 and 1:4), $\Delta\Theta^{\text{TS}}$ turns out to be close to zero for all of the temperatures studied. A comparison of the SS rate measured for the CO+O₂ reaction and the $\Delta\Theta^{\text{TS}}$ shows, in general, the rate maximum occurs when the $\Delta\Theta^{\text{TS}}$ is close to zero and this aspect will be discussed later.

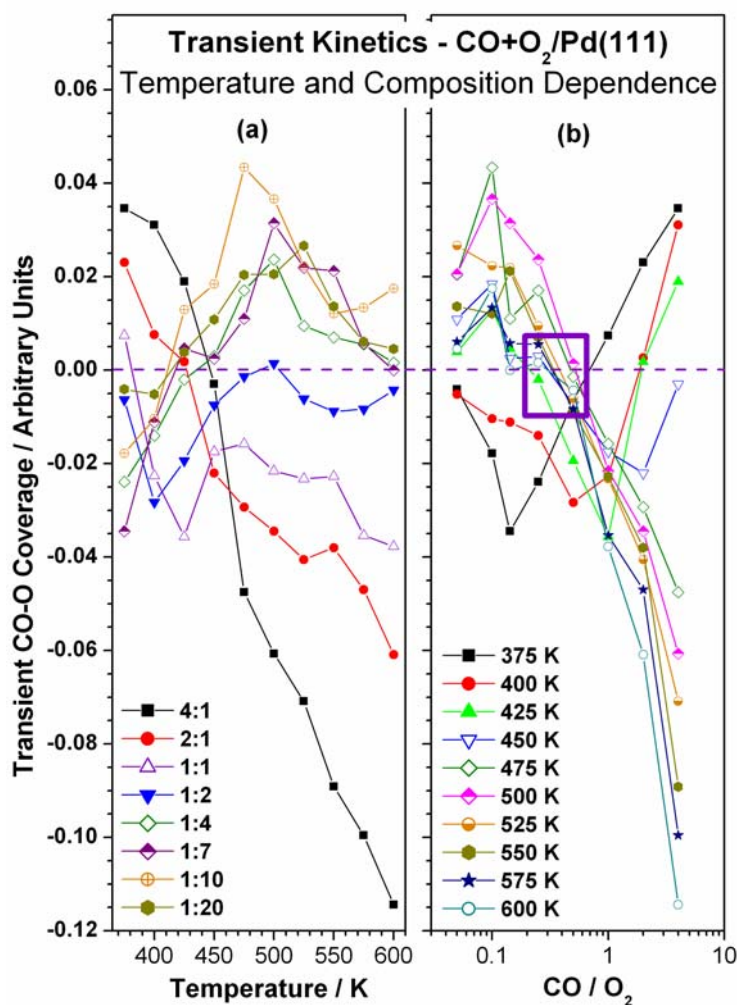


Figure 5.6: Transient CO₂-coverage differential ($\Delta\Theta^{\text{TS}}$) measured for different CO:O₂ beam compositions at different reaction temperatures. $\Delta\Theta^{\text{TS}}$ is plotted as a function of (a) temperature and (b) CO:O₂ ratio. It is to be noted that the steady-state reaction rate reaches the maximum with any beam composition when $\Delta\Theta^{\text{TS}}$ is close to zero and the same is highlighted with a rectangular box for 1:2 and 1:4 beam in panel b.

Figure 5.6b shows the beam composition dependence of $\Delta\Theta^{\text{TS}}$ for all the temperatures employed. Certain important features are worth highlighting here are as follows: (1) 1:2 and 1:4 beam compositions shows a $\Delta\Theta^{\text{TS}}$ value very close to zero for almost the entire active temperature range (shown in a box in Figure 5.6b). (2) Oxygen-

rich (1:20) and CO-rich (4:1) beams show a positive and negative $\Delta\Theta^{\text{TS}}$ value, respectively, in the TS for the active temperature window indicating no oxygen poisoning with oxygen-rich beams, but some oxygen-poisoning associated with CO-rich beams, especially at high temperatures. Indeed, the later observation is not expected. (3) A region, marked by a rectangular box, indicates a regime where $\Delta\Theta^{\text{TS}}$ is close to zero and it comprises, mostly, the high steady-state rate regime. (4) Under most of the active temperature conditions (≥ 425 K), the $\Delta\Theta^{\text{TS}}$ value changes from negative to positive values between 1:2 and 1:4 beam compositions. The last two points clearly suggests a likely possibility of 1:1 surface composition of CO:O and hence the surface coverage in the presence of molecular beam is neither rich in CO nor rich in O. A fast approach towards the SS observed under the above conditions also supports the above point. An exceptional high negative $\Delta\Theta^{\text{TS}}$ value associated with CO-rich beam (4:1) at $T > 500$ K, indicates no net CO-adsorption might be a limiting factor; indeed this is clearly supported by a slow increase in the extent of CO adsorption, but a continuous oxygen adsorption on the surface at high temperatures (see Figure 5.8 and 5.9)

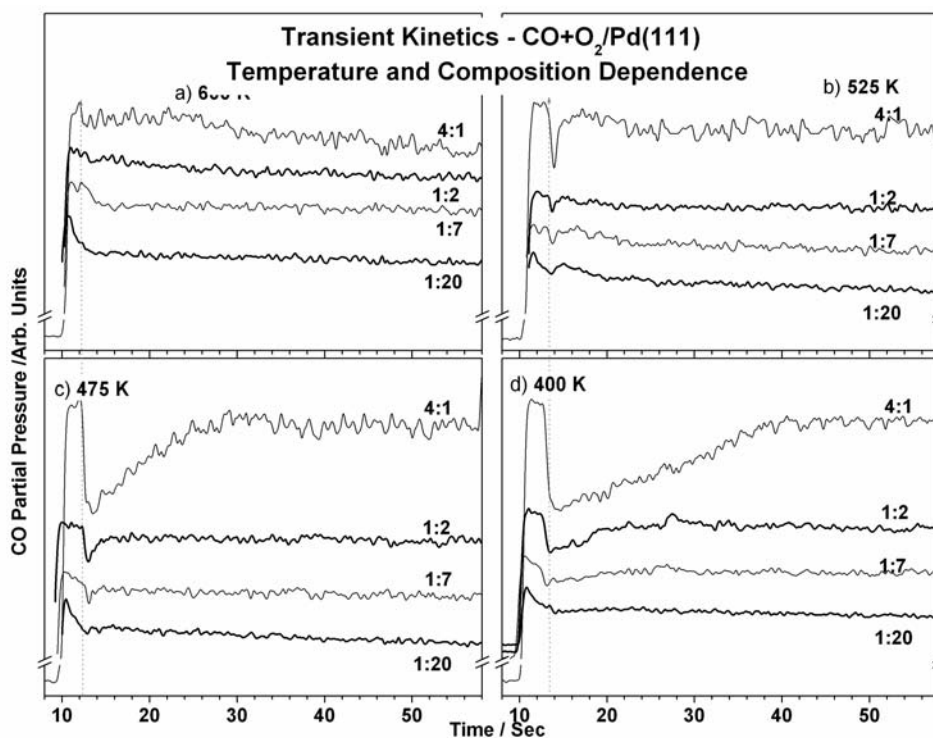


Figure 5.7: Temperature dependence of the CO adsorption in the transient state for four representative beam compositions at (a) 600 K, (b) 525 K, (c) 475 K and (d) 400 K

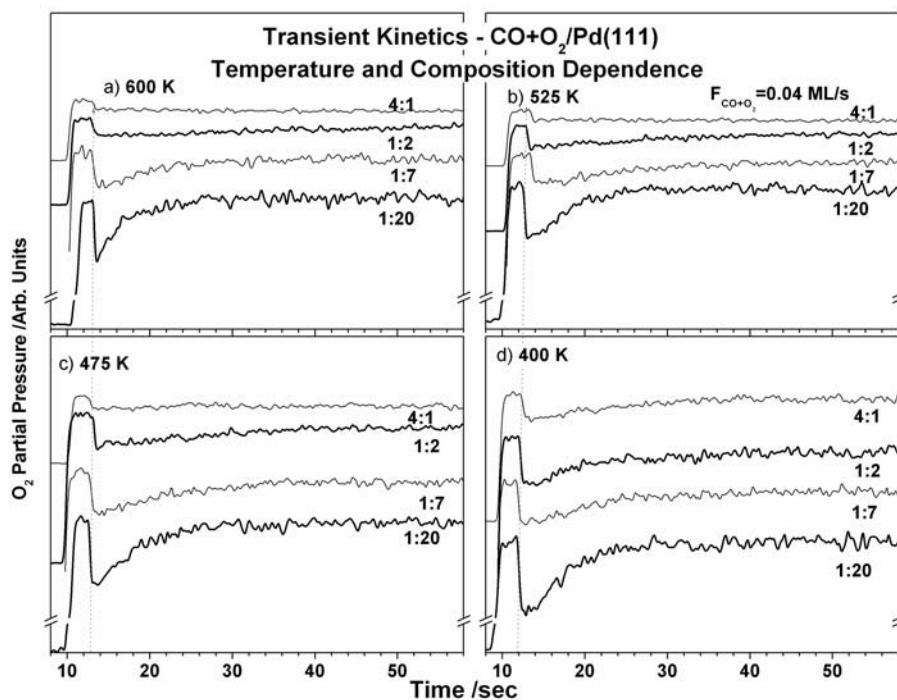


Figure 5.8: Temperature dependence of the O₂ adsorption in the transient state for four representative beam compositions at (a) 600 K, (b) 525 K, (c) 475 K and (d) 400 K

5.3.3.4. CO and O₂ Initial Sticking Coefficients:

Earlier studies have determined that CO adsorption on Pd(111) studies displays high initial sticking coefficients (s^0_{CO}) on the order of 0.96 up to 475 K [118,168,176]. CO and O₂ adsorption from different CO + O₂ beam compositions at four critical temperatures are shown in Figures 5.7 and 5.8, respectively. The adsorption kinetics for CO, however, does change significantly in the presence of oxygen. Figure 5.9 displays the dependence of the (a) s^0_{CO} and (b) $s^0_{\text{O}_2}$ on temperature for all of CO:O₂ ratios the above sticking coefficient values were measured from the data shown in Figures 5.7 and 5.8, but at all temperatures between 375 K and 600 K. It is to be noted that although the total flux was kept constant in all of these experiments, flux of either of the reactants change with the beam composition. The s^0_{CO} were calculated from the drop in CO or oxygen partial pressure at the shutter-removal time, as described in our earlier publication [148 and **Chapter 2**]. It is also to be mentioned here that these values for s^0_{CO} as well as $s^0_{\text{O}_2}$ are not true initial sticking coefficients on the clean surface, but only approximations due to the adsorption from background gases that occurs before the unblocking of the

beam. Pure CO or O₂ adsorption from CO or O₂ beam respectively, was also measured and plotted in Figure 5.9 and shown by a solid line. Data shown in Figure 5.9a indicates that, independent of CO:O₂ compositions, at low temperatures (<425 K) all the beams show high s^0_{CO} values (around 0.9) comparable to that of on clean Pd(111) surface. Above 425 K, there is a gradual decrease in s^0_{CO} with increasing temperature, and above 550 K, sticking coefficient becomes immeasurably small. An important observation to be highlighted here is the qualitative trend in declining s^0_{CO} with increasing temperature remains the same for all beam compositions and it is independent of oxygen content. In a way it is not surprising since CO-adsorption takes place very well on oxygen-saturated Pd(111) surfaces, as shown in Figure 5.2. However a decrease in s^0_{CO} at $T > 425$ K from CO+O₂ beam compared to CO beam, indicates that around the CO-desorption maximum temperatures (450 K), and above, there is a significant decreases in adsorption characteristics especially from mixed beams.

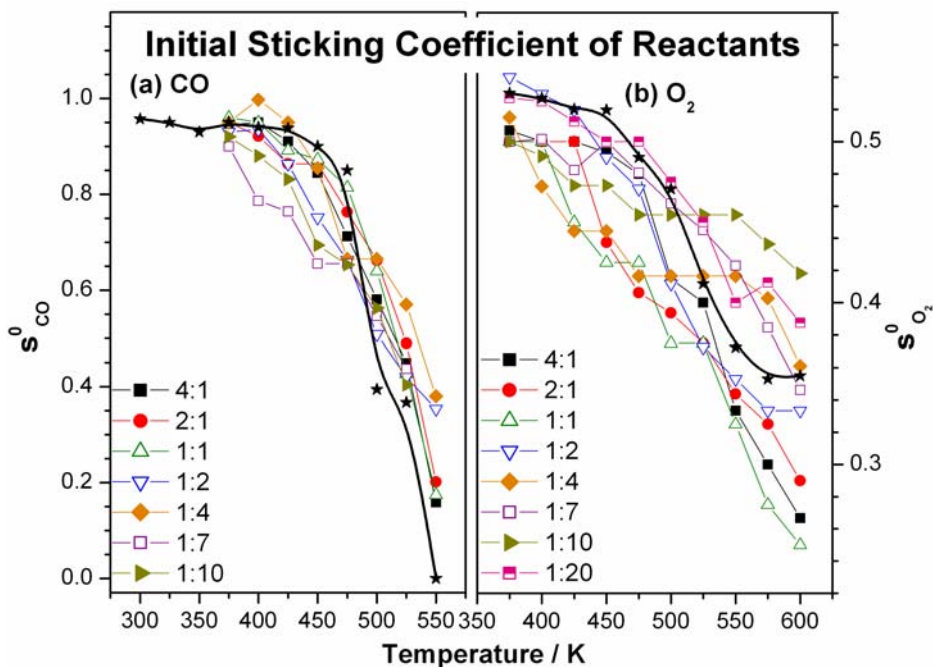


Figure 5.9: Initial sticking coefficients for the adsorption of (a) CO and (b) oxygen from CO+O₂ beams on Pd(111) surface as a function of reaction temperature. Note, solid line in the panels, (a) and (b) indicate initial sticking coefficients of pure CO and oxygen respectively.

Figure 5.9b shows a similar temperature dependence plot of the $s^0_{\text{O}_2}$ for all of the beam compositions. With oxygen also the $s^0_{\text{O}_2}$ decreases with increasing temperature and

there is a general agreement with the data reported by Engel et al [167] on clean Pd(111). There is a subtle difference observed between $s_{O_2}^0$ and s_{CO}^0 dependence on temperature is the highly linear decrease with the former between 375 and 600 K. It is also to be reminded here that a similar linear trend was observed with s_{CO}^0 above the desorption maximum of CO (450 K); however oxygen desorption from O/Pd(111) surfaces starts above 700 K is to be noted. Another important point is the relatively steep decrease in $s_{O_2}^0$ with increasing temperature from CO-rich beams. However, with oxygen rich beams, the rate of decrease in $s_{O_2}^0$ is slower.

5.3.3.5. Any O₂ Poisoning in the CO+O₂ Reaction on Pd(111) Surfaces ?

Figure 5.10 shows the results of CO₂ desorption for the beam compositions ranging from 4:1 to 1:4 of CO:O₂ at a sample temperature of 475 K on (a) O-pre-dosed and saturated, and (b) clean Pd(111) surfaces. The O₂ dosing was carried out as shown in Figure 5.2a to an extent of 100 L, and later CO+O₂ beam was dosed with desired composition at 475 K. Oxygen dosing at 475 K ensures that there is no oxygen diffusion into the sub-surface or oxide formation. CO₂ production in the TS for CO-rich compositions on a clean Pd(111) surface increases slowly and this is attributed in part due to some poisoning of CO (see Figure 5.8). On the other hand explosive production of CO₂ was observed for CO-rich compositions in the TS on O-saturated Pd(111) surface. Indeed the above trend is expected since the CO molecules can consume chemisorbed oxygen instantaneously at the reaction temperature employed. This also indicates the CO-adsorption is independent of oxygen coverage under the above conditions. However, for O-rich beams no transient CO₂ production was observed for both clean and O-pre-covered Pd(111) surfaces and it reaches the SS immediately. It is to be noted that a preferential CO-adsorption was observed in the TS and oxygen uptake increases gradually with time, indicating the fast consumption of oxygen in the TS and hence reaching the SS was smooth and fast. SS rate was measured by beam oscillation at a later time between 60 and 90 s. It should be noticed here that the SS rate was not altered significantly for both clean and O-dosed surfaces for all of the compositions studied and the rates were comparable within an experimental uncertainty limit of ±5%. Our results are in good agreement to that of Libuda et al, carried out on nano-Pd particles supported

on Fe₂O₃ [58,155,172-173] that no significant oxygen poisoning occurs in the presence of significant CO-flux.

5.3.3.6. Flux Dependence:

Figure 5.11 shows the dependence of flux on (a) CO and (b) O₂ adsorption and (c) CO₂ desorption for CO:O₂ = 2:1 beam at 425 K on Pd(111) surfaces. CO and oxygen adsorption continues ($F_{\text{CO+O}_2} < 0.04$ ML/s) and it is difficult to decide the TS and SS. However, CO₂ desorption clearly shows some delay in the beginning of CO₂ desorption at lower $F_{\text{CO+O}_2}$ values. It is likely due to the build-up of required reactants coverages, so that the reactant molecules are in close proximity to form the product. About 8-9 s delay observed with $F_{\text{CO+O}_2} = 0.01$ beam supports the above point. However, the above delay decreases to 3-4 s with $F_{\text{CO+O}_2} = 0.02$ ML/s beam and no more delay observed with

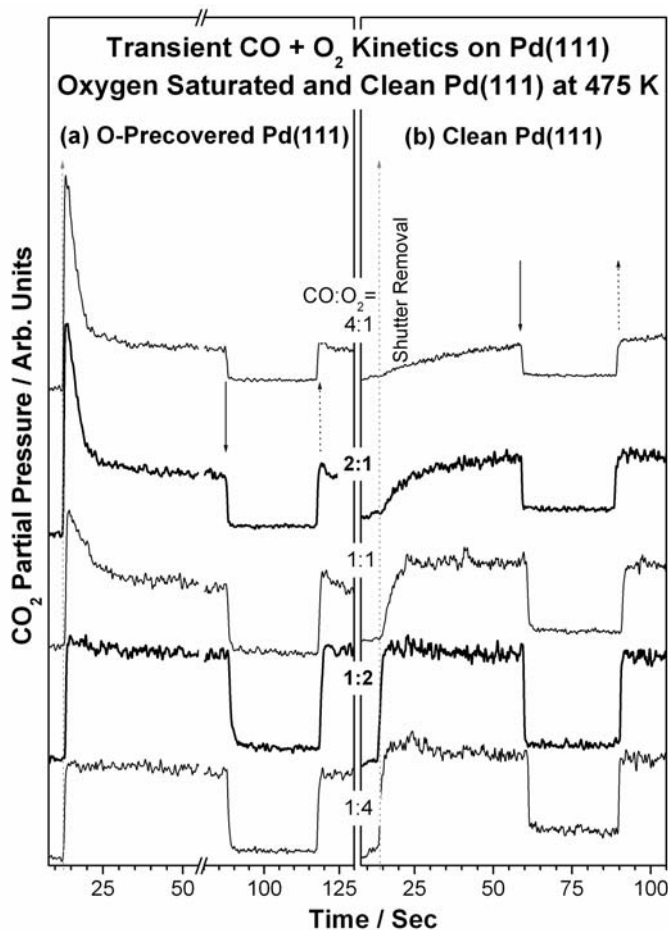


Figure 5.10: Time evolution of CO₂ desorption at 475 K for different CO:O₂ ratios from (a) clean Pd(111) and (b) oxygen pre-dosed and saturated Pd(111) surfaces. Same y-axis scale has been plotted for both panels. Note the change in transient kinetics for CO-rich beams on both the surfaces and identical kinetics with oxygen rich beams.

higher flux beams. With increasing flux, CO and oxygen adsorption reaches the SS level relatively quickly. Initial explosive production of CO₂ is observed for fluxes ≥ 0.08 ML/s. CO₂ desorption trend in the TS changes systematically with increasing flux value. At $F_{\text{CO}+\text{O}_2} = 0.02$ ML/s, a slow and continuous decrease in CO₂ production is seen and it is attributed to the delay in reaching the SS.

Indeed the SS rate value measured at $t = 60-90$ s does not represent the actual rate value and it is clear from the continuous decrease in rate till the beam was shut-off at $t = 120$ s. For $F_{\text{CO}+\text{O}_2} = 0.04$ ML/s the SS rate was reached around $t = 55$ s and at higher fluxes the SS was reached even faster. An interesting observation to be noted is a transition behavior from TS to SS is sharp for $F_{\text{CO}+\text{O}_2} \geq 0.08$; however it is somewhat smooth at lower fluxes.

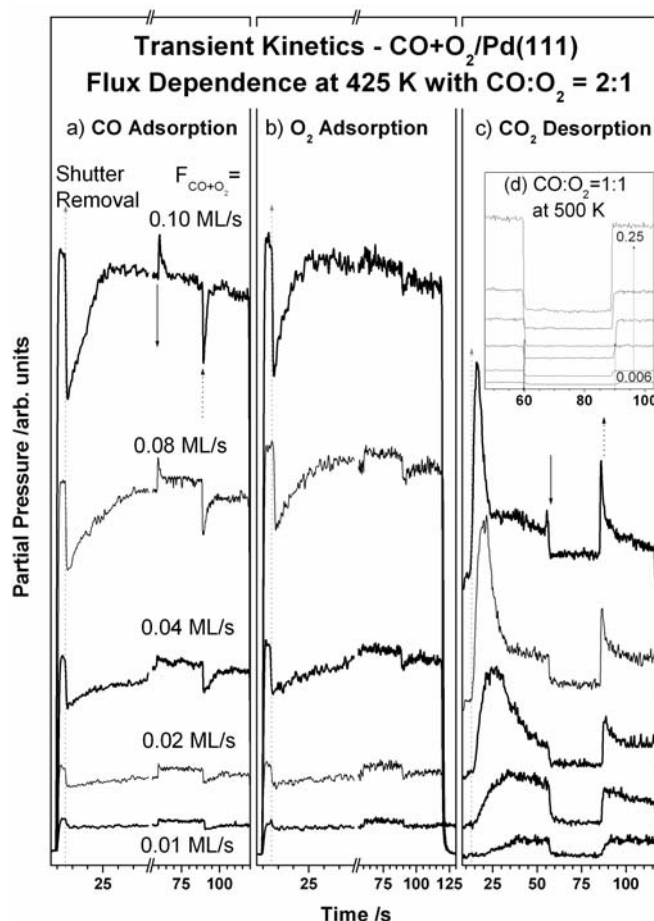


Figure 5.11: Flux dependence of CO+O₂ reaction on Pd(111) surfaces at 425 K for 2:1 CO:O₂ ratio. Adsorption of reactants are shown in a and b and product desorption in c. (d) Inset in c shows a linear increase in rate of CO₂ formation with flux varying from 0.006 to 0.25 ML/s at 500 K with 1:1 beam.

This might be due to a possible change in surface structure and/or composition of reactants on Pd(111). The SS rate measured indicates an increase in rate with increasing flux, but not proportional to the flux values. For example, the SS rate just doubled at $F = 0.1$ ML/s compared to that of 0.01 ML/s. Nonetheless, the SS kinetics shown (Figure 5.11d) at 500 K with 1:1 CO:O₂ beam demonstrate the rate increases linearly with increasing flux and the rate depends on the rate of supply of reactants under favorable conditions of no poisoning (either O or CO). TPD was recorded after the reaction was completed. Almost same CO coverage was found and it is independent of beam flux used at 425 K.

5.3.4. Steady State CO+O₂/Pd(111) Kinetics:

5.3.4.1. Temperature Dependence of Steady State Rate:

Figure 5.12 shows the temperature dependence on the time evolution of the SS rates with a 2:1 CO:O₂ beam for (a) CO, (b) oxygen and (c) CO₂. It is seen here that no considerable conversion of reactants can be catalytically sustained below 400 K, as expected from the CO/Pd(111) TPD results [178-179] and suggests CO-poisoning is the prime reason for no activity. Above 400 K, however, the SS rates for the production of CO₂, which is proportional to the changes in partial pressures, between the shutter close and shutter open operations, increases rapidly with temperature until reaching a maximum value around 525 K. Notice also that the kinetics observed in the new SS for CO and oxygen adsorption; CO (oxygen) adsorption decreases (increases) with increasing temperature. Nonetheless, the extent of CO-adsorption is not zero at ≥ 550 K, but the oxygen adsorption is fairly high. Significant decrease in the rate observed ≥ 550 K suggests an increasing CO-desorption with increasing temperature limits the overall rate of the reaction. Further, oxygen adsorption and CO₂ desorption shows instant partial pressure changes on beam oscillation and hints that they cannot be rate-limiting.

5.3.4.2. Composition Dependence of CO+O₂ reaction on Pd(111) surface at 425 K:

Figure 5.13 shows the kinetic traces obtained from the CO oxidation reaction on Pd(111) surface at a constant temperature, 425 K, for CO:O₂ ratios ranging from 4:1 to 1:20. A general description given in **Sections.5.3.4.1** and **5.3.1** is applicable to this figure too. Of note, when the beam is rich in CO the overall rate of the reaction is low. In fact a clear CO desorption observed, over and above the new SS rate, at the time of shutter

closing ($t = 60$ s) for CO-rich beam indicate a dynamic CO adsorption-desorption equilibrium. CO and oxygen adsorption in the new SS is marginal with CO-rich beams. However the above situation changes drastically with equi-molar (1:1) beam and maximum CO₂ production was observed with 1:2 and 1:4 beams. Comparable amount of CO and oxygen adsorption in the SS is clear from the kinetic data shown in Figure 5.13.

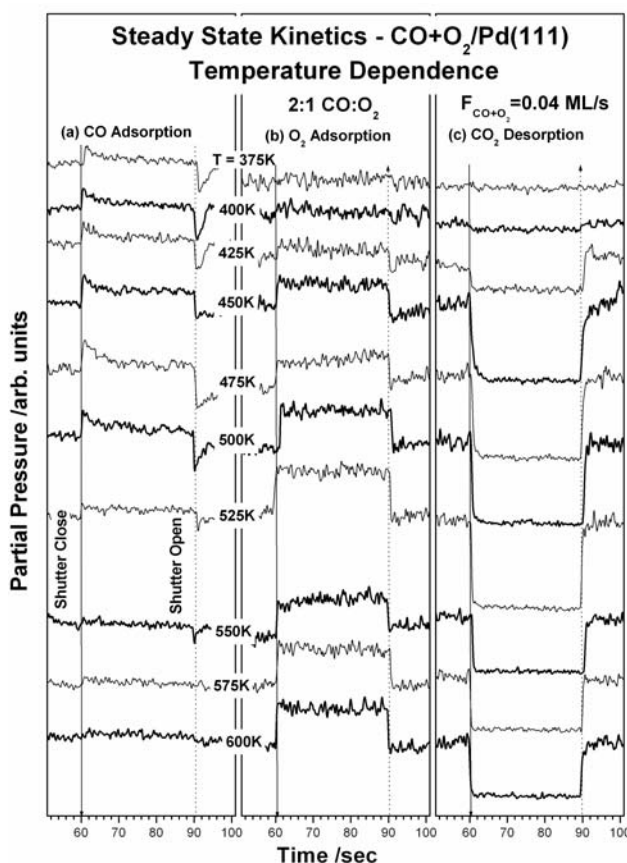


Figure 5.12. Time evolution of the partial pressures of the reactants (CO in (a) and O₂ in (b)) and CO₂ in (c) in steady-state kinetic experiments with a 2:1 CO:O₂ beam composition as a function of temperature. Note an increase in oxygen adsorption in the steady-state above 450 K.

With further increase in oxygen content in the beam, the overall rate of CO₂ formation decreases, mainly due to a decrease in F_{CO} . Nonetheless, CO₂ production observed in the SS with oxygen-rich beam (1:20) is comparable to 4:1 beam, support the oxygen saturated Pd-surfaces does not prevent CO-adsorption and, in fact, it is independent of oxygen coverage.

5.3.4.3. Steady State Rate of CO₂ Production on CO+O₂/Pd(111):

Rate of CO₂ production in the SS is plotted in terms of temperature and beam composition in Figure 5.14. There are few interesting points worth highlighting here about the CO₂ production in the SS. (a) There is a high reaction rate regime observed for CO-rich beams (4:1 and 2:1) between 500 and 575 K. (b)

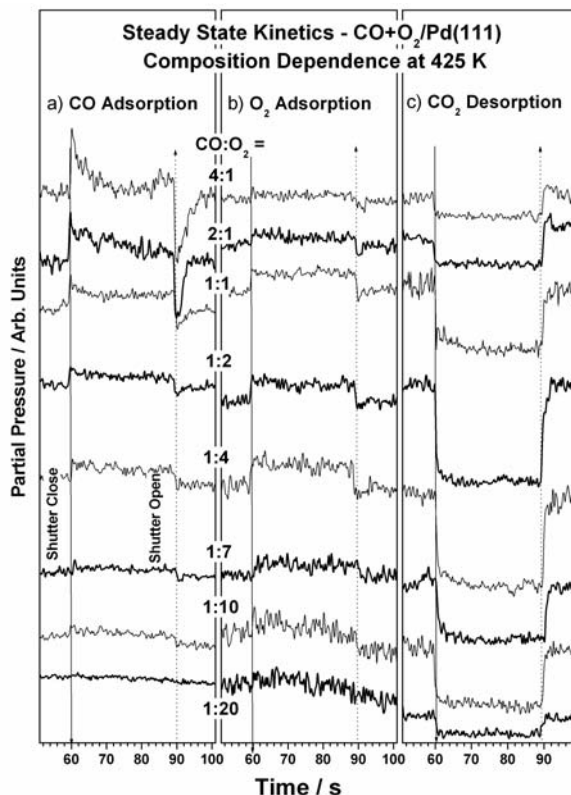


Figure 5.13: Time evolution of the partial pressure of the reactants (CO in (a) and O₂ in (b)) and CO₂ in (c) in the steady-state kinetic experiments at 425 K as a function of CO:O₂ ratio.

Above high rate regime extends to low temperatures with decreasing (increasing) CO (oxygen) content up to 1:4. With 1:2 and 1:4 compositions, comparable rate regime was observed between 400 and 600 K, although the transient kinetic detail varies with temperature. (c) Although an overall decrease in rate is observed with oxygen rich (1:7 and 1:10) beams, the above temperature range holds good for comparable rate regime around 0.0014 ML/s. With further increase in oxygen content (1:20) the rate decreases again. (d) Maximum rate (0.0029 ML/s) is observed with 1:2 and 1:4 beams at 525 K. (e) Wide variation in rate is observed between 375 and 600 K for CO-rich beams; however

the above variation converges towards a single-rate regime around 1:2 and 1:4 beam compositions (Figure 5.14b). Further increase in oxygen content retains the single-rate regime for any given oxygen-rich composition, independent of temperature. All of the above observations demonstrate that the reaction rate is effectively controlled by the beam composition and to a lesser extent by temperature. High rate regime and intermediate-rate regimes are encircled to support the above points.

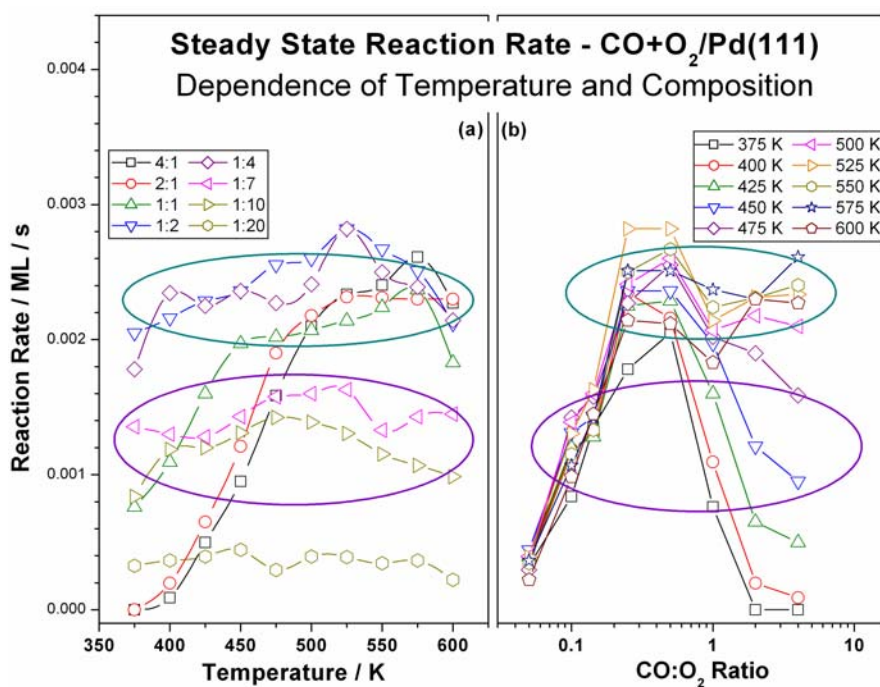


Figure 5.14: CO+O₂ reaction rates both as (a) a function of temperature for beam ratios between 4:1 to 1:20, and (b) as a function of CO/O₂ ratio for temperatures between 375 and 600 K. The maximum in reaction rate widens to lower temperatures with increasing oxygen content in the beam.

5.3.5. A Correlation between R_{SS} and Transient Kinetics:

To underscore the effect of the initial sticking coefficients of CO and O₂ on the SS reaction rates (R_{SS}), Figure 5.15 shows the ratios of those R_{SS} to the (a) s_{CO}^0 and (b) $s_{O_2}^0$ as a function of temperature for all the beam compositions. A striking similarity is observed between the trends in SS rate shown in Figure 5.14a and the trend shown in Figure 5.15b with oxygen. Independent of the reaction temperatures, the sticking coefficient of oxygen decreases dramatically in the steady-state to that of the initial

values with oxygen-rich beams. Similar is the case with CO in CO-rich beams, however, the s^0_{CO} is not measurable at high temperatures. This is the reason for high $R_{\text{SS}}/s^0_{\text{CO}}$ values observed with CO-rich beams, at high temperatures. Nonetheless, the $s^0_{\text{O}_2}$ of oxygen is the same as that observed in the SS with CO-rich beams, and still reproduces the trend shown in Figure 5.14a suggests the initial oxygen adsorption ($s^0_{\text{O}_2}$) may be correlated to SS rate.

The values of $R_{\text{SS}}/s^0_{\text{CO}}$ ratio continue to increase slowly up to 525 K and then rapidly. Very small s^0_{CO} values at high temperatures should lead to high $R_{\text{SS}}/s^0_{\text{CO}}$ values for all beams at $T > 550$ K. Indeed, as the beam becomes richer in CO, the SS to TS oxygen uptake ratio remains at a value close to 1, especially > 450 K. This is mostly due to the decreasing residence time of CO due to fast desorption with increasing temperature. However, below 450 K, large amount of CO molecules remain on the surface and hence low SS to TS uptake ratio of oxygen. At intermediate and stoichiometric compositions the SS to TS oxygen uptake ratio varies from lower values up to 1. From the above results and points, it is clear that oxygen have less significant control over the reaction than CO, since plenty of adsorbed oxygen is present on the surface from the transient state of the reaction, especially above 450 K. Although it is not directly evident from the results, it is implied that CO-adsorption has more significant control over the overall reaction.

5.3.6. Surface Stoichiometry under Steady-State Conditions:

It is expected that the surface stoichiometry plays a crucial role in deciding the rate of the reaction as well as the course of the reaction. In view of this a simple ratio of uptake of reactants – CO/O – was calculated from the steady-state kinetic data. Dissociative adsorption of oxygen molecule is assumed and two vacant sites are occupied upon adsorption. Figure 5.16 shows the results of steady state ratio of CO/O uptake for all of the beam compositions between 375 and 600 K. As already mentioned, the reaction does not sustain with CO-rich beams below 400 K due to CO-poisoning, and hence essentially there is no uptake of either of the reactants in the SS.

High CO/O > 1 was observed with 4:1 and 2:1 beams < 500 K, indicating the equilibrium CO-coverage is still very significant and poisons the surface under the SS conditions. However, the values reaches close to 1 at > 500 K. With 1:1, 1:2 and 1:4

beams the CO/O ratio reaches a value close to 1 around 450 K and remains at the same value up to 600 K. Indeed high CO/O ratio (1.2 – 1.8) was observed at <400 K with the above three beams too. On further increase in the oxygen content (1:7 to 1:20), the CO/O ratio decreases compared to the other beams.

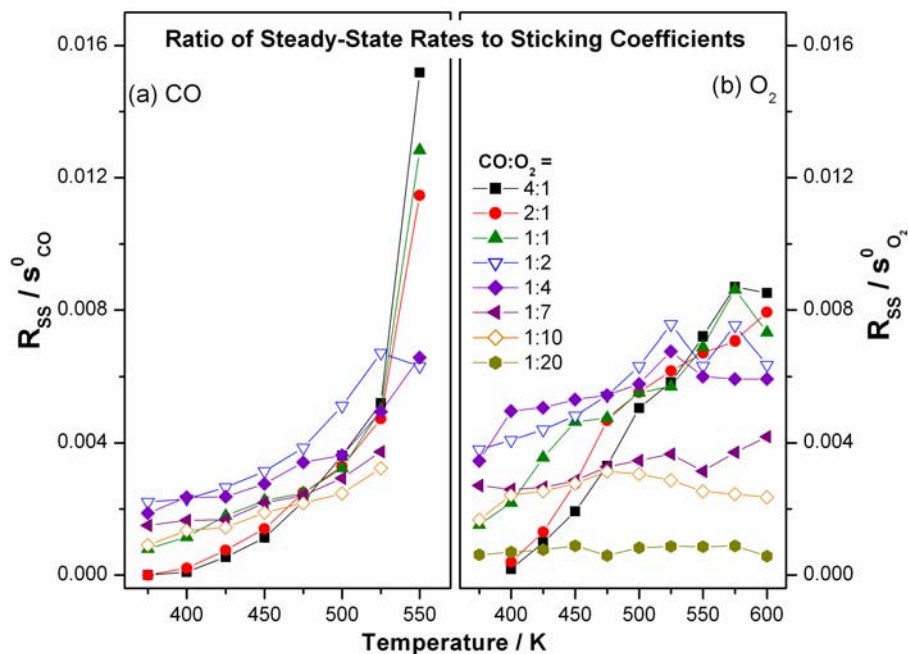


Figure 5.15: Temperature dependence of steady-state rate to initial sticking coefficient ratios for (a) CO and (b) O₂ in the CO+O₂/Pd(111) experiments. A striking similarity is to be noted between the results in oxygen panel and that of SS rate displayed in Fig. 5.12a.

However, the qualitative trend remains the same with oxygen rich beams too. A value higher than one for CO/O ratio is considered to be due to CO-poisoning. It is to be noted that the above values are calculated from the equilibrium uptake in the SS; with CO-rich beams the CO/O ratio at low temperatures essentially means high rate constant of the CO adsorption-desorption equilibrium. A CO/O value closer to one (1 ± 0.25) is considered to be highly favorable due to the reaction stoichiometry involved in the basic reaction of CO+O giving CO₂. Values, that are lower than <0.75 is considered to be due to low CO uptake on the surface and the same occurs with oxygen-rich beams. Indeed low F_{CO} also contributes for low CO-uptake. With CO-rich beams, there is a characteristic drop in the CO/O value occurs >500 K. A comparison between the CO/O ratio and the SS rate given in Figure 5.14 demonstrate an inversely proportional relation

and it is clear with CO-rich beams. CO/O ratio observed close to one with intermediate compositions demonstrates a 1:1 surface stoichiometry of CO/O under the reaction conditions; indeed, TPD also shows hardly any CO and O left on the surface after the reaction. Significant to large amount of oxygen observed with oxygen rich beams indicating the presence of high oxygen coverage, however it does not poisons the surface.

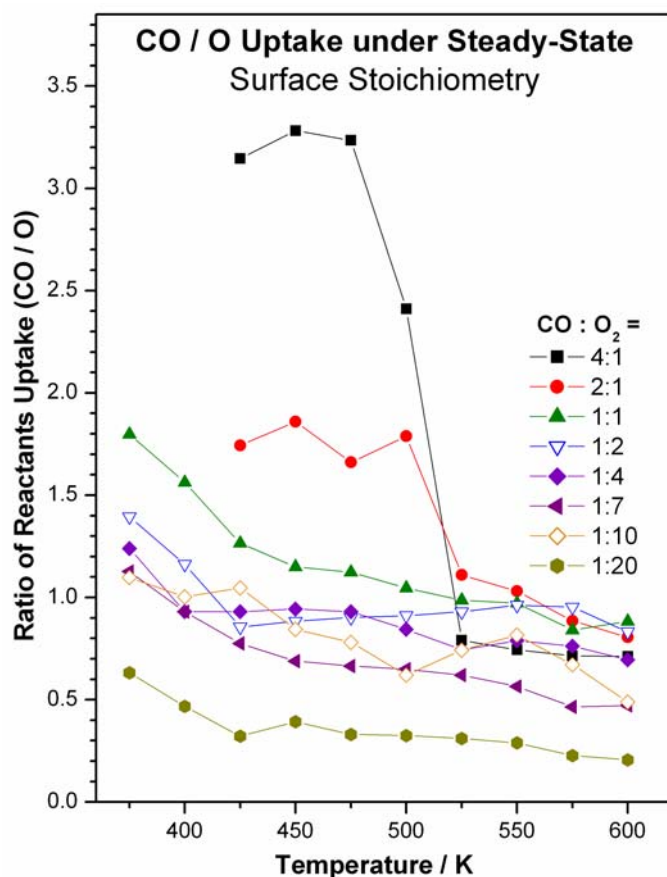


Figure 5.16: Surface stoichiometry (CO/O) of reactants calculated from the steady-state data of uptake of reactants on Pd(111) for all beam compositions between 375 and 600 K. Note the qualitative trend between the above ratio and the steady-state rate is inversely related.

5.3.7. Post-reaction TPD:

Figure 5.17 shows the post-reaction TPD results of all the species, CO, O₂ and CO₂, observed after completing the reaction with all the beam compositions at the sample temperature, 425 K, recorded at a heating rate of 10 K/s. Nature of the adsorbate remains on the surface after the reaction changes from CO-dominated to oxygen dominated from 4:1 to 1:20. Large CO desorption was observed for CO-rich compositions at 445 K shows

the dominant character of CO on the Pd(111) surface over O₂. It clearly suggests that CO poisoning for CO-rich beam compositions and hence no CO₂ desorption in the TPD. However, significant CO₂ desorption observed from oxygen rich compositions (1:20) to equimolar (1:1) composition indicates that oxygen do not seems to poison the surface. Indeed, 1:1 to 1:4 compositions show no oxygen adsorption, but some CO₂ desorption. Minimum reactants and some CO₂ observed on the surface after reaction with 1:2 and 1:4 beam compositions is to be noted and hinting an almost complete utilization of the reactants CO and O₂. High SS rate supports the above fact. O₂ desorption was observed for oxygen rich compositions above 1:4 CO:O₂ beams around 760 K in agreement with literature values [123,159-160]. It is noteworthy to mention here that the CO₂ desorption increases linearly with increasing O-content in the beam.

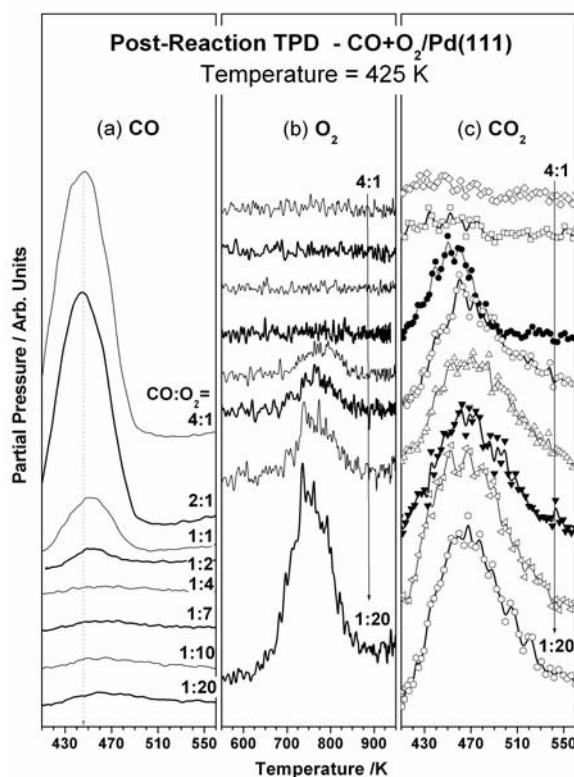
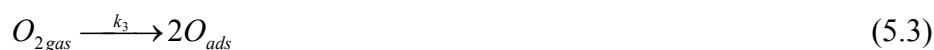


Figure 5.17: (a) CO, (b) Oxygen, and (c) CO₂ TPD experiments that were carried out after performing the CO+O₂ reaction on Pd(111) surfaces at 425 K with different CO:O₂ ratios.

5.4. Discussion

5.4.1. Reaction Mechanism Aspects:

Our present study essentially tries to find out the influence of the interaction of oxygen with Pd(111) surfaces and a special emphasis is given for transient kinetic analysis. In the discussion of the results presented here, it is important to remember that, as opposed to the case of the SS regime, the kinetics in the TS does not require that all the steps in the mechanism display equal rates. In simple terms, as the metal surface system goes from a clean metal in the beginning of the experiment to the SS of the reaction, both the surface concentration and the rates of individual steps change in absolute and relative terms and hence the variations in rates over time seen in Figures 5.1 and 5.3-5.5. As established from the earlier reports [118,167], the CO oxidation reaction goes through the following mechanism:



At lower temperatures, i.e. < 450 K, step (5.1) dominates and poisons the surface. In other words, CO₂ production rate is dependent on the CO-desorption, so that significant oxygen adsorption might occur and sustain the reaction at some rate, depending on the extent of oxygen adsorption. Indeed, as the temperature increases from 375 K to 450 K, a gradual increase in CO-desorption sets-in and simultaneously the overall reaction rate also increases with CO-rich beam compositions. Nonetheless, an overproduction of CO₂ observed with CO-rich compositions of CO:O₂ (4:1 to 1:1), is entirely due to a significant oxygen uptake in the TS at the time of shutter removal on clean Pd(111) surfaces, as seen in Figures 5.3-5.5 and 5.8. Subsequently, oxygen uptake decreases due to predominant CO-uptake at higher times and poisons the Pd(111) surface. Indeed both TS kinetic data of CO and O₂ uptake and large amount of CO species left on the surface after the reaction, measured by the TPD (Figure 5.17), clearly indicates the domination of CO in the reaction. For O₂-rich beams, the situation becomes opposite. However for

intermediate compositions (1:2 CO:O₂), both CO and O₂ peaks were not observed in the TPD in the whole of high-rate regime indicating the complete utilization of the reactants. An immediate attainment of SS and a higher SS rate confirm this fact. We attribute this behavior to a near-stoichiometric (1:1) coverage of both CO and oxygen atoms on the surface under the present experimental conditions in the SS. Indeed, a calculation of ratio of uptake of reactants (CO/O) in Figure 5.16 shows a value very close to one for the high rate regime for all CO-rich and intermediate beam compositions. There are some deviations observed, especially, in the low temperature regime is exclusively due to CO-poisoning. Above 450 K, oxygen adsorption is dominant and it is one of the fast step in the overall reaction. The kinetic data for the TS of the CO oxidation with oxygen on Pd(111) surfaces presented here generally reinforce the conclusions reached by Engle and Ertl and others. [118,156-158,167] Low CO-desorption rate poisons the surface and controls the overall reaction below 450 K, especially with CO-rich beams. High CO-desorption rate at higher temperature seems to decide the rate at higher temperatures with all beam compositions.

An important aspect of the CO+O₂/Pd(111) system relevant to the discussion presented here is related to the dependence of the reaction rates on initial uptake of reactants. This dependence becomes evident by the product desorption patterns observed in the TS as the reaction approaches its SS. A careful look at Figures 5.3-5.5 allows for the realization that there is an inverse correlation between the time evolution of CO₂ either with CO-rich and O₂-rich beams or low and high temperatures. An over-production of CO₂ seen in the TS, at low temperature with CO-rich beams, changes to under-production at high temperatures. Similarly an under-production of CO₂ observed with oxygen-rich beams at low temperature changes to over-production at high temperatures. This result means that, under those conditions, an excess of one of the reactants builds up on the surface at first; only after that excess reactant is removed the adsorption of other species can continue. However, this situation changes drastically with intermediate beam compositions under the high rate-regime, so that adsorption of both reactants seems to be comparable with a CO:O ratio close to one (Figure 5.16). This is further supported by a fast reaching SS without having any significant TS in significant number of cases (Figure 5.5). It is also evident that CO-rich beams never reach the direct SS under any of the

experimental conditions employed. In contrast, oxygen-rich beams reach the direct SS at high temperatures. This also hints that the rate becomes zero-order with respect to oxygen coverage and first order with respect to CO-coverage.

An important aspect, from the CO titration of O-saturated Pd(111) surfaces (Figure 5.2), is the identification of two temperature regions. An active temperature region lying between 400 and 500 K, where the TS CO₂ desorption occurs fast and have a comparable values. However, > 525 K diffusion of oxygen to the subsurface and/or bulk starts to occur (step 5) as reported by Schlögl et al [162-163]. Hence a reduction in the rate as well as the amount of CO₂ desorption above this temperature. Subsurface oxygen species desorbs around 760 K in the post-reaction TPD spectra (see Figure 5.18). Above 600 K, the oxygen species diffuses into the bulk and this oxygen desorption occurs above 1100 K [163] in the TPD. Nonetheless, the CO+O₂ reaction data obtained in the present set of experiments does not necessarily support the oxygen diffusion.

5.4.2. Initial Adsorption of CO and O₂ from CO+O₂ Beams:

An important conclusion from the present work is the fact that the rates of uptake of reactants on Pd(111) surfaces from CO+O₂ mixtures are affected in a significant way both the composition of that mixture and by the presence of adsorbed species on the metal surface. It is clear from Figure 5.9a that the s^0_{CO} decreases with any beam composition at temperatures higher than 425 K. However ≤ 425 K, the s^0_{CO} is very similar to that on clean Pd(111), irrespective of the beam composition. At and above 450 K, there is a gradual decrease in s^0_{CO} mostly due to co-adsorption of oxygen and different from the CO-adsorption on clean Pd(111) [178-179]. Clean metal shows almost same s^0_{CO} up to 475 K and then decreases very fast. This difference indicates that competition with oxygen alters the kinetics of CO-adsorption. However the converse seems not to be true. Under most of the reaction conditions, the $s^0_{\text{O}_2}$ measured on Pd(111) from the molecular beam follows that of clean Pd(111) surfaces [118]. Although the absolute $s^0_{\text{O}_2}$ values may be little different from the clean Pd(111), the overall trend remains the same. This clearly suggests that oxygen adsorption is not considerably affected at least above 450 K, where CO-poisoning is no-longer valid.

The temperature dependence of the $s_{\text{CO}}^0/s_{\text{O}_2}^0$ ratio could provide an indication of the difference in adsorption barriers for the co-adsorbed system and hence a calculation was taken up and the results are given in Figure 5.18. Although $s_{\text{O}_2}^0$ changes only by a factor of 2 between 375 and 600 K, the s_{CO}^0 changes few orders of magnitudes, especially above 525 K. Figure 5.18 demonstrates a clear domination of CO adsorption on Pd(111) surface up to 525 K. However, above 550 K, a marked change in the initial adsorption

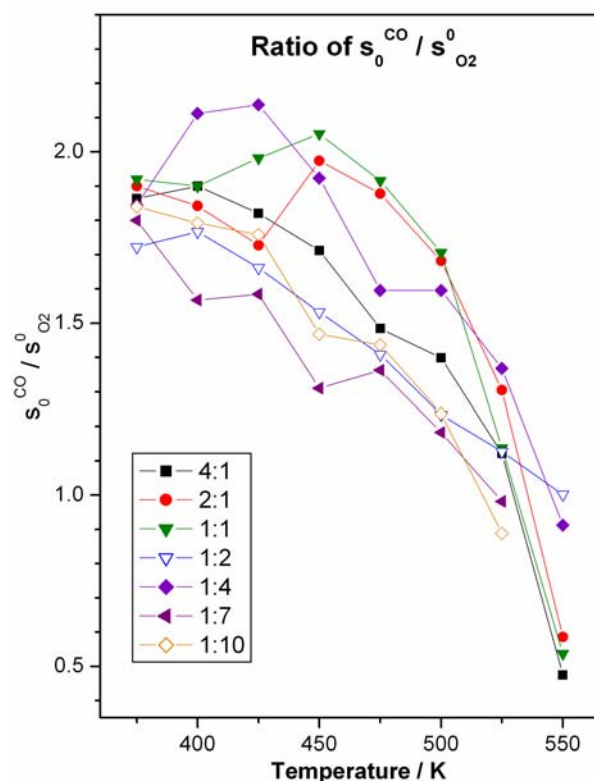


Figure 5.18: Ratio of $s_{\text{CO}}^0/s_{\text{O}_2}^0$ calculated from the data given in Fig. 5.9.

towards oxygen dominated Pd(111) surface is clear from the values shown in Figure 5.18. Any $s_{\text{CO}}^0/s_{\text{O}_2}^0$ value below (above) 1 is due to significant to large adsorption of oxygen (CO) initially. It is known that CO-adsorption on the clean Pd(111) surfaces decreases drastically above 525 K [167] to lower values cannot be measured even with MBI systems. This hints the $s_{\text{CO}}^0/s_{\text{O}_2}^0$ ratio should decrease drastically above 550 K. It is to be noted that the $s_{\text{CO}}^0/s_{\text{O}_2}^0$ ratio turns below 1 around 525 K for all the beam compositions and the maximum rate observed at this temperature correlates well with the surface stoichiometry mentioned earlier. This also suggests the nature of the surface

under reaction conditions changes from CO-dominated below 525 K and hence reducing character to oxygen dominated above 525 K and hence oxidizing. In a way this might also be a reason for decreasing rate with increasing oxygen content at T>550K.

5.4.3. Transient Behavior of Surface Coverages:

We address the relation between the behavior of the CO+O₂ system on the clean Pd(111) surface in the TS to the final SS of the reaction. Indeed Figures 5.6, 5.9, 5.15 and 5.16 are in some way related to the above relation. Especially Figure 5.6 demonstrates a clear trend by the behavior of the $\Delta\Theta^{\text{TS}}$. It is basically the coverage of CO and O that were close enough and formed the product CO₂ and leave two vacant sites on desorption. A wide variation in $\Delta\Theta^{\text{TS}}$ with temperature from large negative value to positive value for CO-rich beam becomes very narrow for intermediate compositions (1:2 and 1:4) and close to zero values. However, for oxygen-rich beams again it widens but more on the positive side above 450 K. It is clear from Figures 5.3-5.5 that CO₂ production is fast in the TS and approaches its SS directly within 1-2 seconds, with intermediate beam compositions >425 K, clearly highlighting the instantaneous approach to the SS coverage and they show $\Delta\Theta^{\text{TS}}$ values close to zero.

There is no overshooting or underproduction of CO₂ in the intermediate compositions, in general. However the over-production observed with CO-rich beams below 450 K is exclusively due to significant adsorption of oxygen in the TS as the oxygen uptake in the SS is much lower. The low SS rate demonstrates a poisoning of the surface by CO molecules depending on the beam compositions. Up to 525 K, equilibrium CO-coverage is significantly high with CO-rich beams under reaction conditions and hence the SS rate increases slowly with increasing temperature, as against intermediate beam compositions. However it changes with increasing temperature and CO-deprived regime occurs above 525 K. A high negative $\Delta\Theta^{\text{TS}}$ value indicates a significant oxygen adsorption first and slow build-up of CO-coverage. However the high SS rate observed at 600 K with CO-rich beams underscores the importance of continuous CO-uptake in the SS, however, on the oxygen-covered Pd(111) surfaces, and not on clean Pd(111), as observed in the low temperature cases. This indeed widens the high rate regime to high temperature side with CO-rich beams.

With oxygen-rich beams, the $\Delta\Theta^{\text{TS}}$ values quickly change from low negative values at $T < 425$ K to positive values >425 K. This is mostly due to slow CO build-up on the surface due to decreasing CO-flux. However, $\Delta\Theta^{\text{TS}}$ reaches positive values indicating a faster build-up of required CO-coverage and hence the reaction reaches SS instantaneously (see Fig. 5.5). Indeed some small overproduction of CO₂ observed around 525 K with O₂-rich beams is due to increasing adsorption of CO at high temperatures, which is unusual. This trend continues until 600 K and higher CO-adsorption was observed.

High SS rate regime observed between 500 and 600 K for the 4:1 to 1:4 beam compositions suggests some contradictory points that are listed below: (a) It is not necessary to have a CO-rich or intermediate composition beams to achieve a high rate. (b) Figure 5.18 confirms that the surface is enriched with oxygen ≥ 525 K, irrespective of the beam compositions. (c) Nonetheless, Figure 5.16 insists on the equi-molar uptake of reactants, which should lead to equi-molar coverage or close to that on the surface, and lead to high SS rate. (d) With oxygen-rich beams, the surface coverage of oxygen is dominant under equilibrium conditions; with low CO-flux it is unlikely to achieve the above equi-molar surface coverage and hence the overall decrease in SS-rate. It is apparent from the above discussion that $\Delta\Theta^{\text{TS}}$ appears to be a good parameter to reflect the changes of coverages of CO and O, in a qualitative manner. In conjunction with other TS and SS data, right explanation is possible for the unusual kinetics.

5.4.4. Unusual Transient Kinetics and High Temperature CO-adsorption:

In the following we provide the first set of evidence for CO-adsorption at high temperatures on mostly oxygen-covered Pd(111) surfaces from the transient kinetics of CO+O₂ reaction with different beam compositions at 600 K. CO₂ Production show in Figure 5.5a at 600 K and corresponding CO adsorption and O₂ adsorption in figures 5.7 and 5.8 are referred again. Indeed, corresponding CO₂ production data is given in Figure 5.5. Immediately upon shutter removal at $t = 13$ s, a clear decrease in oxygen partial pressure is observed with all the beam compositions. Nonetheless, no direct CO uptake is apparent from the kinetic data for the beam compositions between 4:1 and 2:1. It is also surprising to note a reasonable CO uptake from the oxygen rich beam compositions (1:7

and 1:20). A slow and gradual increase in CO adsorption could be seen with CO-rich (4:1) beam after a delay of about 12 sec after the shutter removal. Meanwhile, the direct oxygen adsorption from the beam during the above delay period ($t = 13-26$ s) demonstrates the change in nature of substrate from clean metal to oxygen-covered surface. The above reaction data hints the surface is covered to an extent of about 0.2 ML of oxygen on Pd(111) from 4:1 beam. An onset in CO-adsorption and CO₂ production, immediately after the above delay period correlates very well and indicating that there was no or minimum net CO adsorption till that time ($t \sim 25$ s). It is to be noted that the rate of oxygen adsorption remains the same from the beginning till the beam was shut off, and suggests a zero-order dependence with respect to oxygen coverage. No direct CO uptake at the time of shutter removal from CO-rich beams is in neat agreement with no net CO-adsorption on clean Pd(111) surfaces at 600 K, due to high rate of CO-desorption [178-179]. The above observations unambiguously demonstrate that there is a clear reversal in CO-adsorption characteristics on oxygen covered Pd(111) surfaces at high temperatures.

Beams with intermediate (1:2) composition shows the above trend, but to a lower extent. The initial delay involved in the onset of CO-adsorption and CO₂ production decreases to about 3 sec. Indeed an increasing oxygen content in the beam makes the Pd(111) surface covered with oxygen at a faster rate, and hence a decrease in the above delay. With oxygen rich beams (1:7 to 1:20), both the CO adsorption and CO₂ production involves hardly any delay and it is almost resonant with oxygen uptake at the point of shutter opening at $t = 13$ s. It is also to be noted that the CO partial pressure keep decreasing from the onset to higher times is not due to any change in flux. No change in oxygen partial pressure and CO₂ production clearly demonstrates that it is due to an increasing CO-adsorption, and likely there is a continuous change in CO:O ratio on the surface, till the reaction reaches the SS. CO-rich beams reaches the SS somewhere close to $t = 100$ s; however with oxygen rich beams the SS reaches at lesser times, as seen in Figure 5.7.

We make the following suggestions for the delayed CO-adsorption (CO₂ desorption) observed in the results discussed above. A decrease in both the attractive O-O as well as repulsive O-CO interaction might be a possibility, which also inevitably leads

to CO₂ production. The above scenario is the case on Pt(111) [180] and hence CO-adsorption within the oxygen islands was possible. This indicates the nature of oxygen covered Pd surface changes considerably and favorably towards green chemistry at high temperatures. However, some possibility of Pd_xO_y formation in the TS cannot be ruled out. Indeed, incommensurate 2D surface oxide Pd₅O₄ formation due to oxygen exposure on Pd(111) at 600 K was reported recently [162-163]. A change in surface structure due to reconstruction after a threshold oxygen coverage is another possibility [162-163]. Phenomenon like, ‘capture zone effect’ (initial adsorption occurs on catalytic support at high temperatures and then adsorbate hops onto the metal particles), might be invoked to explain the CO-adsorption on oxygen-covered surfaces at high temperatures. Such effect has been reported on Pd supported on either MgO or Fe₂O₃ [155,172-175], but not on metallic Pd-surfaces.

5.5. Summary

Our revisit on CO oxidation reaction on Pd(111) surface with mixed molecular beams at wide range of temperatures (from 375 K to 600 K) for a variety of beam compositions ranging from 4:1 to 1:20 gave some interesting information about the reaction.

- 1) 1:2 beam composition of CO:O₂ at 525 K shows maximum rate in the steady state and not a stoichiometric beam composition.
- 2) A stoichiometric coverage of both CO and O is required to achieve a maximum in SS rate.
- 3) Below 450 K, the CO oxidation process is mainly controlled by the extent of CO desorption.
- 4) A good correlation was revealed between the SS rate to the transient kinetic parameters such as sticking coefficient, transient state differential coverage.
- 5) It is clearly demonstrated that direct CO adsorption is feasible with significant sticking coefficient at high temperatures (600 K) on oxygen-covered Pd(111) surfaces under steady-state (SS) conditions and hence no significant oxygen poisoning was observed. Further no significant oxygen poisoning is observed under any conditions, if there is sufficient CO-flux.

Chapter 6

NO + CO + O₂ Reaction on Pd(111)

*Surfaces**

“Influence of oxygen on NO+CO reaction on Pd(111) surfaces was studied through mixed molecular beams of ¹⁵NO+CO+O₂ under isothermal conditions as a function of varying beam compositions between 425 K and 575 K. Although the steady state (SS) production of N₂ decreases with increasing oxygen content, more N₂ was produced in the transient state (TS). SS rates for CO₂ increases noticeably with increasing oxygen content in the beam and oxygen does not seem to poison the surface towards CO-oxidation. N₂O production enhances to some extent with oxygen-rich beams due to significant decrease in NO-dissociation. Well above the desorption maximum of 450 K, CO adsorption could be observed, however, on the oxygen-covered Pd(111) surfaces. A time delay observed in the production of CO₂ in the TS decreases with increasing oxygen content in the reaction mixture. At 525 K, irrespective of the beam composition, NO+CO+O₂ reaction on Pd(111) shows maximum reaction rate with respect to CO₂ as well as N₂, but maximum SS rate for N₂O is observed at 475 K. NO-dissociation seems to occur significantly on relatively oxygen-free Pd-surfaces, at least in the transient state, irrespective of the beam composition. Based on the above, a fast beam switching experiment is suggested to manage the NO-reduction at a better level in the existing three-way catalyst setup.”

* Thirunavukkarasu, K., Gopinath, C. S.,
to be submitted to *J. Catalysis*.

NO + CO + O₂ Reaction on Pd(111) Surfaces

6.1. Introduction

Over the last three decades, the introduction of three-way catalysts (TWC) in all types of automobiles leads to a huge reduction in emissions into the atmosphere [181]. Improvements in internal combustion engines and the developments in this field have led to fuel-efficient vehicles. Nonetheless, problems exist in the oxidation of nonvolatile organic species to CO₂ and, in particular, the reduction of NO to N₂. The latter is difficult, especially, under highly oxidizing conditions with fuel-efficient lean-burn engines. [81] In the last decade palladium only TWC converters (Pd supported on γ -alumina support) were introduced increasingly and replacing the traditional Rh-Pt TWCs, due to its reasonable performance to reduce NO in net oxidizing conditions, its low cost and higher abundance of Pd than Rh. Hence an understanding of NO_x reduction reactions under net oxidizing conditions on palladium catalysts is attracting more attention for the last one decade. [82] In the recent past, there have been numerous reports on the NO dissociation [91-100,106-109], NO reduction with reductants like CO, H₂ [101-105] and CO oxidation reaction [118,156-158,167-177] over different facets of Pd-surfaces and a variety of supported systems. Despite that, there is a lack of fundamental understanding of NO dissociation on the Pd surfaces. Moreover interaction of oxygen with Pd surfaces is being paid much attention recently. [123,127-134,159-166] Still very few groups have reported the influence of oxygen on NO+CO reaction on Pd surfaces. [182-185]. Matsushima et al [184-185] studied the branching of the intermediate, N₂O on Pd(110) surfaces, and it was estimated that for a 1:1 NO:CO composition, only 20% of N₂O_(ads) desorbed without decomposition on the surface and an increase in the oxygen content improves N₂O desorption for the same composition on the surface [184]. The O_{ads} decreases the decomposition of N₂O on the surfaces which eventually means that N₂ formation occurs through an N₂O intermediate, because N+N recombination step reduces completely for the sequence of processes they have formulated: [185]





Our continuing efforts on studying NO adsorption and dissociation [117,148, **Chapter 3**], NO+CO reaction [69, **Chapter 4**] and CO+O₂ reaction [71,72, **Chapter 5**] on Pd(111) surface under isothermal conditions in a molecular beam setup shown some light on the understanding of the deNO_x processes. The important conclusions derived from those studies can be summarized below which are essential to the present study of interaction of oxygen on NO+CO reaction on Pd(111) surfaces:

(i) Dissociative adsorption of NO above 400 K, a precursor mediated, Langmuir type, on Pd(111) surfaces was observed in our adsorption studies, [148, **Chapter 3**] though the previous reports stated that the dissociation happens in defect sites. [99,101]

(ii) Comparatively reasonable activity on Pd surfaces for the NO+CO reaction to that of Rh surfaces was observed as reported by us and others [69,99,101, **Chapter 4**] contradicting the hypothesis that NO dissociation activity happens only on defect sites. The reaction shows a maximum in steady-state rate in between 475 K – 525 K for a 1:4 composition of NO:CO with respect to CO₂ and N₂ formation [69, **Chapter 4**].

(iii) O_(ads) mediated adsorption of CO particularly at temperatures above 525 K was observed in our CO+O₂ reaction on Pd(111) surfaces [71, **Chapter 5**] and the delay in transient CO₂ production was addressed in terms of the interaction of O₂ with Pd(111) surfaces above 525 K. [123,127-134,159-166]

The conclusions mentioned above were taken into account carefully for our study of NO+CO+O₂ reaction on Pd(111) surface and some interesting observations made are: CO₂ production increases with increasing oxygen content in the beam, however N₂ production decreases due to inhibited NO dissociation with increasing O₂ content in the beam. However N₂O production remains almost same for temperatures 475 K and 525 K.

6.2. Experimental Section

0.05 ML/s total flux of the NO + CO + O₂ mixture ($F_{NO+CO+O_2}$) with a desired composition of 1:y:z of ¹⁵NO:CO:O₂ where y = 2, 4 or 8 and z = 0, 1, 2 and 4, was used in all the experiments reported here unless otherwise specified. A five-way valve was also fitted to the gas handling system in order to carry out fast beam switching experiments. The common port of the valve is used to connect the doser i.e. precision

leak valve, which is attached to the other four ports. Those four ports are set in a cross pattern; only one port can be connected to the beam at any time and the opposite ports were connected with two separate beam sources and others to a rotary pump to minimize any cross-port flow during beam switching. In experiments with one single beam composition, only one of the beam sources was connected to the beam until the end of the experiment, at which point the valve was switched to the pump by 90° rotation of the main handle. In experiments where the gas composition of the beam needed to be changed rapidly like beam switching experiments, the valve was flipped to 180° quickly within a second in two phases, first to one of the pumping positions (either upwards or downwards), and then to the second beam source. [153] Pd(111) sample was cleaned by the usual procedure described in the previous chapters. The mass spectrometer intensities for ¹⁵NO, CO, and O₂ were calibrated by measuring the ¹⁵NO, CO, and O₂ uptakes on clean Pd(111) at 300 K separately, assuming a saturation coverage of 0.33 monolayer (ML) for NO following Bertolo et al. [93,94], 0.50 ML for CO, and 0.25 ML for O₂. [118] ¹⁵NO, ¹²CO and O₂ were exclusively used for all the experiments reported here. Hence, hereafter ¹⁵NO would be simply noted as NO. Further, the SS rates presented in Figures 6.7, 6.8, and 6.9 have an error margin of ±10%.

6.3. Results

6.3.1. A Typical Isothermal Kinetic Measurement:

All the kinetic measurements reported here, except beam switching experiment, were carried out by following the procedure stated below. A typical raw kinetic data is shown in Figure 6.1 for the NO+CO+O₂ (1:2:2) reaction on Pd(111) surface at 525 K: (a) At t = 10 seconds, a desired beam of 1:y:z of NO:CO:O₂ composition, 1:2:2 in this case, at a desired sample temperature, 525 K in this case, with a beam flux of 0.05 ML/s is turned on. All the experiments reported in this study were carried out with the same total beam flux. An immediate rise in the partial pressure of all of the reactants (NO, CO and O₂) could be observed. The Pd(111) is still blocked and the molecular beam do not interact with the substrate directly at this stage. (b) Around t = 13 seconds, the shutter was opened to allow the beam to interact with the Pd(111) surface directly. The time difference between the beam on and the shutter opening was kept around 2-3 sec to minimize the background reaction. A dip in the partial pressure of all the reactants, NO,

CO and O₂ could be observed along with a rise in the partial pressure of all the products, CO₂, N₂, and N₂O. All the relevant mass species were followed for all the reaction measurements; however, no NO₂ (mass 47) was observed even with oxygen rich beams. (c) The reaction reaches the steady state (SS) in the next 60 seconds, in general. In the present case SS reached at t = 55 sec. However, the reaction was allowed to continue further. (d) The shutter was deliberately closed between t = 90 and 120 seconds to measure the SS rate of the reaction. A new SS for all the reactants and products was reached after closing the shutter. A clear increase (decrease) in the partial pressure of reactants (products) compared to the SS level demonstrates the rate of adsorption (desorption) in the SS. The rise or dip in the partial pressure of reactants or products, respectively, is directly proportional to SS rate of the reaction. In fact the SS rate from the above measurements were made after calibration of individual mass species, as explained earlier [66,148]. (e) At t = 150 seconds, the beam was turned off. The Pd(111) surface was cleaned by flashing it to 1000 K at a rate of 10 K/s after treating with CO beam at reaction temperature. [148]

It is to be noted that there is a delay in the beginning of CO₂ desorption in the TS, in spite of sizeable uptake of all reactants at the time of shutter opening. Similarly nitrogen desorption also exhibits a delay, not only in the TS, but also in the SS after shutter removal at t = 120 s. These points underscore the importance of TS and hence a special emphasis is given for TS analysis for the present reaction, like CO + O₂.

6.3.2. Transient Kinetics of NO+CO+O₂ Reaction on Pd(111):

6.3.2.1. Temperature Dependence:

Figure 6.2 displays the adsorption of reactants ((a) CO, (b) NO and (c) O₂) in the transient kinetic regime with an oxygen rich beam composition of 1:4:4 of NO:CO:O₂. It is clear from Figure 6.2a, that initial CO adsorption at the time of shutter opening decreases with increasing temperature, as expected from the CO-adsorption behavior on clean Pd(111) [118].

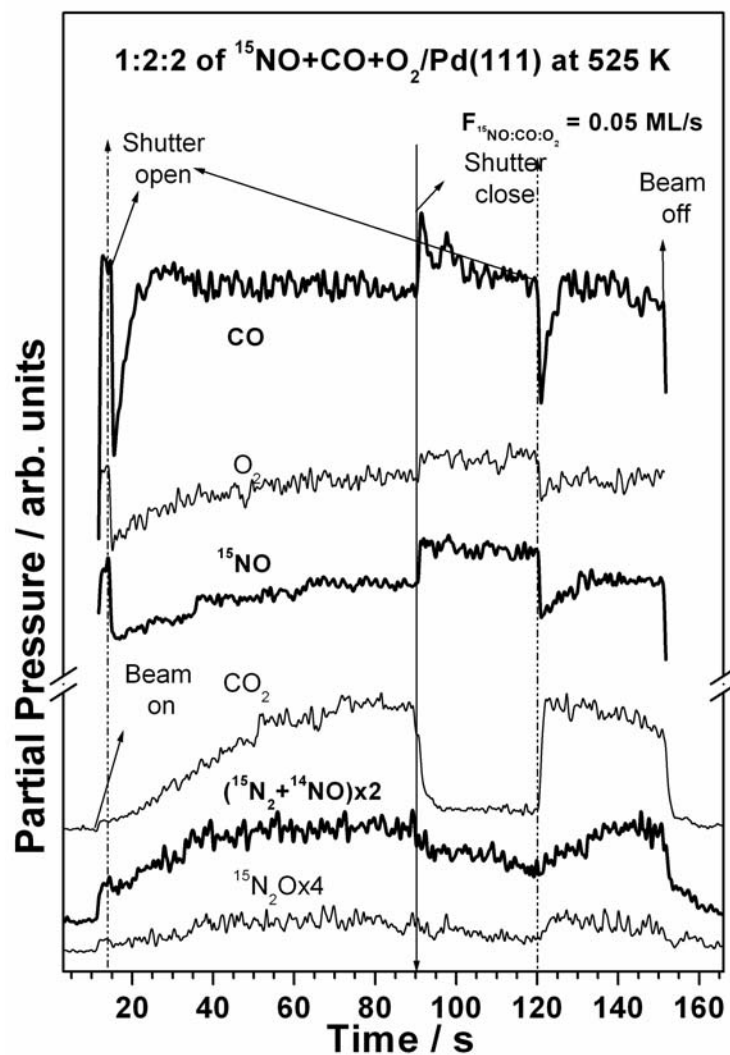


Figure 6.1. Typical raw kinetic data of the type described in this report. A molecular beam of 1:2:2 ¹⁵NO:CO:O₂ composition is allowed to directly impinge onto a clean Pd(111) surface at 525 K. Temporal evolution of the partial pressures of reactants (¹⁵NO, CO, and O₂) and all the products (¹⁵N₂, CO₂ and ¹⁵N₂O) are followed. The beam is blocked and unblocked between t = 90 and 120 s, in order to measure the steady-state rates with respect to both reactants and products (rise in the partial pressures of reactants and drop in the partial pressures of products are directly proportional to the steady-state rate). The instantaneous changes in CO₂ signal with beam perturbation to be noted with the slower response of the ¹⁵N₂ and ¹⁵N₂O signals in the SS.

Nonetheless, an interesting point to be noted here is the delayed onset of CO adsorption after a substantial adsorption/coverage of O_(ads) and NO between 525 and 575 K. This behavior is in good agreement with that of the CO+O₂ reaction, as discussed in the previous chapter. Large NO adsorption observed below 475 K, decreases with increasing temperature. On the other hand a continuing O₂ adsorption could be seen and the same increases with increasing temperature. Indeed, at 575 K, a continuous O₂

adsorption could be seen right from the time of shutter opening. This observation is worth to compare with our previous NO/Pd(111) and NO+CO/Pd(111) results [69,148], whereas the adsorption of NO was not observed ≥ 575 K for any beam composition studied.

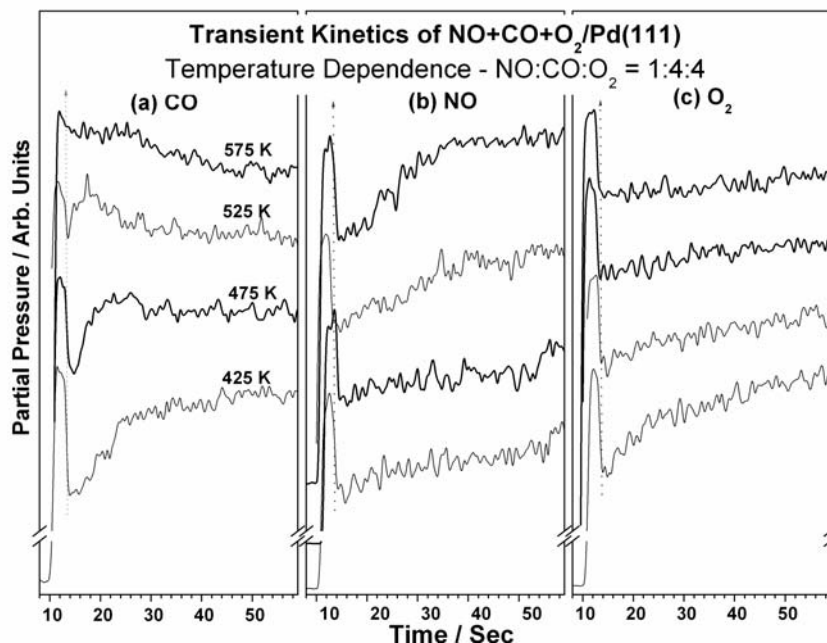


Figure 6.2. Transient uptake of the reactants a) CO, b) NO and c) O₂ for a collimated molecular beam of 1:4:4 ¹⁵NO:CO:O₂ composition on the Pd(111) surface is shown for the temperature between 425 K and 575 K; O_a induced adsorption of CO as well as NO can be observed at 575 K, as seen in the previous chapter and a gradual increase of O₂ uptake can be observed from lower to higher temperature.

Figure 6.3 displays the desorption of products ((a) CO₂, (b) N₂ and (c) N₂O) in the transient kinetic regime for the same oxygen rich beam composition of 1:4:4 of NO:CO:O₂ employed in Figure 6.2. At 425 K, CO₂ desorption starts after shutter removal and reaches a maximum rate after about 10 s and then decreases with increasing time, before it settles to low SS rate. Same trend continues at 475 and 525 K, but with a higher rate in the SS. However a considerable delay can be seen clearly at 575 K for about 10 sec. and then the CO₂ desorption starts and reaches the SS slowly. Almost no nitrogen desorption is observed in the TS as well as in the SS at 425 K; the intensity seen in Fig. 3b for 425 K trace is exclusively due to 1% of unlabelled NO. It is also to be mentioned here that the intensity shown at 425 K should be subtracted for the actual N₂ intensity. In the figures presented in this chapter, no such subtraction was made, mainly to avoid any artifacts that could arise from the subtraction. N₂ production starts ≥ 475 K and produces

excess ≥ 525 K in the TS over and above the SS rate. At 425 K, a small but reproducible amount of N_2O observed and it increases with temperature and reaches the maximum at 525 K. At 575 K, no N_2O production was observed.

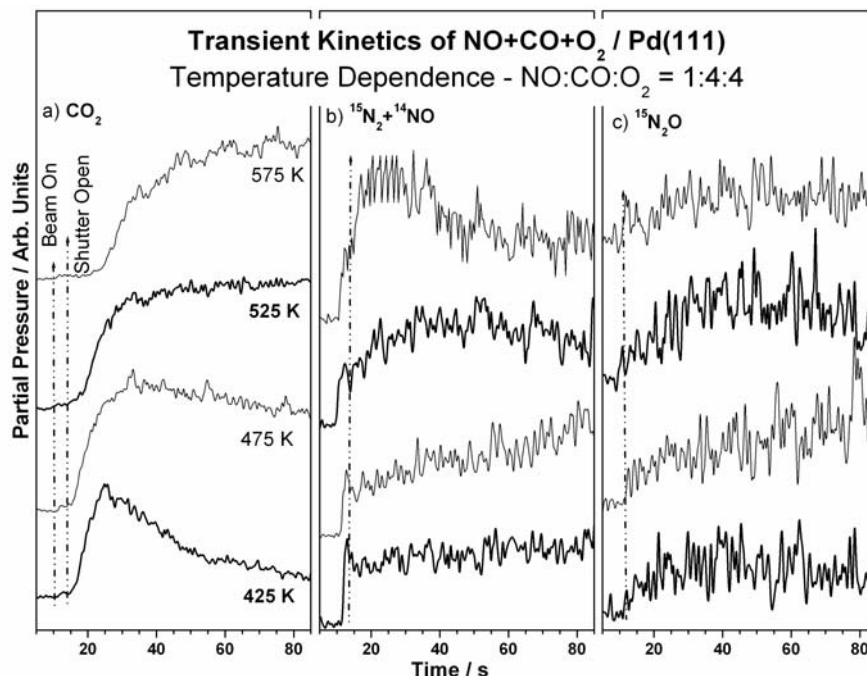


Figure 6.3. Transient state desorption of the products a) CO_2 , b) N_2 and c) N_2O with a collimated molecular beam of 1:4:4 $\text{NO}:\text{CO}:\text{O}_2$ composition on the $\text{Pd}(111)$ surface for the temperature window of 425 K to 575 K. Delay in the evolution of CO_2 is observed at temperatures 525 K and 575 K. At 575 K N_2 is produced in excess in the transient due to the same effect, which clearly reveals that NO dissociation is spontaneous on $\text{Pd}(111)$ surface.

6.3.2.2. Beam Composition Dependence:

Figure 6.4 displays the adsorption of reactants ((a) CO , (b) NO and (c) O_2) in the transient kinetic regime at 525 K with beam composition of 1:4:z of $\text{NO}:\text{CO}:\text{O}_2$ with increasing oxygen content. Figure 6.4a shows no direct CO adsorption from the beam that contains no oxygen at the time of shutter opening in the TS. However, adsorption-desorption equilibrium should maintain some CO coverage and hence CO_2 formation was also seen in the products. No further CO uptake from the beam is evident. With increasing oxygen content in the beam, no CO adsorption was observed at the time of shutter opening, however CO adsorption starts at later time when $t = 35$ s, 25s and 20s with $z = 1, 2$ and 4, respectively. In contrast, NO adsorption was observed at the time of shutter removal in the TS for $z = 0$ and no significant change observed with $z = 1$.

Nevertheless, NO uptake decreases with further increase in oxygen content ($z = 4$) in the beam, as clearly seen in Figure 6.4b. Similarly, oxygen also shows large adsorption in the TS and continues throughout the reaction for $z = 1$. The relative oxygen adsorption extent decreases with increasing oxygen content; however relative oxygen adsorption increases with increasing oxygen content in the beam. Similar adsorption pattern was observed for 1:2:z and 1:8:z series of beam compositions (not shown). Decreasing NO adsorption with increasing oxygen content clearly supports the repulsive interaction between NO and O species. A careful look at the O₂ adsorption trend in the transient state gives an idea about the high initial (threshold) coverage of oxygen along with N and/or NO on Pd(111) surface. Only when the above O-coverage is attained, the CO-adsorption begins. This result is something new and similar to the trend that was observed in CO+O₂ reaction too. As it is addressed in detail in the earlier chapter, it will not be discussed here. It is to be noted that the NO+CO reaction presented in the earlier chapter and in Figure 6.4 shows a significant difference with respect to CO and NO adsorption, and this is attributed to a possible subsurface/bulk oxygen within Pd(111).

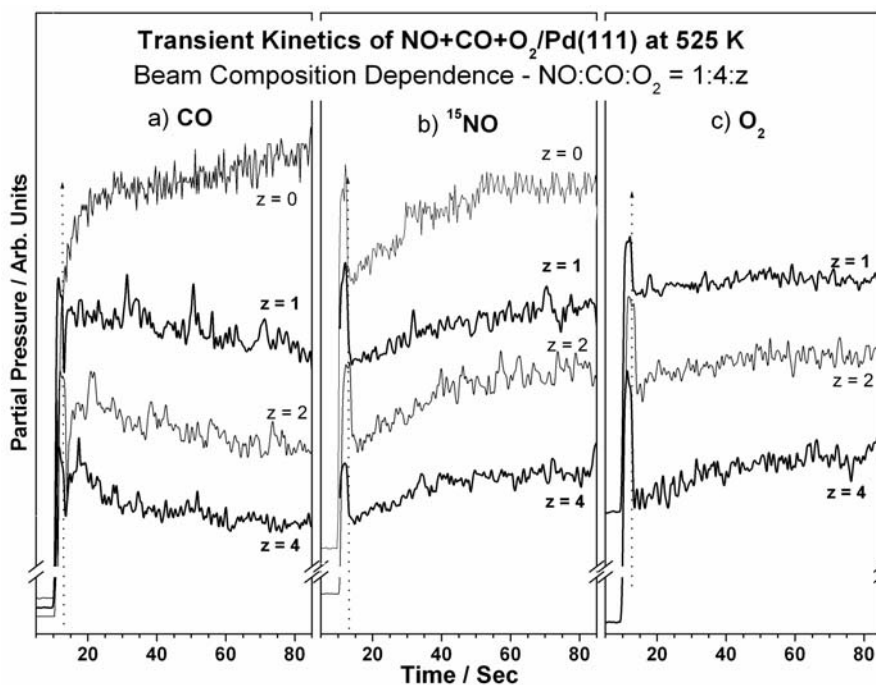


Figure 6.4. Transient uptake of the reactants a) CO, b) NO and c) O₂ from the collimated molecular beams of 1:4:z NO:CO:O₂ compositions, where $z = 0, 1, 2$ and 4 on the Pd(111) surface at 525 K.

Figure 6.5 shows the temporal evolution of products formation for 1:4:z of NO:CO:O₂ at 525 K, for which reactants adsorption was presented above. CO₂ desorption begins almost simultaneously at the time of shutter opening with z = 0 beam. However the delay observed in the production of CO₂ with oxygen containing beam decreases with increasing oxygen content. Hence, a fast SS CO₂ production can be attained with high oxygen content in the beam (>4). Needless to say, that increasing oxygen content in the beam favors CO₂ production. On the other hand, N₂ and N₂O production decreases with increasing oxygen content, as expected since the concentration of NO in the beam decreases with increasing oxygen content for 1:4:z NO:CO:O₂ beam composition. While comparing 1:4:0 beam with a 1:4:4 beam, though the concentration of NO in the beam decreases nearly to half, N₂ production decreases much more. In contrast, N₂O production increases slowly with increasing oxygen content, till z = 2; however it decreases with further increase in oxygen content in the beam. Hence oxygen retards not only the decomposition of NO but favors N₂O formation to some extent.

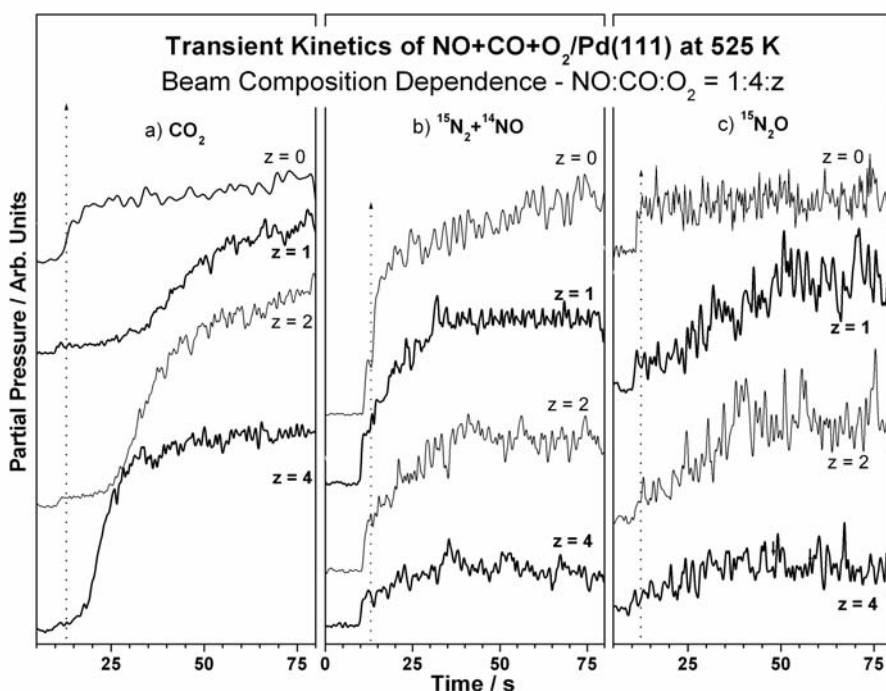


Figure 6.5. Transient production of the products a) CO₂, b) N₂ and c) N₂O for the collimated molecular beams of 1:4:z ¹⁵NO:CO:O₂ compositions, where z = 0, 1, 2 or 4 on the Pd(111) surface at 525 K.

6.3.2.3. Temporal Evolution of N₂ and N₂O from O₂-lean and O₂-rich Beams:

A comparison was made for the production of N₂ and N₂O for the compositions, 1:4:0 (oxygen lean) and 1:2:2 (oxygen rich) of NO:CO:O₂ beams. It is to be noted here that these compositions contains same NO concentration in both the beam; two parts of CO was replaced by two parts of oxygen in 1:2:2 beam and the total flux remains the same. Hence a comparison of these two beams for NO reduction and the influence of oxygen on the production of N₂ and N₂O will be highly valid. Figure 6.6 shows the results of such comparison; left panel contains the transient and steady state productions of (a) N₂ and (c) N₂O for a 1:4:0 NO:CO:O₂ beam compositions; right panel contains (b) N₂ and (d) N₂O productions for a 1:2:2 beam. Introduction of oxygen in the beam reduces the N₂ production, as expected. Nonetheless, a large production of N₂, compared to the SS values, was observed for the 1:2:2 beam in the TS. Oxygen-less and oxygen-rich beams differ in their NO-reduction and N₂ formation kinetics in the SS, and the TS is relatively unaffected. Almost comparative production of N₂O is observed for both the cases, hinting that the N₂ formation might be through N₂O_(ads) intermediate, in addition to N_(ads)+N_(ads) recombination.

Temporal evolution of N₂ and N₂O from 1:4:0 and 1:2:2 beams of NO+CO+O₂ compositions shows a slow response for beam oscillations during SS is evident from Figure 6.6. A close observation on the perturbation responses for both N₂ and N₂O SS production clearly reveals that the response for N₂ is slower than that of N₂O. In fact it is more clear for 1:2:2 NO:CO:O₂ beam composition than 1:4:0. However, CO₂ partial pressure displays fast changes on beam oscillations in the SS. The above observations clearly indicate that the rate determining step is predominantly controlled by N₂ formation step, as in NO + CO reaction.

6.3.3. Steady State Kinetics of NO+CO+O₂ /Pd(111):

Figures 6.7, 6.8 and 6.9 shows SS rates measured for N₂, N₂O, and CO₂, respectively, for 1:y:z NO:CO:O₂ beam compositions, where y = 2, 4 and 8 and z = 0, 1, 2 and 4. Compositions with each y (CO-content) with different z values (O₂-content) were plotted in separate panels, (a) 1:2:z, (b) 1:4:z, and (c) 1:8:z of NO:CO:O₂ compositions for all three products separately for better clarity. Generally the maximum rate of formation of all products lies in the range of 475 and 525 K, which is in good agreement with our earlier results on NO+CO/Pd(111) [69, Chapter 4].

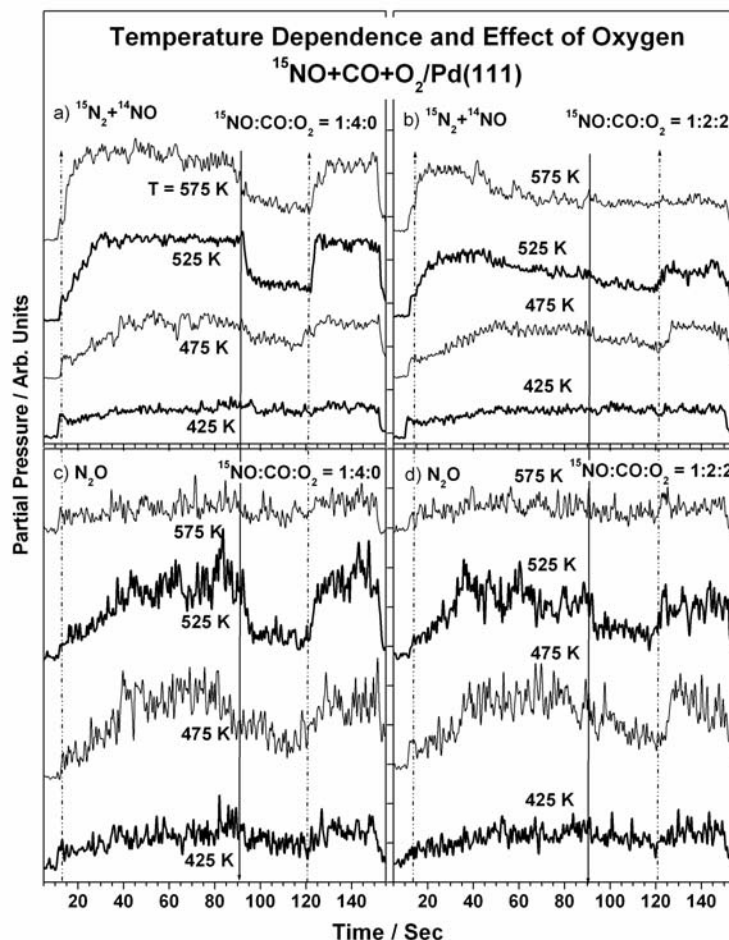


Figure 6.6. Temporal evolution of N-containing products N₂ (a and b) and N₂O (c and d) from the collimated molecular beams of 1:4:0 and 1:2:2 NO:CO:O₂ compositions.

The rate maximum decreases for all the products on either side of the above temperature range. Further, N₂ and CO₂ shows exactly an opposite trend in rate changes with oxygen content in Figs. 6.7 and 6.9. An important point to be noted is that a small amount of oxygen ($z=1$ and 2) does not influence the N₂ rate very significantly, although it almost stops NO reduction at high oxygen content ($z = 4$ and 8). Rather a sizeable increase in N₂O production observed at 525 K is to be noted with small amount of oxygen in the beam ($z = 1$ and 2). Some of the specific results are of particular interest to highlight the above points, are listed below: The SS rate for both N₂ and N₂O reduces nearly to half when comparing 1:4:0 beam with that of 1:2:2 beam, where the NO concentration remains the same in both the beams (see Figures 6.6, 6.7 and 6.8). While comparing a 1:8:0 NO:CO:O₂ beam with a 1:4:4 beam, (NO content is same again in these two compositions) the N₂ production reduces to half but N₂O production remains the same

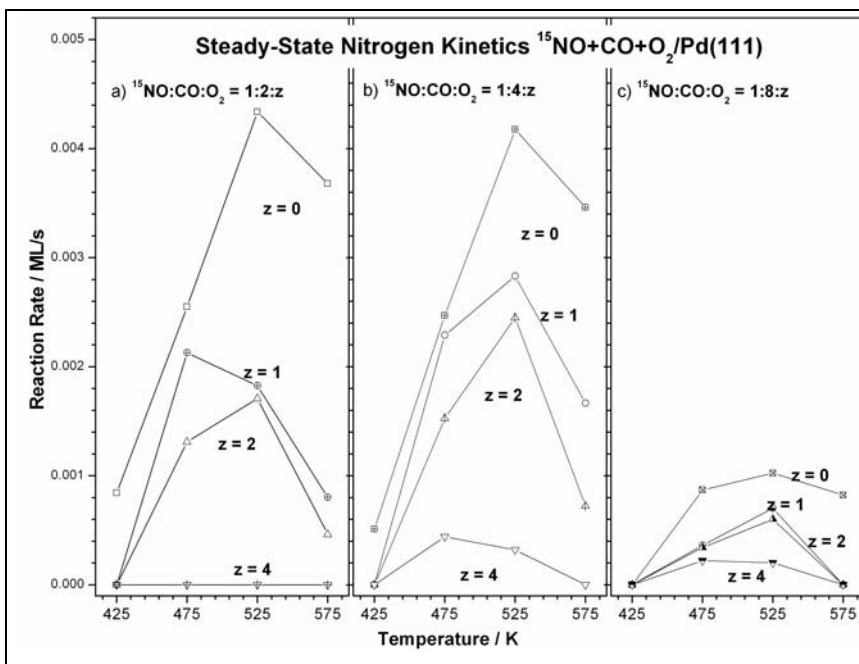


Figure 6.7. Steady state rates of N_2 production are presented for a) 1:2:z, b) 1:4:z, c) 1:8:z of $\text{NO}:\text{CO}:\text{O}_2$ beam compositions, where $z = 0, 1, 2$ or 4.

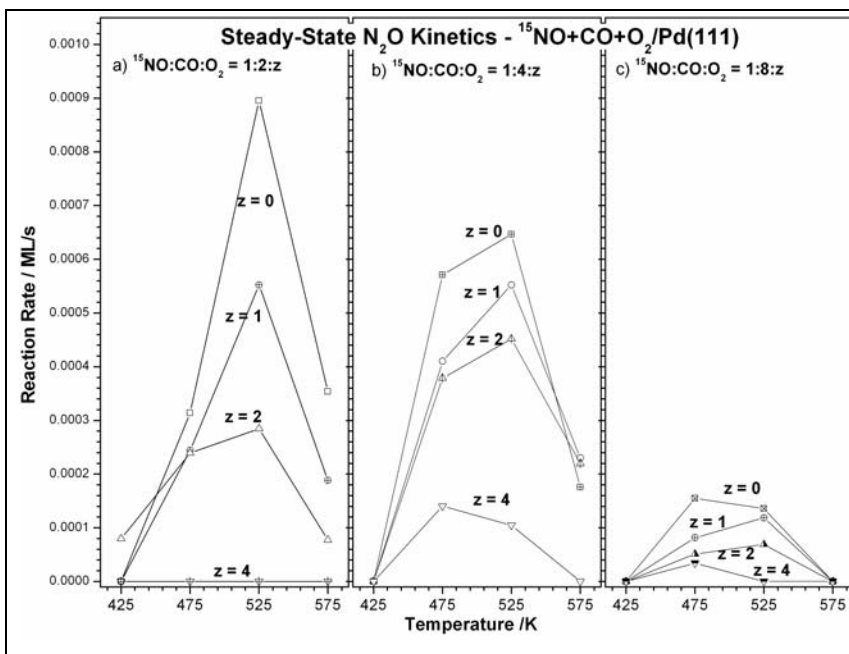


Figure 6.8. Temperature dependence of steady state rates of N_2O production are displayed for a) 1:2:z, b) 1:4:z, c) 1:8:z of $\text{NO}:\text{CO}:\text{O}_2$ beam compositions, where $z = 0, 1, 2$ or 4.

(see figures 6.7 and 6.8). This observation also hints that N_2 formation might be through another channel of dissociation of N_2O intermediate. However, $\text{N}+\text{N}$ recombination is still a major channel for N_2 production under any of the experimental conditions employed. An important observation to be highlighted here is the considerable production

of N_2 observed with O-rich beams clearly reveals the efficiency of Pd-based TWC's for NO reduction in net oxidizing conditions in the real world conditions.

Figure 6.8 shows SS N_2 production rates and it is interesting to note that for 1:2:z series of NO:CO:O₂ compositions when $z = 4$, no SS production of both N_2 and N_2O was observed at all the temperatures investigated. But for the same z value ($z = 4$), 1:y:z NO:CO:O₂ beam compositions, where $y = 4$ and 8, produces same SS N_2 at temperatures 475 and 525 K, because the oxygen content in the beam equates when $y = 4$, i.e. 4 parts of CO, and becomes half when $y = 8$. The above indicate that an effective surface oxygen removal were assisted by an increasing CO content in the beam. In other words, the chances of NO adsorption and dissociation under the oxygen-rich conditions are also sizeable.

On the other hand, CO_2 production rate increases with z value, i.e. O-content in the beams of type 1:y:z of NO:CO:O₂. SS rate of CO_2 reaches its maximum at 525 K for all the compositions studied under the present conditions. Thus increasing oxygen content increases the rate of CO_2 production with another oxidant molecule, NO, present in the beam (Figure 6.9) for all the compositions of the type 1:y:z of NO:CO:O₂ reported here.

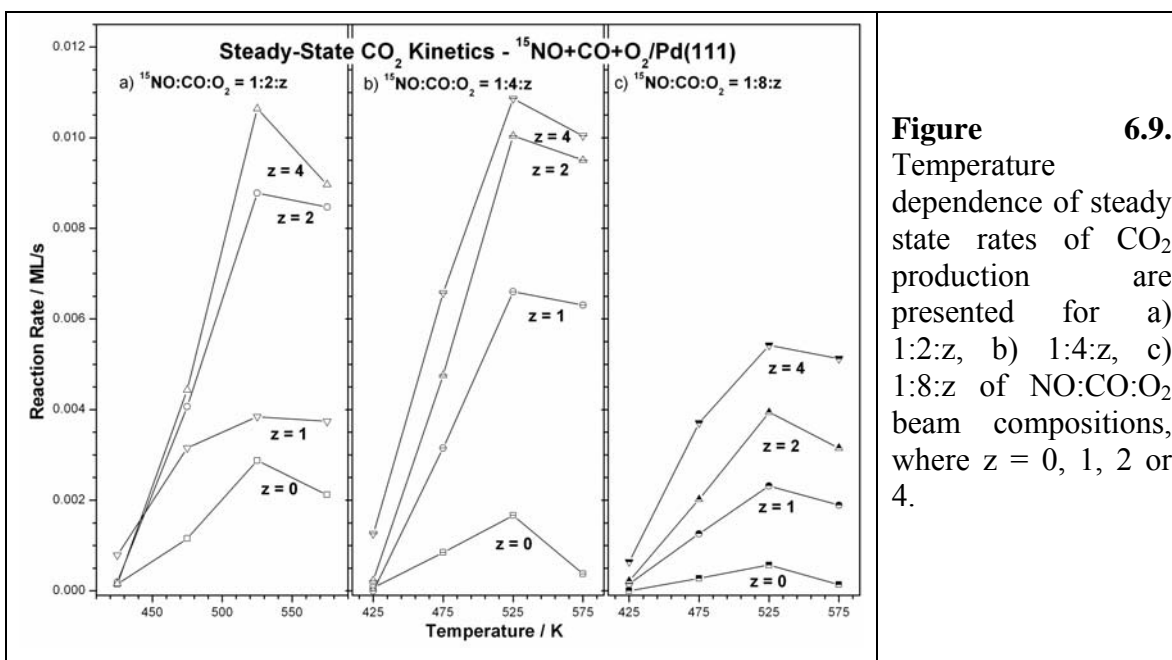


Figure 6.9. Temperature dependence of steady state rates of CO_2 production are presented for a) 1:2:z, b) 1:4:z, c) 1:8:z of NO:CO:O₂ beam compositions, where $z = 0, 1, 2$ or 4.

6.3.3.1. The Effect of NO on the Steady State CO₂ Production for CO+O₂ Reaction on Pd(111) Surface:

As far as CO+O₂ reaction on Pd(111) surface is concerned, the influence of NO on CO oxidation has to be understood, since Pd surfaces are well known for hydrocarbons and CO oxidations particularly in the SS. Hence a comparison was made for the SS CO₂ productions from 8:2 and 8:4 CO:O₂ beam compositions to that of 8:2:1 and 8:4:1 CO:O₂:NO beam compositions, respectively, with the same total flux (Figure 6.10). At 425 K, comparatively smaller SS CO₂ production was observed with 8:2:1 CO:O₂:NO beam composition than 8:2 CO:O₂ beam composition. But ≥ 475 K a comparable production of CO₂ in SS is observed for both the beams (panels (a) and (b) in

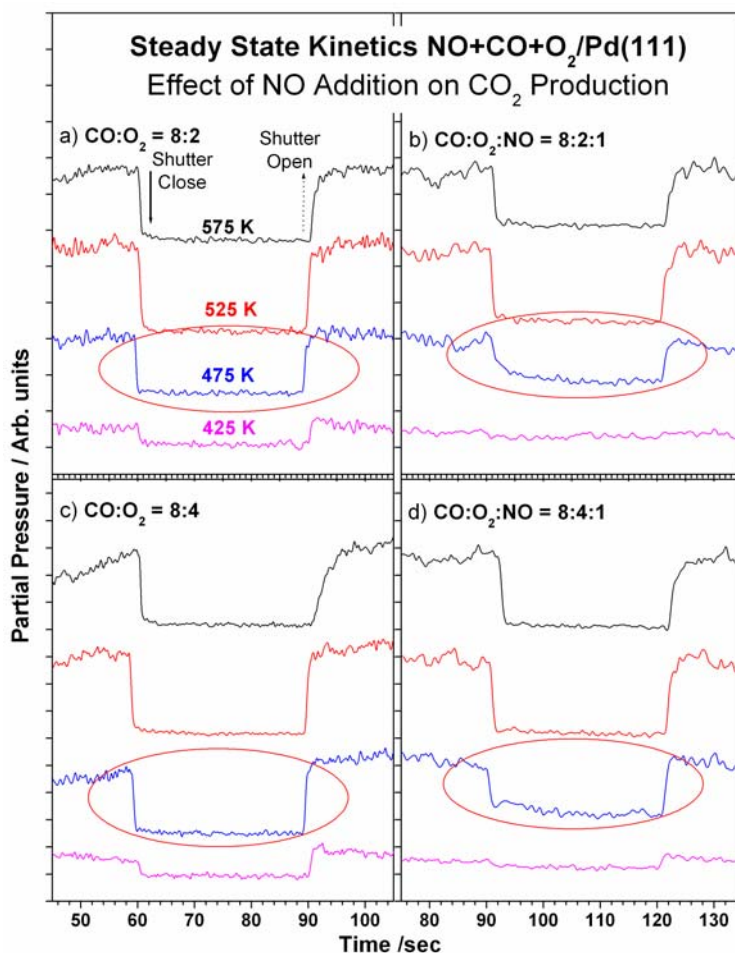


Figure 6.10. Effect of NO addition to the CO+O₂ beam towards the production of CO₂. CO₂ production for CO+O₂ beam on Pd(111) surface is shown in the left panel, ((a) 8:2 and (c) 8:4 of CO:O₂ composition) along with the same for CO+O₂+NO beam in right panels ((b) 8:2:1 and (d) 8:4:1 of CO:O₂:NO composition).

figure 6.10). A slow decay CO₂ production for beam blocking has to be noticed after the addition of NO in the beam. This clearly reveals that NO decomposition and its presence on the surface delays CO₂ production to some extent. The above mentioned effect was not observed ≥ 525 K. Hence the addition of NO to a CO+O₂ beam changes the SS CO₂ production rate to a somewhat lower value at temperatures < 475 K. It is to be mentioned here that, NO decomposition becomes spontaneous ≥ 525 K and hence a fast response to the beam perturbation treatments was observed as in CO+O₂ reaction on Pd(111) surface. However it need not be true below 525 K, especially on oxygen covered Pd(111) surfaces. Hence above 475 K, N+N recombination or N₂O decomposition on the surface determines the overall rate of NO+CO+O₂ reaction on Pd(111) in oxidizing atmosphere. As shown in Figure 6.6, N+N recombination might be the rate determining step for the overall NO+CO reaction on Pd(111) surface in oxidizing atmosphere. N-being a common intermediate to both nitrogen and nitrous oxide and the latter being a minor product, it is likely that N+N recombination might be an overall RDS as in NO + CO reaction.

6.3.4. Beam Switching Experiments:

Beam switching experiments were performed for two principal reasons: (1) to analyze the reversibility of the reaction under oxygen poor and oxygen rich conditions on Pd(111) surfaces; and (2) to observe the difference between the product evolution under these two opposing conditions especially in the transient state. Beam switching experiments were performed by following the procedure described below and a representative example is given in Figure 6.11: two mixtures of compositions 1:2 of NO:CO (Oxygen poor - beam P) and 1:1:1 of NO:CO:O₂ (oxygen rich - beam R) were taken separately in two beam mixing reservoirs. 1:2 NO:CO beam was switched on at $t = 10$ s; and the shutter was opened at around $t = 13$ s to allow the beam to directly interact with the Pd(111) substrate kept at 525 K. SS rates were measured by blocking the beam at $t = 60$ s and 100 s for 20 s each; After the reaction reached the SS above $t > 120$ s, at $t = 150$ s the beam P was switched off. Beam R was switched on at $t = 165$ s for another 150 s and the SS rates were measured twice before $t = 300$ s.

The two beams were alternated one by one on Pd(111) for 20 s each and the treatment was repeated again for 10 s and then for 5 s. SS CO₂ production rate increased visibly from oxygen lean to oxygen rich beam in spite of halving CO-flux, whereas N₂

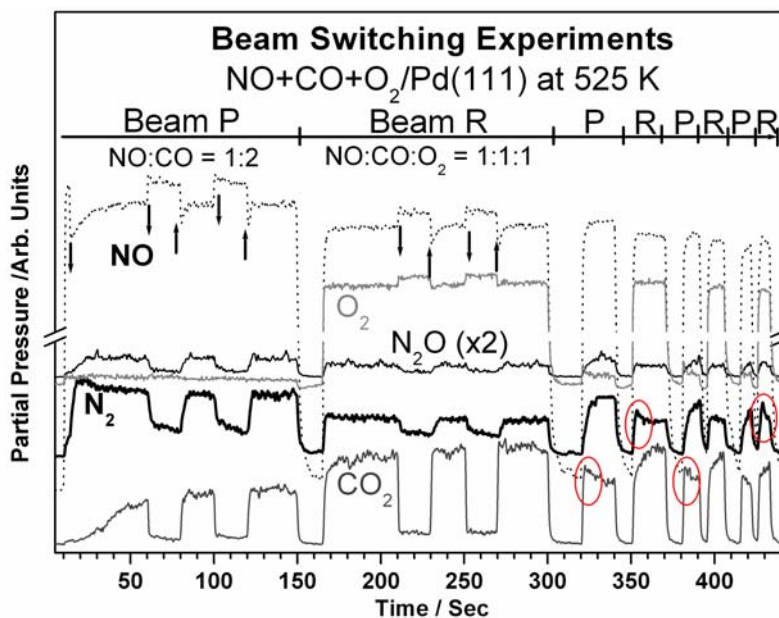


Figure 6.11. Raw data obtained in beam switching experiments for Pd(111) surface. In this example, the traces for CO₂, N₂, O₂, N₂O, and NO are shown as a function of time as the composition of the beam is switched between 1:2:0 (beam P) and 1:1:1 (beam R) NO:CO:O₂ compositions. The Pd(111) substrate was kept at 525 K. Clearly, the SS rate of CO₂ production is higher with the O₂-containing beam and N₂ and N₂O in oxygen-poor beam. The changes in reactivity for both the beams are completely reversible. Traces for all the masses are stacked vertically for better clarity. Encircled region in the transient state for nitrogen and CO₂ shows the large production.

and N₂O rates were decreased to nearly half though NO concentration remains constant in both the beams. A decrease in CO concentration to half with beam R (compared to beam P) does not reduce the rate of CO₂ production; indeed an increase was observed. Switching again to beam P gave more transient CO₂ production. Presumably, CO in the beam consumes some amount of oxygen on the Pd(111) surface from the earlier beam's exposure. However, a time delay of 3-5 s was observed after switching again to beam R with CO₂ production. The situation is just the reverse for N₂ and N₂O which essentially means that both N₂ and N₂O production is relatively high in the TS than in the SS. The reversibility of the Pd(111) surface for the fluctuation in the oxygen content is clear from this experiment.

A careful analysis of the CO₂ production with beam P and N₂ production with beam R in the transient state between $t = 320$ and 430 s suggest the following: (a) Predominantly oxygen covered Pd(111) surface at the end of the exposure of beam R,

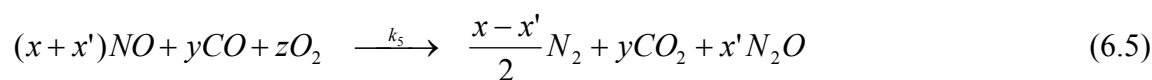
results in high transient state CO₂ production with subsequent beam P. (b) In contrast, relatively O-free Pd(111) surface at the end of the exposure of beam P, results in high transient state N₂ production with subsequent beam R. Main results to be noted here is the high N₂ production with oxygen-rich beam R. High transient state N₂ production observed with beam P on clean Pd(111) at the beginning of reaction demonstrate the requirement of relatively oxygen free Pd(111) surface for high NO dissociation and N₂ formation. However, N₂O production does not show this trend. Large N₂ production observed in the TS with oxygen-rich beam from fast beam switching experiments is in contradiction to that of from oxygen-poor beam on Rh(111). [153]

6.4. Discussion

The kinetic data reported in this manuscript focus on the characterization of the effect of oxygen on the reduction of NO by CO on Pd(111) surfaces. It is generally believed that the addition of oxygen is detrimental to the reduction of NO, because oxygen is expected to consume the carbon monoxide on any Pt-group metal surfaces. Indeed a logical argument of NO-reduction in a net oxidizing environment is just not possible. In fact O₂ competes highly to NO for the CO in the mixture and the adsorption behavior shown in the results section is evident for this. In particular, the deposition of oxygen can alter the adsorption properties of the palladium surfaces. Oxygen diffuse into the subsurface region above 500 K [45] and it changes the nature of the metal at temperatures above 500 K. Another related issue pertinent to the kinetics of this system is the change in adsorption dynamics due to a competition among NO, CO, and O₂ molecules for adsorption sites. Both CO and NO exhibit a large extent of adsorption with high sticking coefficient below 500 K; however, oxygen adsorption is predominant above 500 K on Pd(111) surfaces. Oxygen may inhibit the adsorption of the other reactants, but may also remove excess CO in some circumstances, and hence helping (but not poisoning), the overall NO reduction reaction as in Rh(111) case [153]. Other effects like the influence of NO on CO + O₂ reaction need to be considered to understand the overall reactivity of the NO + CO + O₂ mixture. NO + CO + O₂/Pd(111) has the same the sequence of elementary steps formulated by us for NO + CO/Pd(111) system [69] along with a dissociative oxygen adsorption,



The overall reaction may be written as



The rate-determining step does not change due to the addition of oxygen in the reactant mixture. The slow decay kinetics observed with nitrogen production in the SS for beam oscillation is the striking evidence that N+N recombination controls the overall rate of the reaction, as in NO+CO reaction. However, oxygen addition affects the overall reaction kinetics, including a significant formation of N₂O, compared to that in NO+CO reaction, for the present ternary system and those factors are discussed below:

6.4.1. The Effect of O₂ on NO Adsorption and Dissociation:

From the results derived from Figures 6.4, and 6.5, the addition of O₂ to the NO+CO mixture has a definite positive impact in the production of CO₂. As long as the CO-flux with sufficient intensity is used, oxygen does not poison the surface and large CO₂ production was observed. Indeed this conclusion is in good agreement with our results on CO + O₂ reaction as well as with that of Schalow et al on Pd/Fe₂O₃. [172] Though initial sticking coefficient of CO is negligible ≥ 525 K, it increases after few seconds with increasing O-coverage on Pd(111) from the NO+CO+O₂ mixture ≥ 525 K (Figure 6.4). On the other hand, O-atoms occupy the adsorption sites and NO adsorption capacity decreases with increasing temperature as well as with increasing oxygen coverage on the surface. The formation of subsurface diffusion of oxygen likely prevents NO adsorption with increasing oxygen content in the reactants mixture. Hence a reasonable retardation for NO decomposition on Pd(111) surface was observed due to oxygen and probability of N₂O formation increases especially at temperatures between 475 K and 525 K. At higher temperatures (>525 K), NO decomposition also contributes to the rate determining step as observed for NO+CO/Pd(111) system. At temperatures below 475 K, CO₂ production follows the trend of CO+O₂/Pd(111) reaction [chapter 5] (see Figure 6.3). Presence of oxygen thus significantly decreases the dominance of NO over CO for adsorption on Pd(111) observed in the case of NO+CO reaction. [69]

6.4.2. The Effect of NO on CO+O₂ Kinetics:

The role NO on the overall NO + CO + O₂ reaction could be better understood from the experiments carried out below 525 K. Figure 6.10 provides such an example. At 425 K, presence of NO almost completely suppresses CO₂ production. It has to be remembered here that NO dissociation starts around 400 K [Chapter 3], but still it is not complete at 475 K. Further, under the reaction conditions the equilibrium coverage of CO and oxygen should be considerably high and hence finding two adjacent vacant sites for NO-dissociation is difficult. CO-desorption is relatively fast above 450 K, and hence sizeable NO dissociates at 475 K and starts contributing to the overall reaction. Nonetheless, due to the incomplete dissociation of NO around 475 K, the beam perturbation treatment shows slower response than that of CO+O₂ reaction at 475 K. Alternatively, the adsorbed NO dissociates at the time of shutter closing and make the oxygen and nitrogen available for CO oxidation and N+N recombination. It is well known that N+N recombination is a diffusion controlled process, which is a slow process and controls the overall rate to a large extent. The presence of oxygen adsorbate retards the NO dissociation and hence a sizeable molecular NO available on the surface makes the N₂O formation relatively easier. Increasing oxygen content increases CO₂ production rate at all the temperatures investigated. But when we compare these rates of CO₂ formation for NO + CO + O₂ reaction with CO + O₂ reaction, lower rates were observed ≤475 K. Relatively large oxygen adsorption between 500 and 700 K, with decreasing NO-adsorption changes the nature of the overall reaction increasingly towards CO + O₂ reaction at high temperatures.

6.4.3. Beam Switching Experiments:

Real world three-way catalysts employed in the automobiles face a significant fluctuation depending on the driving conditions and hence the composition of the auto exhaust varies significantly. Although we cannot explore into the minor details of all the possible fluctuations, two extreme situations are easy to be modeled based on either the oxygen/fuel rich or poor conditions. Most of the above mentioned fluctuations should be between the above two extreme conditions. Reversibility between the above conditions is

mandatory for the best performance of TWCs. Fast molecular beam switching experiments performed (Figure 6.12) was to simulate the above conditions. First of all, an excellent reversibility for both the conditions on Pd(111) surface was observed. Surprising thing to be noticed here is an increase in the SS CO₂ production; though the concentration of CO reduced to half in oxygen rich conditions (compared to fuel rich conditions) in Figure 6.11, which should lead to more N₂ and N₂O. Expectedly, a large increase in both N₂ and N₂O production was observed with fuel-rich conditions in the SS. Nonetheless, more interesting is the observation of large N₂ production in the TS with oxygen-rich beam. As mentioned in the results section, relatively clean or less-oxygen-covered Pd-surfaces help in NO dissociation in the TS. Similar condition was achieved by exposing the Pd-surface to beam P with 1:2 NO:CO ratio, which avoids or decreases oxygen accumulation from NO-dissociation. However, subsequent oxygen-rich beam builds up significant oxygen coverage on Pd and hence SS NO-dissociation decreases. Nonetheless, the above significant oxygen coverage helps for fast CO-oxidation in the next half-cycle of beam P and significant NO-reduction could be achieved in the SS. Although the above method might not reach 100% efficiency towards NO-reduction, by fast and appropriate cycling between the oxygen-rich and oxygen-poor exhaust compositions, a better NO-reduction management is possible. Making use of a significantly large NO-dissociation on relatively oxygen-free Pd-surface is the key finding from this experiment.

6.4.4. Comparison with Previous Reports:

Very few studies were reported on NO + CO + O₂ reaction on Pd surfaces. [182-185] Graham et al [183] found that the rate of CO₂ production for NO + CO + O₂ reaction was two orders of magnitude greater than that of NO + CO reaction on a Pd(100) surface, which is in qualitative agreement with our results on Pd(111) surfaces too. However, at temperatures below 480 K, the rates for NO + CO + O₂ reaction were greater than CO + O₂ reaction on the Pd(100) surface, which is in contradiction to our observation. This difference in behavior may be attributed due to the possible structure sensitivity of the reaction, like the NO+CO reaction on Pd surfaces as observed by Goodman et al [186]. Ma et al, [184-185] observed that the production of N₂ occurs

through N₂O intermediate with increasing surface oxygen species on a Pd(110) surface, matching with our observation on Pd(111) surface. As their main objective was the spatial distribution of the products, we cannot make a direct comparison with their study. While comparing this reaction with Rh surfaces [153], the efficacy of the Pd surfaces can be understood clearly under net oxidizing conditions as a TWC from our present studies, especially in view of the present generation fuel-efficient automobiles.

6.5. Summary

An investigation on the influence of oxygen in NO + CO reaction on Pd(111) surfaces was made between 425 and 575 K. Isothermal kinetic measurements were performed with all the beam conditions employed. These experiments were carried out in ultra high vacuum, but under conditions where the NO reduction reaction could be sustained in a catalytic regime similar to that encountered in a realistic three-way catalytic converter.

High reactivity was found in the temperature window of 475 K to 575 K. A detailed analysis of the kinetic data led to the conclusion that the main effect of the oxygen addition to the NO+CO mixture is to inhibit the NO-dissociation rates and clearly enhance the rate of CO₂ production under most circumstances. This effect is more pronounced at and above 525 K. However, the domination of NO-adsorption over CO on Pd(111) surface remains operative below 475 K even in the presence of surface oxygen with a low CO₂ production rate than CO + O₂ reaction on Pd(111) surface. Surface oxygen seems to decrease NO dissociation for the overall reaction above 525 K and enhances the CO-oxidation rates. The kinetic data clearly point to a preferential reaction of CO with oxygen, instead of NO, especially above 475 K. Although it is not explored in detail, diffusion of oxygen into the sub-surfaces of Pd(111) might be responsible for higher CO₂ rates observed. An increasing direct CO-adsorption observed in our experiments on the oxygen-covered Pd surfaces at high temperatures (525 K and above) supports the above. The overall reaction was largely controlled by the N+N

recombination below 525 K and NO-dissociation also increasingly contributes to the RDS at high temperatures and oxygen content in the beam.

Pd(111) surface shows complete reversibility for the fluctuations between oxygen-rich and oxygen-lean conditions. Large NO-dissociation on relatively oxygen-free Pd-surfaces may be exploited through fast beam-switching for better de-NO_x management.

Chapter 7

Conclusions and Future Outlook

“Our objectives to build MBI and study and explore the microkinetic details of deNO_x reactions on Pd(111) surfaces were accomplished to a reasonable extent. However, our studies does not stop here and a future outlook of what can be done further is narrated briefly.”

Conclusions and Future Outlook

The importance of fundamental kinetic studies to the catalytic science, particularly with molecular beams, was emphasized in **Chapter 1**. A molecular beam instrument was fabricated successfully at National Chemical Laboratory, Pune, India, as the first phase of the dissertation work presented here and the important aspects of fabrication details and experimental methods were discussed in **Chapter 2**.

MBI was successfully employed to probe NO adsorption and its dissociation on Pd(111) surface through isothermal kinetic experiments between 300 and 525 K and presented in **Chapter 3**. Molecular NO adsorption was observed below 400 K. NO dissociation starts on Pd(111) surfaces above 400 K and the dissociation products, N₂ (major product) and N₂O (minor product) was observed clearly in the transient state at temperatures >425 K. Nitrogen formation occurs through a diffusion-controlled mechanism and it could be the rate limiting step, at least below 500 K. Substantial NO equilibrium coverage was observed below 500 K. Oxygen diffusion into the subsurface starts around 475 K and increases significantly above 525 K. Sticking coefficient measurements for NO adsorption between 300 and 350 K up to high coverage, indicating the precursor mediated adsorption. s_{NO} decreases with increasing coverage and temperature. Some inherent NO dissociation activity on Pd(111) surfaces suggests that more spectroscopic and *in-situ* structural works can shed more light on this.

A kinetic study on the NO + CO reaction on Pd(111) surfaces carried out at a wide range of temperature, beam composition and total flux was reported in **Chapter 4**. A significant and comparable catalytic activity as that of Rh(111) in the narrow temperature window 475-575 K was observed. N₂ formation limits the rate of the overall reaction below 525 K and NO dissociation step also contributes toward the RDS above 525 K. Direct displacement of CO_{ads} by NO was observed between 375 and 475 K and the transient state coverage calculations show that the surface composition was different from the NO:CO beam composition at low temperatures. The rate of NO + CO reaction increases linearly with increasing total beam flux and indicates a first order dependence on F_{NO}. Irrespective of the NO:CO composition, a rate maximum always occurs between 475 and 525 K for all the beam compositions investigated. However, there is a

broadening of the active rate regime from 475 to 525 K for 2:1 to 475-625 K for 1:4 NO:CO. Both NO-rich and CO-rich beams show poor catalytic activity and is attributed to surface poisoning by those species.

Revisit on CO oxidation reaction on Pd(111) surface with mixed molecular beams at wide range of temperatures (from 375 K to 600 K) for a variety of CO+O₂ beam compositions ranging from 4:1 to 1:20 provided interesting information about the reaction (**Chapter 5**). 1:2 beam composition of CO:O₂ at 525 K shows maximum rate in the steady state and not a stoichiometric beam composition. However, a stoichiometric coverage (1:1) of both CO and O on the surface is essentially required to achieve a high steady state rate. Below 450 K, the CO oxidation process is mainly controlled by the extent of CO desorption. It is clearly demonstrated that direct CO adsorption is feasible with significant sticking coefficient at high temperatures (≥ 550 K) on oxygen-covered Pd(111) surfaces under steady-state conditions. Further no significant oxygen poisoning is observed under any conditions, if there is sufficient CO-flux. Broadening of temperature window for high rate regime with any CO:O₂ composition highlight the relevance of this chapter work to green chemistry. However the mechanism is different with different CO:O₂ ratios and oxygen sub-surface diffusion complicates the analysis; nevertheless it is worth further investigating with Pt-group metals

An investigation on the influence of oxygen in NO+CO+O₂ reaction on Pd(111) surfaces was made between 425 and 575 K under isothermal kinetic measurements and discussed in **Chapter 6**. Though the experiments were carried out in ultra high vacuum, a catalytic regime similar to that encountered in realistic three-way catalytic converters was maintained. High reactivity was found in the temperature window of 475 K to 575 K. A detailed analysis of the kinetic data led to the conclusion that the main effect of the oxygen addition to the NO+CO mixture is to inhibit the NO-dissociation rates and clearly enhance the rate of CO₂ production under most circumstances. This effect is more pronounced at and above 525 K. However, the domination of NO-adsorption over CO on Pd(111) surface remains operative below 475 K even in the presence of surface oxygen. Surface oxygen seems to decrease the extent of NO dissociation for the overall reaction above 525 K and enhances the CO-oxidation rates. The kinetic data clearly point to a preferential reaction of CO with oxygen, instead of NO, especially above 475 K. An

Chapter 7 – Conclusions

increasing direct CO-adsorption observed in our experiments on the oxygen-covered Pd surfaces at high temperatures (525 K and above) indicates a reversal in CO-adsorption at high temperatures on O/Pd(111) surfaces.. The overall reaction was largely controlled by the N+N recombination below 525 K and NO-dissociation also increasingly contribute to the RDS with increasing temperature and oxygen content in the beam. Beam switching experiments suggests a better way to manage NO-reduction by fast oscillation between oxygen-rich and oxygen-lean compositions. Indeed this is highly worth exploring with a practical TWC and any little success would contribute to make our environment greener.

Above studies clearly indicate that more studies, especially spectroscopic studies, are required for the reactions discussed in this dissertation particularly on Pd supported on a metal oxide support.

References*

1. Somorjai, G. A. in Introduction to Surface Chemistry and Catalysis, *John Wiley & Sons, New York, 1994*.
2. Ertl, G. *Adv. Catal.* **2000**, 45, 1.
3. Schlögl, R. *Cat. Tech.* **2001**, 5, 146.
4. Schlögl, R. *Angew. Chem. Int. Ed.* **1998**, 37, 2333.
5. Goodman, D. W. *Ann. Rev. Phys. Chem.* **1986**, 37, 425.
6. Goodman, D. W. *Surf. Sci.* **1994**, 299/300, 837.
7. Boudart, M. *Adv. Catal.* **1969**, 20, 156.
8. Goodman, D. W.; Kelley, R. D.; Madey, T.E.; Yates, Jr. J. T. *J. Catal.* **1980**, 63, 226.
9. Zhu, G.; Han, J.; Zemlyanov, D. Y.; Ribeiro, F. H. *J. Am. Chem. Soc.* **2004**, 126, 9896.
10. Campbell, C. T.; Goodman, D. W. *Surf. Sci.* **1982**, 123, 413.
11. Goodman, D. W.; Kiskinova, M. *Surf. Sci.* **1981**, 105, L265.
12. Kiskinova, M.; Goodman, D. W. *Surf. Sci.* **1981**, 108, 64.
13. Goodman, D. W. *Appl. Surf. Sci.* **1984**, 19, 1.
14. Rostrup-Nielsen, J. R.; Pedersen, K. *J. Catal.* **1979**, 59, 395.
15. Bonn, M.; Funk, S.; Hess, Ch.; Denzler, D. N.; Stampfl, C.; Scheffler, M.; Wolf, M.; Ertl, G. *Science* **1999**, 285, 1042.
16. Ertl, G. *Chem. Rec.* **2000**, 1, 33.
17. Ribeiro, F.H.; Gerken, C. A.; Rupprechter, G.; Somorjai, G. A.; Kellner, C.S.; Coulston, G.W.; Manzer, L. E.; Abrams, L. *J. Catal.* **1998**, 176, 352.
18. Bonzel, H. P.; Krebs, H. J. *Surf. Sci.* **1982**, 117, 639.
19. Bonzel, H. P. *Surf. Sci. Rep.* **1987**, 8, 43.
20. Nørskov, J. K.; Holloway, S.; Lang, N. D. *Surf. Sci.* **1984**, 137, 65.
21. Groff, A. *Appl. Phys. A* **1998**, 67, 627.
22. Gravil, P. A.; Toulhoat, H. *Surf. Sci.* **1999**, 430, 176.

* Follows ACS journals format

References

23. Freund, H-J.; Bäumer, M.; Libuda, J.; Risse, T.; Rupprechter, G.; Shaikhutdinov, S. *J. Catal.* **2003**, *216*, 223.
24. Hoffmann, J.; Meusel, I.; Hartmann, J.; Libuda, J.; Freund, H-J. *J. Catal.* **2001**, *204*, 378.
25. Bertarione, S.; ... Freund, H-J. *J. Phys. Chem. B* **2004**, *108*, 3603.
26. Bäumer, M.; Freund, H-J. *Prog. Surf. Sci.* **1999**, *61*, 127.
27. Somorjai, G. A.; Yang, M. *Top. Catal.* **2003**, *24*, 61.
28. Somorjai, G. A.; Rioux, R. M. *Catal. Today* **2005**, *100*, 201.
29. Hoffmann, J.; Schauer mann, S.; Johánek, V.; Hartmann, J.; Libuda, J. *J. Catal.* **2003**, *213*, 176.
30. Xu, C.; Lai, X.; Goodman, D. W. *Faraday Discuss.* **1996**, *105*, 247.
31. Luo, K.; Yi, C-W.; Davis, K. A.; Gath, K. K.; Goodman, D. W. *J. Phys. Chem. B* **2005**, *109*, 4064.
32. Xu, X.; Szanyi, J.; Xu, Q.; Goodman, D. W. *Catal. Today.* **1994**, *21*, 57.
33. Choi, Y-K.; Zhu, J.; Grunes, J.; Bokor, J.; Somorjai, G. A. *J. Phys. Chem. B* **2003**, *107*, 3340.
34. Kónya, Z.; Puentes, V.F.; Kiricsi, I.; Zhu, J.; Ager, J.W.; Ko, M.K.; Frei, H.; Alivisatos, P.; Somorjai, G.A. *Chem. Mater.* **2003**, *15*, 1242.
35. Freund, H-J.; Bäumer, M.; Libuda, J.; Risse, T.; Rupprechter, G.; Shaikhutdinov, S. *J. Catal.* **2000**, *216*, 223.
36. Schmidt, J.; Risse, T.; Hamann, H.; Freund, H-J. *J. Chem. Phys.* **2002**, *116*, 10861.
37. Bowker, M.; Holroyd, R. P.; Sharpe, R. G.; Corneille, J. S. Francis, S. M.; Goodman, D. W. *Surf. Sci.* **1997**, *370*, 113.
38. Bukhtiyarov, V. I.; Kaichev, V. V.; Prosvirin, I. P. *Top. Catal.* **2005**, *32*, 3.
39. Ozensoy, E. PhD Thesis, Texas A&M University **2004**.
40. Hess, C.; Ozensoy, E.; Yi, C-W.; Goodman, D.W. *J. Am. Chem. Soc.* **2006**, *128*, 2988.
41. Wallace, W. T.; Cai, Y.; Chen, M. S.; Goodman, D. W. *Phys. Chem. B* **2006**, *110*, 6245.

References

42. Kaichev, V. V.; Bukhtiyarov, V. I.; Rupprechter, G.; Freund, H-J. *Kine. Catal.* **2005**, *46*, 269.
43. Shen, Y. R. *Surf. Sci.* **1994**, *300*, 551.
44. Dellwig, T.; Hartmann, J.; Libuda, J.; Meusel, I.; Rupprechter, G.; Unterhalt, H.; Freund, H-J. *J. Mol. Catal. A* **2000**, *162*, 51.
45. Cremer, P. S.; Su, X.; Somorjai, G. A.; Shen, Y. R. *J. Mol. Catal. A* **1998**, *131*, 225.
46. McCrea, K.; Parker, J. S.; Chen, P.; Somorjai, G. A. *Surf. Sci.* **2001**, *494*, 238.
47. Rupprechter, G. *Annu. Rep. Prog. Chem. Sect. C* **2004**, *100*, 237.
48. Boronin, A. I.; Bukhtiyarov, V. I.; Vishnevskii, A. L.; Boreskov, G. K.; Savchenko, V. I. *Surf. Sci.* **1988**, *201*, 195.
49. Ogletree, D.; Bluhm, H.; Lebedev, G.; Fadley, C.; Hussain, Z.; Salmeron, M. *Rev. Sci. Instrum.* **2002**, *73*, 3872.
50. Bluhm, H.; Havecker, M.; Kleimenov, E.; Knop-Gericke, A.; Liskowski, A.; Schlögl, R.; Su, D. S. *Top. Catal.* **2003**, *23*, 99.
51. Kaichev, V. V.; Sorokin, A. M.; Timoshin, A. I.; Vovk, E. I. *Instrum. Exp. Tech.* **2002**, *45*, 50.
52. Pauly, H. in: Scoles, G. (Ed.) **1988** Atomic and Molecular Beam Methods, *1* (Oxford University Press) 99.
53. King, D. A.; Wells, M. G. *Surf. Sci.* **1972**, *29*, 454.
54. Libuda, J.; Freund, H-J. *J. Phys. Chem. B* **2002**, *106*, 4901 and references therein.
55. Zaera, F. *Prog. Surf. Sci.* **2001**, *69*, 1 and references therein.
56. Kleyn, A. W. *Chem. Soc. Rev.* **2003**, *32*, 87 and references therein.
57. Zaera, F. *Int. Rev. Phys. Chem.* **2002**, *21*, 433 and references therein.
58. Johanek, V.; Laurin, M.; Hoffmann, J.; Schauermaun, S.; Grant, A. W.; Kasemo, B.; Libuda, J.; Freund, H-J. *Surf. Sci.* **2004**, *561*, L218.
59. Rettner, C. T.; Pfnür, H. E.; Auerbach, D.J. *Phys. Rev. Lett.* **1985**, *54*, 2716.
60. Ceyer, S. T.; Beckerle, J. D.; Lee, M. B.; Tang, S. L.; Yang, Q. Y.; Hines, M. A. *J. Vac. Sci. Technol. A* **1987**, *5*, 501.
61. Doyen, G. *Top. Curr. Phys.* **1987**, *43*, 301.
62. Bowker, M. *Appl. Catal. A* **1997**, *160*, 89.

References

63. Madey, T. E. *Surf. Sci.* **1972**, *33*, 355.
64. Liu, J.; Xu, M.; Nordmeyer, T.; Zaera, F. *J. Phys. Chem.* **1995**, *99*, 6167.
65. Liu, J.; Xu, M.; Zaera, F. *Catal. Lett.* **1996**, *37*, 9.
66. Gopinath, C. S.; Zaera, F. *J. Catal.* **1999**, *186*, 387.
67. Gopinath, C. S.; Zaera, F. *J. Phys. Chem. B* **2000**, *104*, 3194.
68. Zaera, F. *Acc. Chem. Res.* **2002**, *35*, 129.
69. Thirunavukkarasu, K.; Thirumoorthy, K.; Libuda, J.; Gopinath, C. S. *J. Phys. Chem. B* **2005**, *109*, 13272.
70. Thirunavukkarasu, K.; Gopinath, C. S. Submitted to *J. Chem. Sci.* **2006**.
71. Thirunavukkarasu, K.; Gopinath, C. S. *in preparation*.
72. Gopinath, C. S.; Thirunavukkarasu, K. *in preparation*.
73. Cardillo, M.J. *Ann. Rev. Phys. Chem.* **1981**, *32*, 331 and references therein.
74. Prada-Silver, G.; Kester, K.; Loftier, D.; Hailer, G. L.; Fenn, J.B. *Rev. Sci. Instrum.* **1977**, *48*, 897.
75. Sawin, H. H.; Merrill, R. P. *J. Vac. Sci. Technol.* **1981**, *19*, 40.
76. Taylor, K. C. *Catal. Rev. Sci. Eng.* **1993**, *3*, 457.
77. Shelef, M.; Graham, G. W. *Catal. Rev. Sci. Eng.* **1994**, *36*, 433.
78. Kreuzer, T.; Lox, S. E.; Lindner, D.; Leyrer, J. *Catal. Today.* **1996**, *29*, 17.
79. Tagliaferri, S.; Köppel, R. A.; Baiker, A. *Stud. Surf. Sci. Catal.* **1998**, *116*, 61.
80. van Yperen, R.; Lindner, D.; Mussmann, L.; Lox, E. S.; Kreuzer, T. *Stud. Surf. Sci. Catal.* **1998**, *116*, 51.
81. Jobson, E. *Top. Catal.* **2004**, *28*, 191.
82. Salasc, S.; Skoglundh, M.; Fridell, E. *Appl. Catal. B* **2002**, *36*, 145.
83. Holles, J. H.; Davis, R. J.; Murray, T. M.; Howe, J. M. *J. Catal.* **2000**, *195*, 193.
84. Martinez-Arias, A.; Soria, J. *J. Catal.* **2001**, *204*, 238.
85. Berndt, H.; Schutze, F. W.; Richter, M.; Sowade, T.; Grunert, W. *Appl. Catal. B* **2003**, *40*, 51.
86. Olsson, L.; Persson, H.; Fridell, E.; Skoglundh, M. *J. Phys. Chem. B* **2001**, *105*, 6895.
87. Zhdanov, V. P.; Kasemo, B. *Surf. Sci. Rep.* **1997**, *29*, 31.

References

88. Peden, C. H. F.; Goodman, D. W.; Blair, D. S.; Berlowitz, P. J.; Fisher, G. B.; Oh, S. H. *J. Phys. Chem.* **1988**, *92*, 1563.
89. Permana, H.; Ng, K. Y. S.; Peden, C. H. F.; Schmiege, S. J.; Lambert, D. K.; Belton, D. N. *J. Catal.* **1996**, *164*, 194.
90. Borg, H. J.; Reijerse, J. F. C.-J. M.; van Santen, R. A.; Niemantsverdriet, J. W. *J. Chem. Phys.* **1994**, *101*, 10052.
91. Schmick, H.-D.; Wassmuth, H.-W. *Surf. Sci.* **1982**, *123*, 471.
92. Conrad, H.; Ertl, G.; Küppers, J.; Latta, E. E. *Surf. Sci.* **1977**, *65*, 235.
93. Bertolo, M.; Jacobi, K.; Nettesheim, S.; Wolf, M.; Hasselbrink, E. *Vacuum* **1990**, *41*, 76.
94. Bertolo, M.; Jacobi, K. *Surf. Sci.* **1990**, *226*, 207.
95. Ramsier, R. D.; Gao, Q.; Waltenburg, N.H.; Lee, K.-W.; Nooij, O. W.; Leerts, L.; Yates, Jr., J. T. *Surf. Sci.* **1994**, *320*, 209.
96. Ramsier, R. D.; Gao, Q.; Neergaard Waltenburg, H.; Yates, Jr., J. T. *J. Chem. Phys.* **1994**, *100*, 6837.
97. Sugai, S.; Watanabe, H.; Kioka, T.; Miki, H.; Kawasaki, K. *Surf. Sci.* **1991**, *259*, 109.
98. Nakamura, I.; Fujitani, T.; Hamada, H. *Surf. Sci.* **2002**, *514*, 409.
99. Sharpe, R. G.; Bowker, M. *Surf. Sci.* **1996**, *360*, 21.
100. de Wolf, C. A.; Nieuwenhuys, B. E. *Surf. Sci.* **2000**, *469*, 196.
101. Rainer, D. R.; Vesecky, S. M.; Koranne, M.; Oh, W. S.; Goodman, D. W. *J. Catal.* **1997**, *167*, 234.
102. Ozensoy, E.; Hess, C.; Goodman, D. W. *J. Am. Chem. Soc.* **2002**, *124*, 8524.
103. Piccolo, L.; Henry, C. R. *Appl. Surf. Sci.* **2000**, *162-163*, 670.
104. Piccolo, L.; Henry, C. R. *Surf. Sci.* **2000**, *452*, 198.
105. Prévot, G.; Henry, C. R. *J. Phys. Chem. B* **2002**, *106*, 12191.
106. Seldmair, C.; Seshan, K.; Jentys, A.; Lercher, J. A. *J. Catal.* **2003**, *214*, 308.
107. Hirsimaki, M.; Valden, M. *J. Chem. Phys.* **2001**, *114*, 2345.
108. Johánek, V.; Schauerer, S.; Laurin, M.; Libuda, J.; Freund, H.-J. *Angew. Chem. Int. Ed.* **2003**, *42*, 3035.

References

109. Johánek, V.; Schauermaun, S.; Laurin, M.; Gopinath, C. S.; Libuda, J.; Freund, H.-J. *J. Phys. Chem. B* **2004**, *108*, 14244.
110. Clausing, P. *J. Vac. Sci. Tech.* **1932**, *8*, 636.
111. Scoles, G. in: Scoles, G. (Ed.), *Atomic and Molecular Beam Methods, Vol. 1* (Oxford University Press) **1988**, 1.
112. Piccolo, L.; Henry, C.R. *J. Mol. Catal. A: Chemical* **2001**, *167*, 181,
113. Judai, K.; Abbet, S.; Wörz, A.S.; Heiz, U.; Henry, C.R. *J. Am. Chem. Soc.* **2004**, *126*, 2732.
114. Campbell, C. T.; Valone, S. M. *J. Vac. Sci. Technol. A* **1985**, *3*, 408.
115. Guevremont, J. M.; Sheldon, S.; Zaera, F. *Rev. Sci. Instrum.* **2000**, *71*, 3869.
116. Fisher, G.L.; Meserole, C.A. *J. Vac. Sci. Technol. A* **2005**, *23*, 722.
117. Thirunavukkarasu, K.; Nagarajan, S.; Gopinath, C.S.; Prasad, S.D. *in preparation*.
118. Engel, T.; Ertl, G. *J. Chem. Phys.* **1978**, *69*, 1267.
119. D'Evelyn, M. P.; Madix, R. *J. Surf. Sci. Rep.* **1984**, *3*, 413.
120. Asscher, M.; Somorjai, G. A. In *Atomic and Molecular Beam Methods*; Scoles, G. Ed. *Oxford University Press: Oxford, U.K.* **1988**, *2*, 489.
121. Rettner, C. T.; Auerbach, D. J.; Tully, J. C.; Kleyn, A. W. *J. Phys. Chem.* **1996**, *100*, 13021.
122. Libuda, J.; Meusel, I.; Hartmann, J.; Freund, H.-J. *Rev. Sci. Instrum.* **2000**, *71*, 4395.
123. Leisenberger, F. P.; Koller, G.; Sock, M.; Surnev, S.; Ramsey, M. G.; Netzer, F. P.; Klötzer, B.; Hayek, K. *Surf. Sci.* **2000**, *445*, 380.
124. Belton, D. N.; DiMaggio, C. L.; Ng, K. Y. S.; *J. Catal.* **1993**, *144*, 273 and references therein.
125. Zaera, F.; Gopinath, C. S. *J. Chem. Phys.* **2001**, *116*, 1128.
126. Bowker, M.; Guo, Q.; Joyner, R. W. *Surf. Sci.* **1991**, *257*, 33.
127. Klötzer, B.; Hayek, K.; Konvicka, C.; Lundgren, E.; Varga, P. *Surf. Sci.* **2001**, *482*, 237.
128. Zheng, G.; Altman, E. I. *Surf. Sci.* **2000**, *462*, 151.
129. Zheng, G.; Altman, E. I. *Surf. Sci.* **2002**, *504*, 253.
130. Zheng, G.; Altmann, E. I. *J. Phys. Chem. B* **2002**, *106*, 1048.

References

131. Bondzie, V. A.; Kleban, P. H.; Dwyer, D. J. *Surf. Sci.* **2000**, *465*, 266.
132. Todorova, M.; Reuter, K.; Scheffler, M. *J. Phys. Chem. B* **2004**, *108*, 14477.
133. Lundgren, E.; ... Scheffler, M. *Phys. Rev. Lett.* **2004**, *92*, 046101.
134. Teschner, D.; Pestryakov, A.; Kleimenov, E.; Hävecker, M.; Bluhm, H.; Sauer, H.; Knop-Gericke, A.; Schlögl, J. *Catal.* **2005**, *230*, 186.
135. Jiang, L. Q.; Koel, B. E. *J. Phys. Chem.* **1992**, *96*, 8694.
136. Wickham, D. T.; Banse, B. A.; Koel, B. E. *Surf. Sci.* **1991**, *243*, 83.
137. Aryafar, M.; Zaera, F. *J. Catal.* **1998**, *175*, 316.
138. Takahashi, N.; ... Kasahara, K. *Catal. Today* **1996**, *27*, 63.
139. Fridell, E.; Persson, H.; Olsson, L.; Westerberg, B.; Amberntsson, A.; Skoglundh, M. *Top. Catal.* **2001**, *16*, 133.
140. Berndt, H.; Schutze, F. W.; Richter, M.; Sowade, T.; Grunert, W. *Appl. Catal. B* **2003**, *40*, 51.
141. Hammer, B. *J. Catal.* **2001**, *199*, 171.
142. Bowker, M.; Bennett, R. A.; Jones, I. Z. *Top. Catal.* **2004**, *28*, 25.
143. Loffreda, D.; Simon, D.; Sautet, P. *J. Chem. Phys.* **1998**, *108*, 6447.
144. Loffreda, D.; Simon, D.; Sautet, P. *Chem. Phys. Lett.* **1998**, *291*, 15.
145. Loffreda, D.; Simon, D.; Sautet, P. *J. Catal.* **2003**, *213*, 211.
146. Prevot, G.; Meerson, O.; Piccolo, L.; Henry, C. R. *J. Phys. Condens. Matt.* **2002**, *14*, 4251.
147. Burghaus, U.; Jones, I. Z.; Bowker, M. *Surf. Sci.* **2000**, *454-456*, 326.
148. Thirunavukkarasu, K.; Thirumoorthy, K.; Libuda, J.; Gopinath, C.S. *J. Phys. Chem. B* **2005**, *109*, 13283.
149. Haq, S.; Hodgson, A. *Surf. Sci.* **2000**, *463*, 1.
150. Prevot, G.; Meerson, O.; Piccolo, L.; Henry, C. R. *J. Phys. Cond. Matt.* **2002**, *14*, 4251.
151. Haq, S.; Hodgson, A. *Surf. Sci.* **2000**, *463*, 1.
152. Zaera, F.; Gopinath, C. S. *J. Chem. Phys.* **1999**, *111*, 8088.
153. Gopinath, C. S.; Zaera, F. *J. Catal.* **2001**, *200*, 270.
154. Zaera, F.; Gopinath, C. S. *Chem. Phys. Lett.* **2000**, *332*, 209.

References

155. Johánek, V.; Laurin, M.; Grant, A. W.; Kasemo, B.; Henry, C. R.; Libuda, J. *Science* **2004**, *304*, 1639.
156. Szanyi, J.; Kuhn, W. K.; Goodman, D. W. *J. Phys. Chem.* **1994**, *98*, 2978.
157. Salo, P.; Honkala, K.; Alatalo, M.; Laasonen, K. *Surf. Sci.* **2002**, *516*, 247.
158. Nakai, I.; Kondoh, H.; Shimada, T.; Resta, A.; Andersen, J. N.; Ohta, T. *J. Chem. Phys.* **2006**, *124*, 224712.
159. Ketteler, G.; Ogletree, D. F.; Bluhm, H.; Liu, H.; Hebenstreit, E. L. D.; Salmeron, M. *J. Am. Chem. Soc.* **2005**, *127*, 18269.
160. Han, J.; Zemlyanov, D. Y.; Ribeiro, F. H. *Surf. Sci.* **2006**, *600*, 2752.
161. Rose, M.K.; Borg, A.; Dunphy, J.C.; Mitsui, T.; Ogletree, D.F.; Salmeron, M. *Surf. Sci.* **2000**, *561*, 69.
162. Zemlyanov, D.; ... Klötzer, B. *Surf. Sci.* **2006**, *600*, 983 and references therein.
163. Gabasch, H.; ... Zemlyanov, D. *Surf. Sci.* **2006**, *600*, 2980 and references therein.
164. Klötzer, B.; Hayek, K.; Konvicka, C.; Lundgren, E.; Varga, P. *Surf. Sci.* **2001**, *482-485*, 237.
165. Gabasch, H.; Unterberger, W.; Hayek, K.; Klötzer, B.; Klein, C.; Schmid, M.; Varga, P.; Kresse, G. *Surf. Sci.* **2006**, *600*, 205.
166. Voogt, E. H.; Mens, A. J. M.; Gijzeman, O. L. J.; Geus, J. W. *Surf. Sci.* **1997**, *373*, 210.
167. Engel, T.; Ertl, G. *Adv. Catal.* **1979**, *28*, 1, Engel, T. *J. Chem. Phys.* **1978**, *69*, 373.
168. Berlowitz, P. J.; Peden, C. H. F.; Goodman, D. W. *J. Phys. Chem.* **1988**, *92*, 5213.
169. Szanyi, J.; Kuhn, W. K.; Goodman, D. W. *J. Vac. Sci. Technol. A* **1993**, *11*, 1969.
170. Szanyi, J.; Goodman, D. W. *J. Phys. Chem.* **1994**, *98*, 2972.
171. Jones, I. Z.; Bennett, R.A.; Bowker, M. *Surf. Sci.* **1999**, *439*, 235.
172. Schalow, T.; Brandt, B.; Laurin, M.; Schauer mann, S.; Libuda, J.; Freund, H-J. *J. Catal.* **2006**, *242*, 58 and references therein.
173. Dellwig, T.; Hartmann, J.; Libuda, J.; Meusel, I.; Rupprechter, G.; Unterhalt, H.; Freund, H.-J. *J. Mol. Catal. A: Chemical* **2000**, *162*, 51.
174. Piccolo, L.; Becker, C.; Henry, C. R. *Appl. Surf. Sci.* **2000**, *164*, 156.
175. Becker, C.; Henry, C.R. *Surf. Sci.* **1996**, *352-354*, 457.

References

176. Eriksson, M.; Ekedahl, L-G. *Surf. Sci.* **1998**, *412/413*, 430.
177. Imbihl, R. *Prog. Surf. Sci* **1993**, *44*, 185 and references therein.
178. Kuhn, W. K.; Szanyi, J.; Goodman, D. W. *Surf. Sci.* **1992**, *274*, L611.
179. Unterhalt, H.; Rupprechter, G.; Freund, H-J. *J. Phys. Chem. B* **2002**, *106*, 356.
180. Wintterlin, J.; Voelkening, S.; Janssens, T. V. W.; Zambelli, T.; Ertl, G. *Science* **1997**, *278*, 1931.
181. Twigg, M. V. *Phil. Trans. R. Soc. A* **2005**, *363*, 1013.
182. Pyatnitskii, Y.I.; Martsenyuk-Kukharuk, M. G.; Orlik, S. N.; Ostapyuk, V. A. *Theor. Exp. Chem.* **1988**, *23*, 454.
183. Graham, G. W.; Logan, A. D.; Shelef, M. J. *J. Phys. Chem.* **1993**, *97*, 5446.
184. Ma, Y-S.; Rzeznicka, I. I.; Matsushima, T. *Catal. Lett.* **2005**, *101*, 109.
185. Ma, Y-S.; Rzeznicka, I. I.; Matsushima, T. *Appl. Surf. Sci.* **2005**, *244*, 558.
186. Vesecky, S. M.; Xu, X.; Chen, P. J.; Goodman, D. W. *J. Vac. Sci. Technol. A* **1995**, *13*, 1539.